South Taranaki Bight Iron Sand Mining: Oceanographic measurements data report

Prepared for Trans-Tasman Resources Ltd

Updated November 2015

Authors/Contributors:
Iain MacDonald
Rod Budd
Dave Bremner
Scott Edhouse

For any information regarding this report please contact:
Iain MacDonald
Scientist
Coastal and Estuarine Processes Group
+64-7-859 1818
i.macdonald@niwa.co.nz

National Institute of Water & Atmospheric Research Ltd
Gate 10, Silverdale Road
Hillcrest, Hamilton 3216
PO Box 11115, Hillcrest
Hamilton 3251
New Zealand

Phone +64-7-856 7026
Fax +64-7-856 0151

NIWA Client Report No: HAM2012-147
Report date: August 2012
NIWA Project: TTR11201 and TTR12202

Contents

Tables

Figures

Reviewed by

M. Green

Approved for release by

R. Bell

Formatting checked by:

Executive summary

As part of wide-ranging biogeophysical studies, NIWA was commissioned by Trans-Tasman Resources Ltd (TTR) to undertake a field programme to measure currents, waves and sediment transport in the South Taranaki Bight (STB). The primary goal of the field programme was to collect an oceanographic data set that would support the development by NIWA of numerical models of current flows, waves and suspended-sediment plume dispersion in the STB.

Initially, NIWA was contracted to undertake a measurement programme that consisted of two 6-week deployments. This was later extended to include an additional 6-week deployment. The locations occupied during the third deployment were different to the sites occupied during the first two deployments. No wave data was collected during the third deployment as sufficient wave data had been collected during the first two deployments.

A comprehensive set of current, wave and suspended-sediment measurements was collected during the approximate 7-month period from 09 September 2011 to 01 July 2012 (excluding gaps between deployments). The range of winds experienced during the field programme were typical of the long-term wind climate and included a more extreme weather-bomb event (3 March 2012).

This report presents a synthesis the oceanographic field measurements.

Current velocities were measured at five sites in the STB and represent a significant dataset in their own right, as few current-meter moorings have been undertaken in this region off Hawera and Patea. The data show the prevailing patterns of water movements in the STB, with tides and winds being the main contributors. Tidal currents account for a significant proportion of the measured currents at all sites, with the proportion explained by the tidal constituents ranging from 40% to 78%. The peak ebb or flood current speed of the main twice-daily lunar (M2) tide, which is an average tide, ranged between 0.13 m/s and 0.25 m/s. Somewhat higher and lower tidal speeds occur on spring and neap tides respectively. At all sites the M2 tide was oriented in the SE–NW direction (parallel with the coastline). The presence of such tidal current speeds well offshore in the STB arises from the alternate flow of water over the extensive, relatively-shallow, shoals off Hawera and Patea.

The tidal currents, however, only comprise part of the story. Currents in the STB are also substantially affected by wind conditions. Large current speeds of around 1 m/s were measured on a number of occasions during periods of high winds. Winds blowing from the W and the SE sectors had the most pronounced influence on currents. Moderate to strong winds not only increased current speeds but also greatly altered current direction. During strong winds, currents could set in a constant direction for more than 24 hours; during calm conditions, currents reversed approximately every 6.2 hours with the tides re-asserting dominance.

At most sites during periods of light winds the prevailing current drift was towards the SE, which is consistent with the influence of the d'Urville Current, which sweeps past Farewell Spit and turns around in the STB to head south. However, current drift directions were significantly altered by moderate to strong SE winds which reversed the drift towards the NW. During times of moderate to strong W to NW winds, the prevailing SE drift was considerably enhanced.

These results have implications for the hydrodynamic and sediment modelling as both tidal and meteorological forcing contributes to the observed water movements in the STB.

Waves were measured at eight sites in the STB, in water depths ranging from 50 m offshore to 9 m near the coast. Wave measurements in both deep and shallow water have captured the transformation of wave trains as they move and shoal from deep to shallow water.

The wave data clearly show that the STB is a high-energy environment. At the deep sites, significant wave heights in excess of 4.0 m were routinely observed. The highest significant wave height of 7.1 m was recorded on 03/03/2012 at 05:40 during the South Taranaki weather bomb. The spectral mean wave period at the surface at that time was 8.4 seconds and the waves arrived from the south. Local 10-minute average winds at Whanganui preceding this event were very strong (~17 m/s or 61 km/hr) with gusts up to 100 km/hr and blew from the SSW within a deep-low depression.

Considering only waves greater than 2 m in height over all deployments showed they arrived mainly from either the S–SSE or from the SW–WSW sectors. There was a reduction in wave height moving from the offshore deeper sites into the shallower sites close to the shoreline, which is part of the wave shoaling process. There was also a reduction in wave height moving down coast in a S–SE direction, caused by sheltering of the prevailing SW to WSW swell by the tip of the South Island (Farewell Spit).

Temperature and salinity measurements show that the water column in the STB was generally well mixed with only small vertical differences in temperature and salinity. Slightly lower salinity is likely to be found in the vicinity of major rivers in the STB (e.g., Patea, Waitotara and Whanganui).

Concentrations in the water column of suspended sands and suspended fine sediments (clays, silts and muds) were made at several sites and heights above the bed within the STB.

In the near-surface waters, the maximum suspended-fine-sediment concentration (*SSCm*) was 0.025 grams/litre. At some sites *SSCm* varied over the deployment period, with peaks in *SSCm* tending to occur during or just after periods of significant rainfall. At these times it is likely that rivers were discharging fine sediments into the STB, which were then being transported in suspension through the measurement site. Some of the peaks in *SSCm* also coincided with times of large waves. While it is possible that large waves resuspended fine sediments from the sea bed and increased *SSCm* near the surface, it is also possible that the increase resulted from an increase in optical backscatter generated by the entrainment of air bubbles into the water column by an energetic sea. For most of the time, the near-surface background *SSCm* was typically less than 0.01 grams/litre, which is close to the lower detection limit of an OBS.

Near the sea bed, the maximum *SSCm* was 0.08 grams/litre, and peaks in concentration near the bed did not always coincide with peaks in wave height. This implies that increases in concentration were not always driven by resuspension of local bed sediments. Instead, fine suspended sediment may have been advected through the measurement site from some “upstream" location. During calm periods, background suspended-fine-sediment concentration at the seabed was similar to the background concentration at the surface (~ 0.01 grams/litre).

When there was any sand in suspension, suspended-sand concentration (*SSCs*) close to the sea bed was typically much greater than *SSCm*. The largest suspended-sand concentration very close to the seabed was 1.9 grams/litre. At all sites, periods of increased sand concentration coincided with periods of large waves, thus highlighting the importance of waves in resuspending sand from the seabed in the STB. During calm periods, no sand was found to be in suspension.

Over the duration of the largest sediment-transport event, 3355 kg of sand per metre width of sea bed was transported in suspension by currents. This equates to a volume of 2.1 m^3 of sand transported per metre width of sea bed. These are gross transport rates in any direction.

Overall, the field dataset provides a coherent picture of currents, waves and suspended-sediment concentrations in the STB. The datasets, which have been carefully calibrated to produce accurate measures, can be used with confidence in the development of numerical models of current flows, waves and suspended-sediment plume dispersion in the STB.

Information relating to TTR's additional scientific work undertaken since 2014 has been provided and the conclusions is this report remain valid.

1 Introduction

Trans-Tasman Resources Ltd (TTR) has secured permits for prospecting for offshore iron sands along the West Coast, North Island. The areas of interest lie within the 12 nautical mile (nm) territorial sea along the North Taranaki Bight (NTB) and South Taranaki Bight (STB) (area PP 50 383), and beyond the 12 nm boundary (area PP 50 753). NIWA is undertaking a range of biogeophysical studies in the STB for TTR to meet the likely requirements of the consenting procedures.

Mining operations will involve dredging depressions in the sea bed, concentrating iron ore on board vessels, and then returning the residual sand to the sea bed where it will partially fill the depressions and also form mounds. Mining sites and tailings deposition areas are about 15 to 35 km offshore from Patea (see Figure 2-1).

As part of the wide-ranging biogeophysical studies, NIWA was commissioned by TTR to undertake a field programme to measure currents, waves and sediment transport in the STB. The primary goal of the field programme was to collect a data set that would support the development by NIWA of numerical models of current flows, waves and suspended-sediment plume dispersion in the STB. Both the field and model studies were undertaken to help assess the potential effects of offshore sand extraction on the surrounding environment.

Initially NIWA was contracted to undertake a measurement programme that consisted of two 6-week oceanographic deployments (D1 and D2). This was later extended to include an additional 6-week deployment (D3). The locations occupied during the third deployment were different to the sites occupied during the first two deployments. No wave data were collected during the third deployment as sufficient wave data had been collected during the first two deployments.

This report provides TTR with a summary of the current, wave, water temperature, salinity and suspend-sediment concentration measurements recorded in the STB during all three deployments, which altogether cover an approximate 7-month period from 09 September 2011 to 01 July 2012 (excluding gaps between deployments).

2 Methods

2.1 Instrumentation

2.1.1 Currents

Current velocities in the STB were measured using Acoustic Doppler Current Profilers (ADCP). ADCPs measure currents in "bins" throughout the water column, thus providing the user with a velocity profile over the entire water column.

ADCPs were deployed on the sea bed facing the water surface, which is known as a bottom-mounted upward-looking configuration. ADCP acoustic transducers were nominally positioned 0.4 m above the sea bed.

2.1.2 Waves

Significant wave height[1] (H_s), mean spectral period (T_m) and, where possible, mean direction of wave propagation (D_p) were measured using three different instruments, these being (1) ADCPs, (2) DOBIE Wave Gauges (DWGs) and (3) a surface-following Datawell wave rider buoy (WRB).

The ADCP calculates the wave parameters H_s, T_m and D_p from the current velocity measured in the bin closest to the sea surface. For a comprehensive overview of how the wave parameters are derived by the ADCP, the reader is directed to the Waves primer technical report[2] published by the ADCP manufacturer (Teledyne RD Instruments Inc.). All wave parameters were calculated using the software supplied by the ADCP manufacturer.

In contrast to the ADCP, which calculates wave parameters from current velocities measured close to the sea surface, the DWG calculates wave parameters from pressure fluctuations measured at the height of the instrument. (The DWG in this study was always located on the sea bed.) Pressure fluctuations beneath waves attenuate with depth through the water column at a rate that depends on the wave frequency (where wave frequency is the inverse of wave period). The rate of attenuation is higher for high-frequency waves than it is for low-frequency waves. Therefore, not only will the total variance of the pressure spectrum at depth be less than the total variance of the pressure spectrum at the sea surface, but also the shape of the spectrum will be different, due to the relatively greater attenuation of the high-frequency (short-period) components. H_s is calculated from the total variance of the pressure spectrum, and must be adjusted for the depth-attenuation of pressure. T_m is calculated from the shape of the pressure spectrum, and can either be adjusted for depth attenuation so that it accurately represents the period of the waves at the surface, or it can be left un-adjusted, in which case it can be interpreted as the mean spectral period of the wave-orbital motions at the level of the measurement. T_m adjusted for depth attenuation will always be smaller than T_m at the level of the measurement, because the higher-frequency components of the wave spectrum are attenuated more than the lower-frequency components. Care is required when comparing wave parameters from difference sources (e.g., field measurements and a wave model) to ensure that like terms are being compared. No information about wave direction can be derived from pressure measured at a single location.

[1] Defined as the average of the top 33% (1/3) of wave heights over the measurement cycle
[2] http://www.rdinstruments.com/pdfs/waves_primer.pdf

The Wave Rider Buoy floats on the water surface and uses accelerometers to measure the 3-dimensional motion that results from the propagating wave train. The accelerometer data are used to derive H_s, T_m and D_p. All wave parameters were calculated using the software supplied by the instrument manufacturer.

2.1.3 Temperature and Salinity

Conductivity and temperature, from which salinity can be derived, were measured using Sea-Bird Electronics 37-SMP MicroCATs. All MicroCAT data were processed and salinity calculated using the software supplied by the instrument manufacturer. Some additional temperature measurements were made using RBR temperature loggers.

2.1.4 Suspended Sediment Concentration

Suspended-sediment concentration (SSC) in the STB was measured using two types of instrument, these being (1) the Acoustic Backscatter Sensor (ABS) and (2) the Optical Backscatter Sensor (OBS).

The ABS is a highly specialised instrument which is typically deployed looking down towards the sea bed from a height of approximately 1 m. It works by transmitting short-period high-frequency acoustic pulses. As the pulse propagates through the water column a proportion of the transmitted pulse is scattered back to the ABS by suspended particles in the water column. By “listening” at fixed time intervals after each transmitted pulse the ABS generates a profile of backscattered sound intensity at known distances from the transducer face (distance and time are related via the speed of sound in water ~1500 m/s). The profiles of backscattered sound may then be inverted to provide profiles of suspended-sediment concentration. Since the ABS has a far greater sensitivity to coarser sediments (sand) than to fine sediments (clays and muds), it is reasonable to treat this as a suspended-sediment sand concentration, which is here denoted by *SSCs*. The reader is directed to Thorne and Hanes (2002) and Moate and Thorne (2012) for more information on how the ABS works and about the data inversion process.

In order to invert the ABS data, the ABS system constants (K_t) are required, which need to be obtained by laboratory calibration against an accurate standard. The two ABSs used in this study were calibrated in a recirculating tank against 4 test suspensions of a known concentration. The sediments used in the calibration came from bed sediments collected at two of the ABS deployment sites. The K_t values were obtained by minimising the differences (in a least squares sense) between the known concentration and the concentration obtained by the ABS through the inversion process across all 4 test concentrations.

The two ABSs used in this study both featured multiple simultaneous operating frequencies (Table 2-1). The multi-frequency data from each ABS can be used in a multi-frequency inversion (e.g., Hunter et al. 2011) to generate estimates of the concentration of different sediment grainsizes in suspension. Specifically, the inversion requires data from any two frequencies. In this study, the multi-frequency inversion was performed using the 2- and 3-MHz frequencies for ABS#1 and the 1- and 2-MHz frequencies for ABS#2. The inversion method requires information about the particle size distribution (PSD) of the sediment in suspension, which was obtained from grain size analysis of bed sediments that were collected near the ABS deployment sites. The assumption here is that the PSD of the

suspended sediments is the same as that of the bed sediments. Given the energetic conditions in the STB, this would seem to be a reasonable assumption.

ABS	Number of frequencies	Frequencies (MHz)
ABS#1	4	1,2,3 and 4
ABS#2	3	1,2 and 4

Table 2-1: ABS information.

In contrast to the ABS, the OBS is much more sensitive to fine sediments (silts, clays and muds) than it is to coarse sediments (sand). The voltage output by the optical backscatter sensor (*V*) is related to the suspended-mud concentration *SSCm* by a linear relationship:

$$SSCm = G*V + O$$

where *G* is the sensor gain (unit of g/l per volt) and *O* is the sensor offset (units of g/l).

Each sensor gain and offset were determined by calibrating the sensor against a series of test suspensions of a known concentration in the laboratory. The sediment used in the calibration came from bed sediments collected near the mouth of the Whanganui River. Reflecting the greater sensitivity to fine sediments, the collected sediment was sieved through a 63-micron sieve to form a slurry of fine sediment, which was used in calibration process. A linear regression was used to fit the linear relationship to the calibration dataset (sensor output versus reference suspended solids concentration) to determine the sensor's gain and offset.

2.2 Deployment considerations

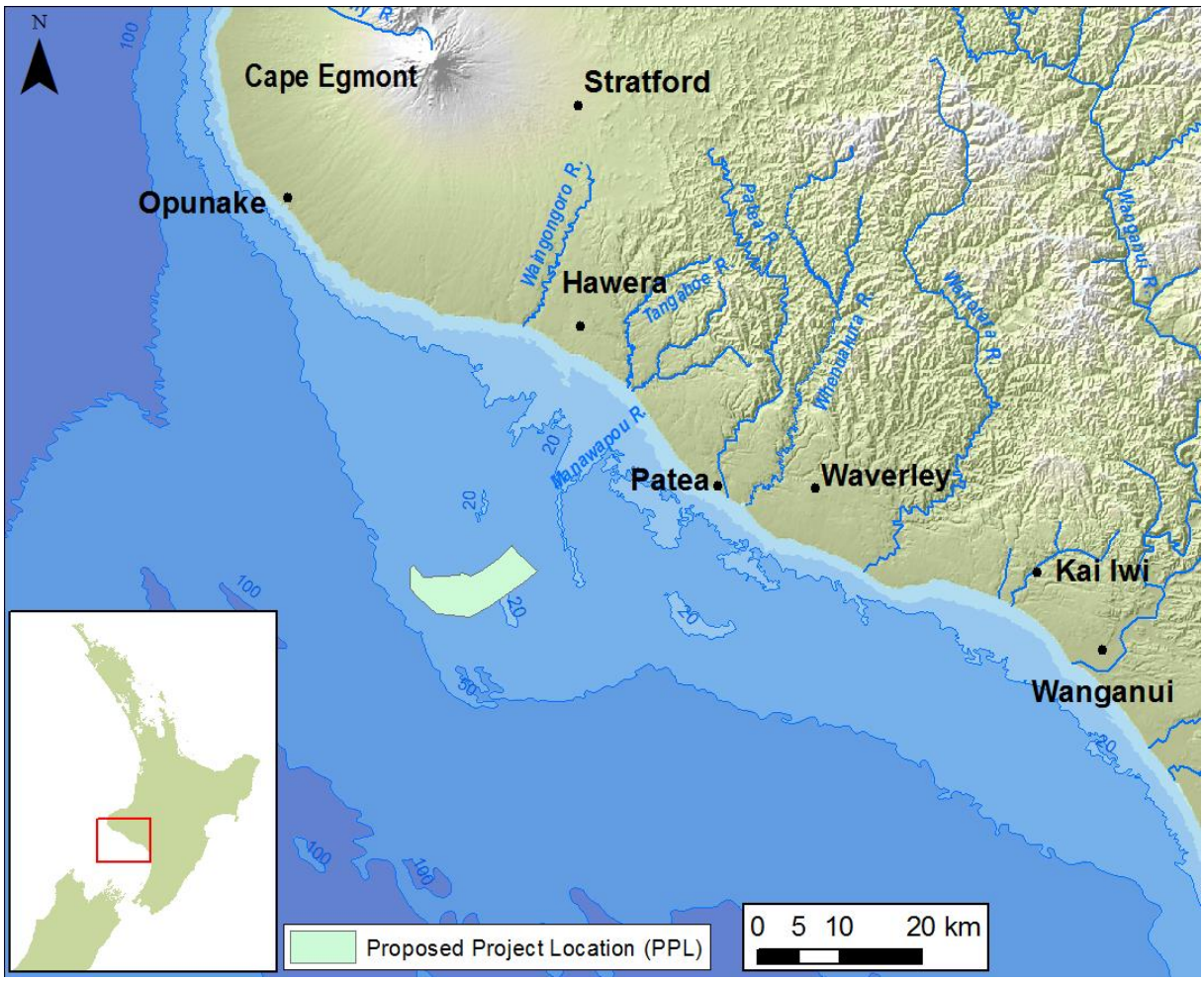

Figure 2-1: Study area of the South Taranaki Bight, showing the proposed project location (PPL).

2.2.1 Currents

In order to accurately model the dispersal of any sediment plumes generated by the mining process, a good understanding of current flows in the STB is required, particularly in the vicinity of the mining operations (Figure 2-1). However, plumes may also move a significant distance from the point of generation. Accordingly, it was deemed necessary to measure currents widely through the STB for the purposes of calibrating and verifying the current model.

2.2.2 Waves

Wave measurements in both deep and shallow water are required to calibrate and verify the simulations of wave propagation through the mining operations area and towards shore. Shoreline change is driven by breaking waves at the outer edge of the surf zone, which also must be captured by the wave model. Accordingly, it was deemed necessary to measure waves both in deep water and close to the shoreline.

2.2.3 Suspended Sediment Concentration

To develop an understanding of sediment-transport processes and to determine background suspended-sediment concentrations in the vicinity of the mining operations, measurements are required close to the sea surface and close to the sea bed. Suspended sediments in near-surface water are likely to be exclusively mud (including clays and silts), but close to the sea bed both mud and sand could be present in suspension. Hence, it was deemed necessary to deploy OBSs throughout the water column (to measure *SSCm*), but it was only necessary to deploy ABSs close to the sea bed (to measure *SSCs*). Sand in suspension close to the seabed is likely to have been placed in suspension by the shear stress exerted on the sea bed by waves and current. Mud in suspension near the water surface may likewise have been placed in suspension by waves and currents, or it may have arrived in freshwater runoff discharged to the coastal ocean by rivers.

2.2.4 Temperature and Salinity

Sea temperature and salinity are required to characterise the vertical water column structure, which can play a role in the dispersal of any sediment plumes generated by mining operations. Lower salinity indicates the presence of freshwater runoff.

2.2.5 Winds

Winds during the deployment period were obtained from the Automatic Weather Station at Hawera (NIWA Climate Database Agent number 25222). The station at Hawera is located 98 m above sea level. Therefore, all wind speed data presented in this report was collected 98 m above sea level.

3 Results

3.1 Instrument locations and deployment information

Following a consideration of logistics and the issues discussed in section 2.2, a field programme was designed.

Figure 3-1 shows locations occupied during the planned three 6-week deployment periods[3]. At some of these sites multiple instruments were deployed. The periods over which the three deployments took place are shown in Table 3-1.

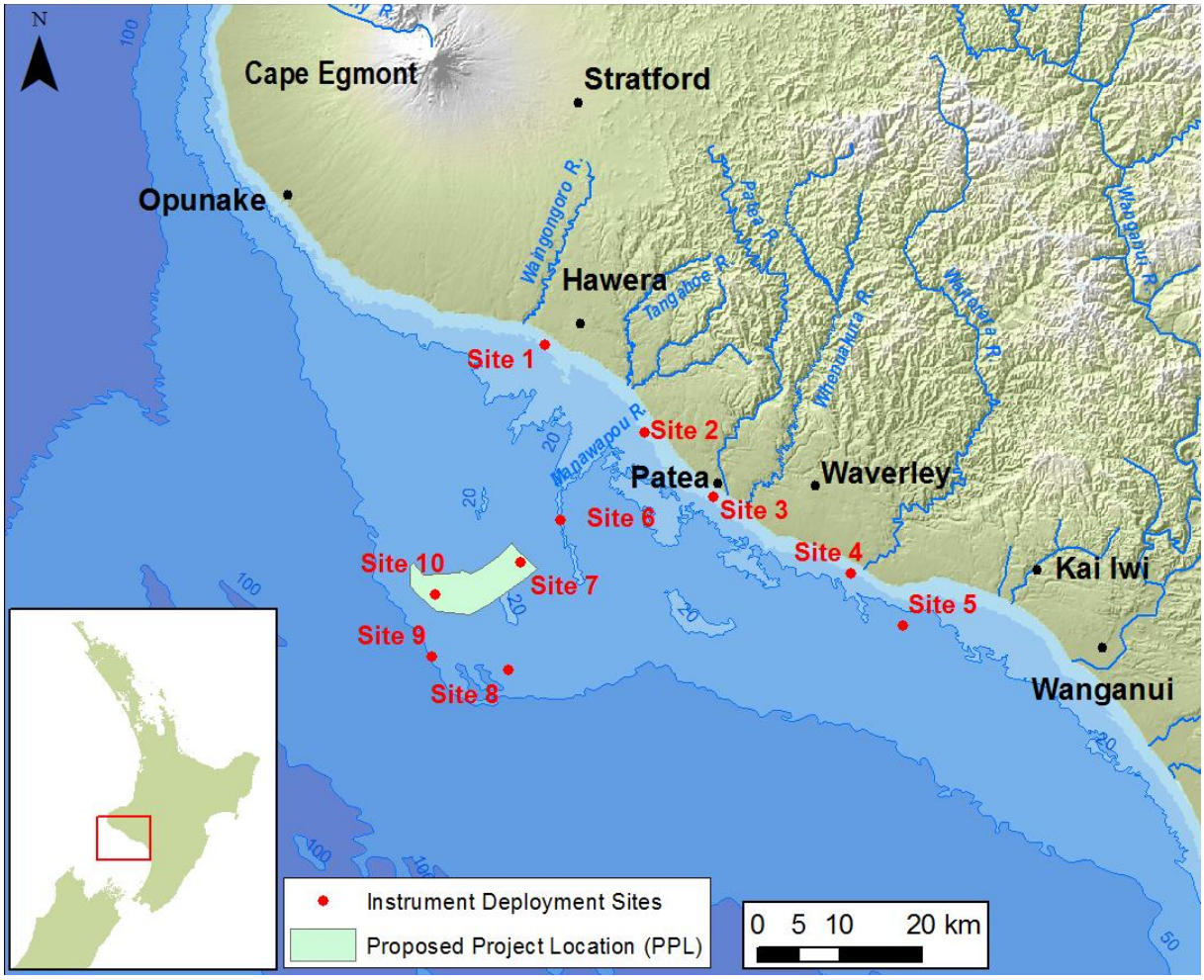

Figure 3-1: Site map, showing instrument locations and the proposed project location (PPL).

[3] Due to infrequent fine weather periods in which instrument could be retrieved the deployments periods for all three deployments exceeded the planned 6 week duration.

Deployment number	Deployment ID	Period
1	D1	06/09/2011 to 01/12/2011
2	D2	08/12/2011 to 09/02/2012
3	D2	24/04/2012 to 01/07/2012

Table 3-1: Deployment periods.

The details of what instruments were deployed at each of the sites and over which deployment period are shown in Table 3-2. The WGS-84 coordinates of the sites are also given in Table 3-2.

Site	Latitude (S)	Longitude (E)	Instrument (parameter measured)	Deployment period	Approximate water depth
1	39˚ 36.652	174˚ 13.459	DWG (waves)	D1 and D2	12
2	39˚ 42.286	174˚ 22.085	DWG (waves)	D1 and D2	15
3	39˚ 46.471	174˚ 28.114	DWG (waves)	D1 and D2	9-11
4	39˚ 51.333	174˚ 39.945	DWG (waves)	D1 and D2	11-13
5	39˚ 54.754	174˚ 44.498	ADCP (currents and waves) OBS (near-surface *SSCm*)	D1 and D2	26
6	39˚ 48.179	174˚ 15.033	ADCP (currents and waves) ABS (*SSCs*) 2 x OBS (near-bed and near-surface *SSCm*)	D1 and D2	23
7	39˚ 50.973	174˚ 11.625	ADCP (currents and waves) ABS (*SSCs*) 2 x OBS (near-bed and near-surface *SSCm*) Temperature and salinity	D1 and D2	31
8	39˚ 58.092	174˚ 10.788	ADCP (currents only) ABS (SSC) 2 x OBS (near-bed and near-surface *SSCm*)	D3	45
9	39˚ 57.301	174˚ 4.158	WRB (waves) Temperature and salinity	D1* D1 and D2	>50
10	39˚ 53.166	174˚ 4.350	ADCP (currents only) ABS (*SSCs*) 2 x OBS (near-bed and near-surface *SSCm*) Temperature and salinity	D3	42

Table 3-2: Locations (WGS-84) and deployment information. * The WRB had sufficient memory and battery endurance to span the entire deployment period (shaded regions help differentiate the different sites).

Table 3-2 shows that currents were measured at sites 5, 6 and 7 during deployments D1 and D2, and at sites 8 and 10 during deployment D3. In order to have current meter data in areas where plumes may be generated, sites 6, 7, 8 and 10 were located in the vicinity of the mining operations. Site 5, which was chosen to increase the spatial coverage of the current measurements, was selected by referring to model predictions of the tidal current velocities in the STB which showed that site 5 is on the main path of the D'Urville current through Cook Strait and is therefore of interest for model validation (see the scoping report by MacDiarmid et al. 2010). Additional deployment information relating to the current measurements is shown in Table A-1 in Appendix A.

Table 3-2 shows that waves were measured at sites 1, 2, 3, 4, 5, 6, 7 and 9 during deployments D1 and D2. To capture the wave transformation from deep to shallow water, wave measurements were taken at water depths ranging from greater than 50 m (Site 9) to 9 m (Site 3). Additional deployment information relating to the wave measurements is shown in Table A-2 in Appendix A.

Table 3-2 shows that temperature and salinity were measured at sites 7, 9 and 10. Sites 7 and 10 are located in the vicinity of the mining operations. The purpose of site 9 is to increase the spatial coverage of the temperature and salinity measurements. Additional deployment information relating to the temperature and salinity measurements is shown in Table A-3 in Appendix A.

Table 3-2 shows that SSC was measured at sites 5, 6, 7, 8 and 10. As with the current measurements, sites were selected to be in the vicinity of the proposed mining operations. At sites 6, 7, 8 and 10, both near-bed and near-surface SSC measurements were made. The purpose of site 5 was to increase the spatial coverage of the measurements. Additional deployment information relating to the SSC measurements is shown in Table A-4 in Appendix A.

3.2 Winds

The long-term wind climate for the STB was derived from hourly observations at Hawera Automatic Weather Station over an 8-year period from January 2004 to July 2012. The wind rose is shown in Figure 3-2.

The mean wind speed over the 8-year period was 5.3 m/s, with a maximum of 21.1 m/s on 15 February 2004 from the S (170˚). The wind directions exhibit a tri-modal distribution, dominated by winds from the N, SE and W.

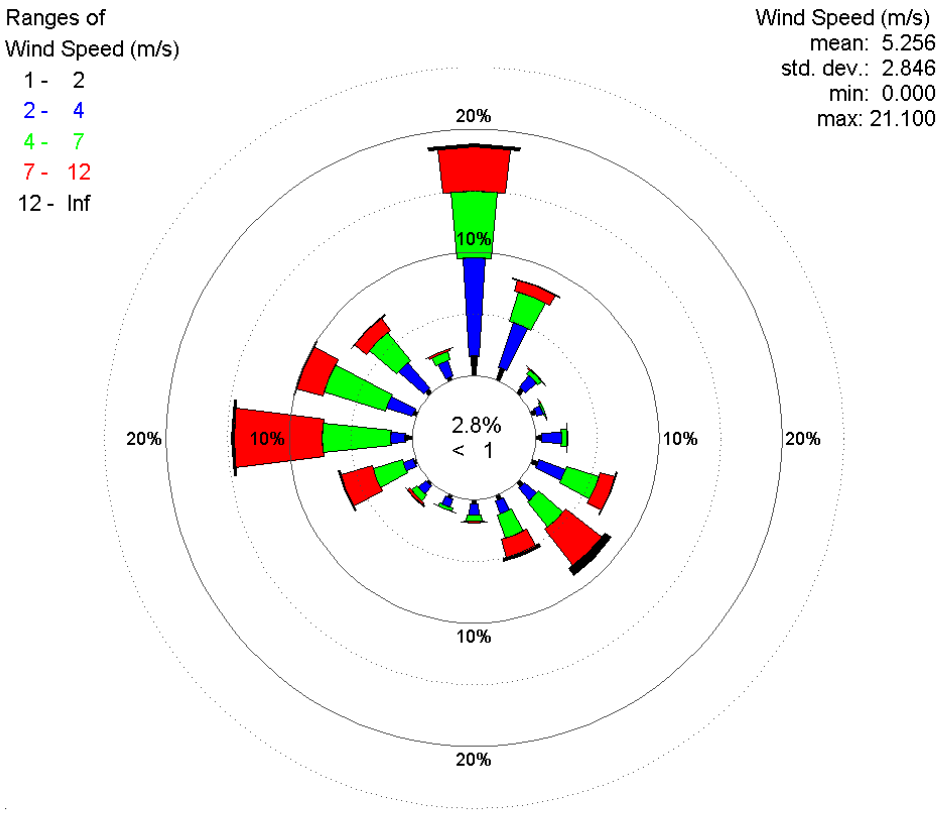

Figure 3-2: Wind rose for winds measured at Hawera over a period of 8-years (January 2004 to July 2012). Meteorological convention is used in expressing the direction that the wind "blows from".

The wind rose for the deployment period (September 2011 to July 2012) is shown in Figure 3-3. The mean wind speed over the deployment period was 5.2 m/s, which is similar to the mean wind speed from the 8-year record. The maximum wind speed during the deployment period was 17.0 m/s, which was reached on 3 March 2012 when the wind blew from the NW (313˚). Overall, the distribution of wind speeds and directions during the field deployment was similar to the long-term distribution (cf. Figure 3-2 and Figure 3-3). Therefore, the range of wind conditions experienced during the field programme was representative of the long-term wind climate.

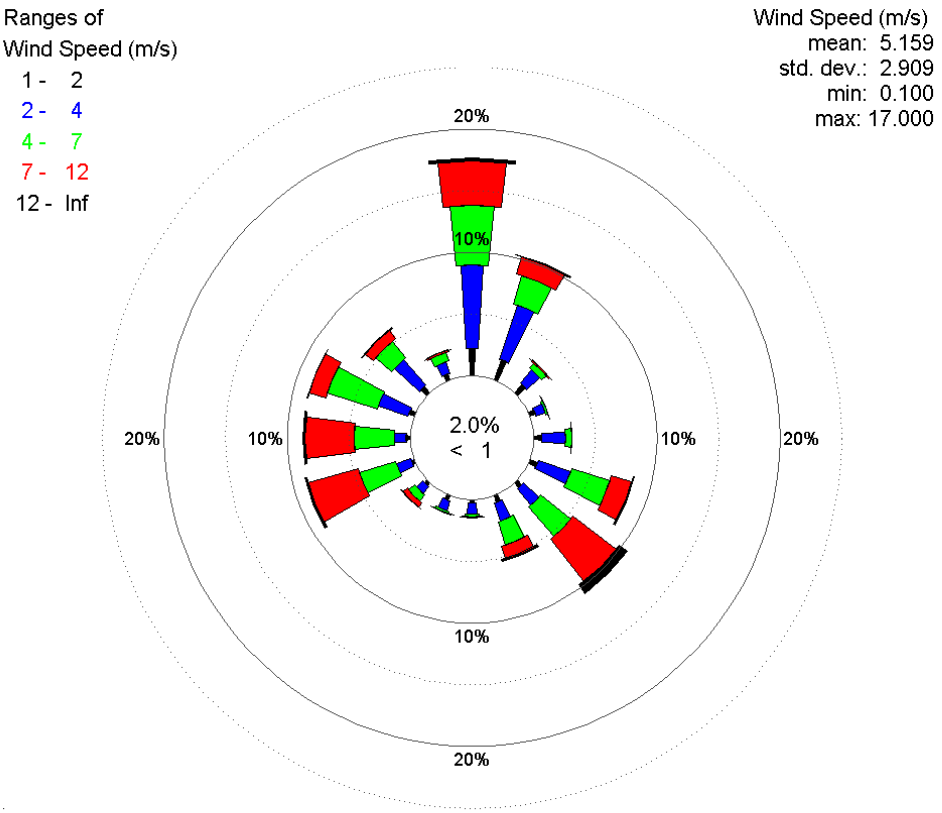

Figure 3-3: Wind rose for winds measured at Hawera over the deployment period (September 2011 to July 2012).

3.3 Currents

The results from each of the ADCP deployments are shown in this section in the form of:

- Time series plots of current speed and direction at various heights above the sea bed, water depth, and wind speed and direction.
- Scatter plots of current velocity components *u* (east–west component, with east positive) and *v* (north–south, with north positive).
- Tidal analysis of the *u* and *v* velocity components.
- Progressive vector plots for the cumulative current-velocity run at various elevations above the sea bed. Although net drift can be inferred from these plots, they cannot account for spatial changes in currents (speed and direction) well away from the deployment site, and therefore need to be interpreted with caution.

3.3.1 Site 5 (near-shore site off Kai iwi)

Two separate ADCP deployments were carried out at site 5 (S5), the details of the location and deployment periods are listed in Table 3-2 and Table A-1 (Appendix A).

Deployment S5/D1

Time-series plots for S5 during deployment 1 (D1) are shown in Figure 3-4.

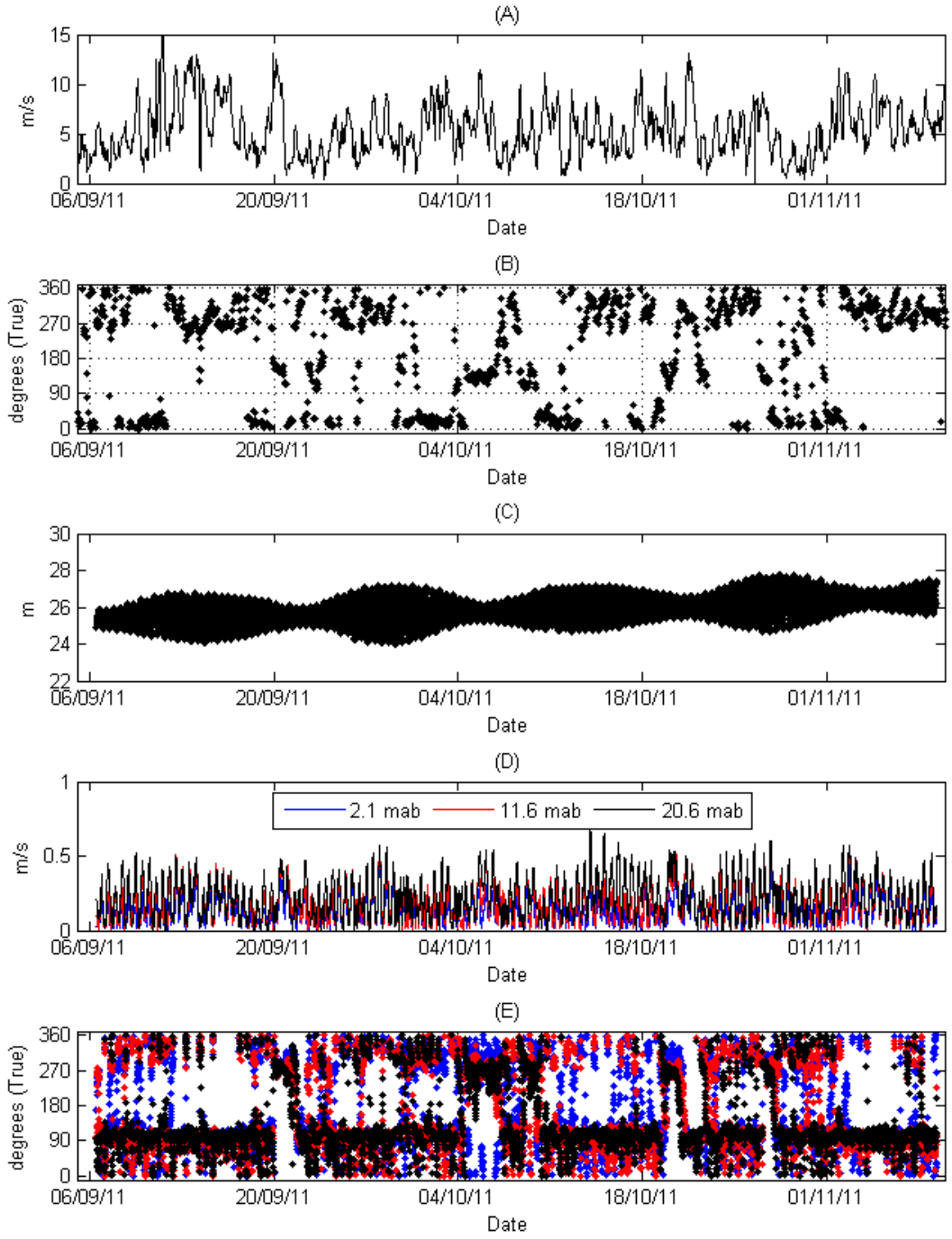

Figure 3-4: Current and wind time series for deployment S5/D1. Panels: (A) wind speed, (B) wind direction (in meteorological convention "blowing from"), (C) water depth, (D) current speed at three elevations above the bed, and (E) current direction (in oceanographic convention "flowing to").

For deployment S5/D1, Figure 3-4D shows that currents were typically less than 0.5 m/s. Near the sea bed, the maximum recorded current speed of 0.50 m/s was measured on 27/09/2011 at 23:45. In the 12-hour period prior, wind speeds ranged between 4.1 and 8.8 m/s (mean 6.4 m/s) with direction from the W. Higher in the water column, at 20.6 metres above bed (mab), the maximum recorded current speed of 0.71 m/s was measured on 14/10/2011 at 01:00. In the 12-hour period prior, wind speeds ranged between 3.8 and 8.1 m/s (mean 6.4 m/s) with direction from the NW.

Scatter plots of the velocity data from the three elevations above the sea bed are shown in Figure 3-5. Here, the east–west velocity component (*u*) is plotted against the north–south velocity component (*v*). In addition to the velocity data, Figure 3-5 displays the results of a principal component analysis (PCA) of the current data. PCA is an orthogonal transformation in which the *u* and *v* velocity components are oriented (rotated) such that the variance along the principal (major) axis is a maximum, and consequently the variance along the minor axis is a minimum. The usefulness of PCA is that the major axis defines the main orientation of the flow. In Figure 3-5, the major and minor axes are displayed as the thick and thin lines respectively (both lines span ± 1 standard deviation). The results of the PCA are also summarised in Table 3-3. Currents measured during the S5/D1 deployment had a principal orientation of ESE–WNW. As expected, Figure 3-5 also shows that current speeds increased with elevation above the sea bed.

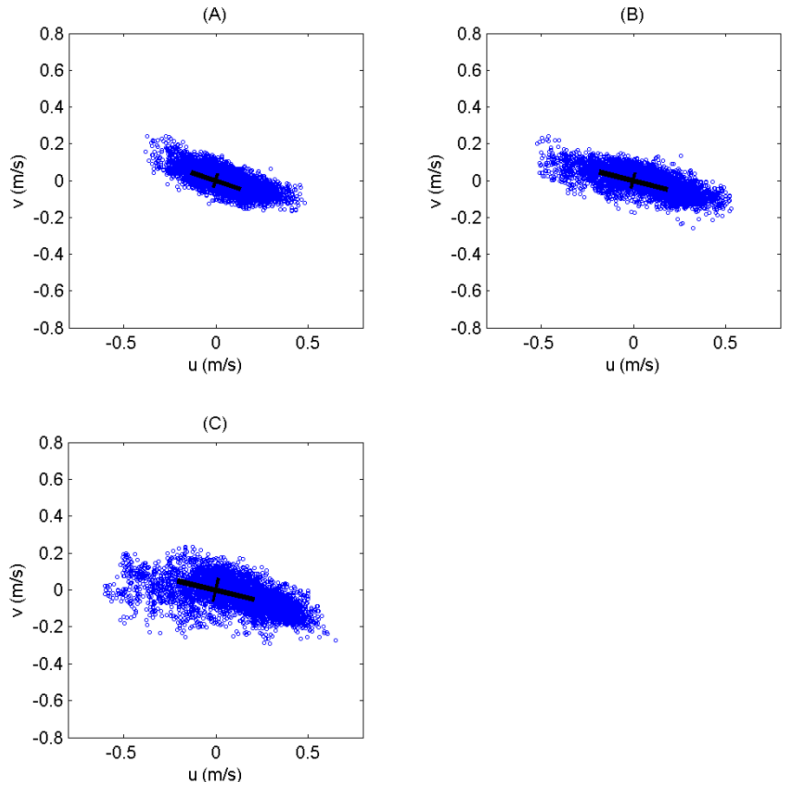

Figure 3-5: Scatter plots of currents at three elevations above the bed from deployment S5/D1: Panels: (A) data from 2.1 mab, (B) data from 11.6 mab, and (C) data from 20.6 mab. Note: the *u* and *v* velocity components relate to the east–west and north–south directions, respectively. The thick line is the major axis and the thin line is the minor axis (both lines span ± 1 standard deviation).

Bin No.	Depth (mab)	Major axis orientation (˚ True North)	Major axis std dev. (m/s)	Minor axis std dev. (m/s)
1	2.1	109	±0.142	±0.039
20	11.6	105	±0.190	±0.043
38	20.6	103	±0.214	±0.06

Table 3-3: Summary of principal component analysis for currents during deployment S5/D1.

A tidal analysis of the ~64-day record of near-bed currents at 2.1 mab for the S5/D1 deployment was conducted. This consisted of fitting a number of tidal constituents to the data by adjusting amplitudes and phases of the constituents such that the least-squares difference between fitted and measured data was minimised. The results of the tidal analysis are given in Appendix B, which shows the amplitude, phase and orientation of each tidal constituent, and in Figure 3-6, which shows measured and predicted *u* and *v* (panels A and B); residual *u*, *v* and magnitude (panel C); wind speed (panel D); and wind direction (panel E). Predicted *u* and *v* are formed from the fitted tidal constituents. Residual *u* is the difference between predicted and measured *u*, and likewise for residual *v*. The residual magnitude is formed from residual *u* and residual *v*.

The fitted tidal constituents explain 46% of the total variability in the current velocities (47% and 45% in the *u* and *v* directions, respectively). The largest constituent was the twice-daily lunar (M2) tide[4], which has an amplitude (maximum speed) of 0.13 m/s and is oriented in the SE–NW direction.

Figure 3-6 shows that the largest residual were associated with two types of wind events: (1) wind from the W and (2) wind from the SE. The winds from the W are characterised by a large positive residual in the *u* component (to the east), while the SE winds are characterised by a large negative residual in the *u* component (to the west).

Times series plots for a wind from the W and for a wind from the SE are shown in Figure 3-7. The panels on the left-hand side of Figure 3-7 show the W wind, while the panels on the right-hand side show the SE wind. The current speeds were clearly affected by the winds, but the most striking effect of the winds was on the current direction: panels E and J show that currents set to a practically constant direction for periods in excess of 24 hours during these wind events.

[4] M2 tide is equivalent to an average tide range – spring tides relate to the combination of M2 with the main solar tide (S2)

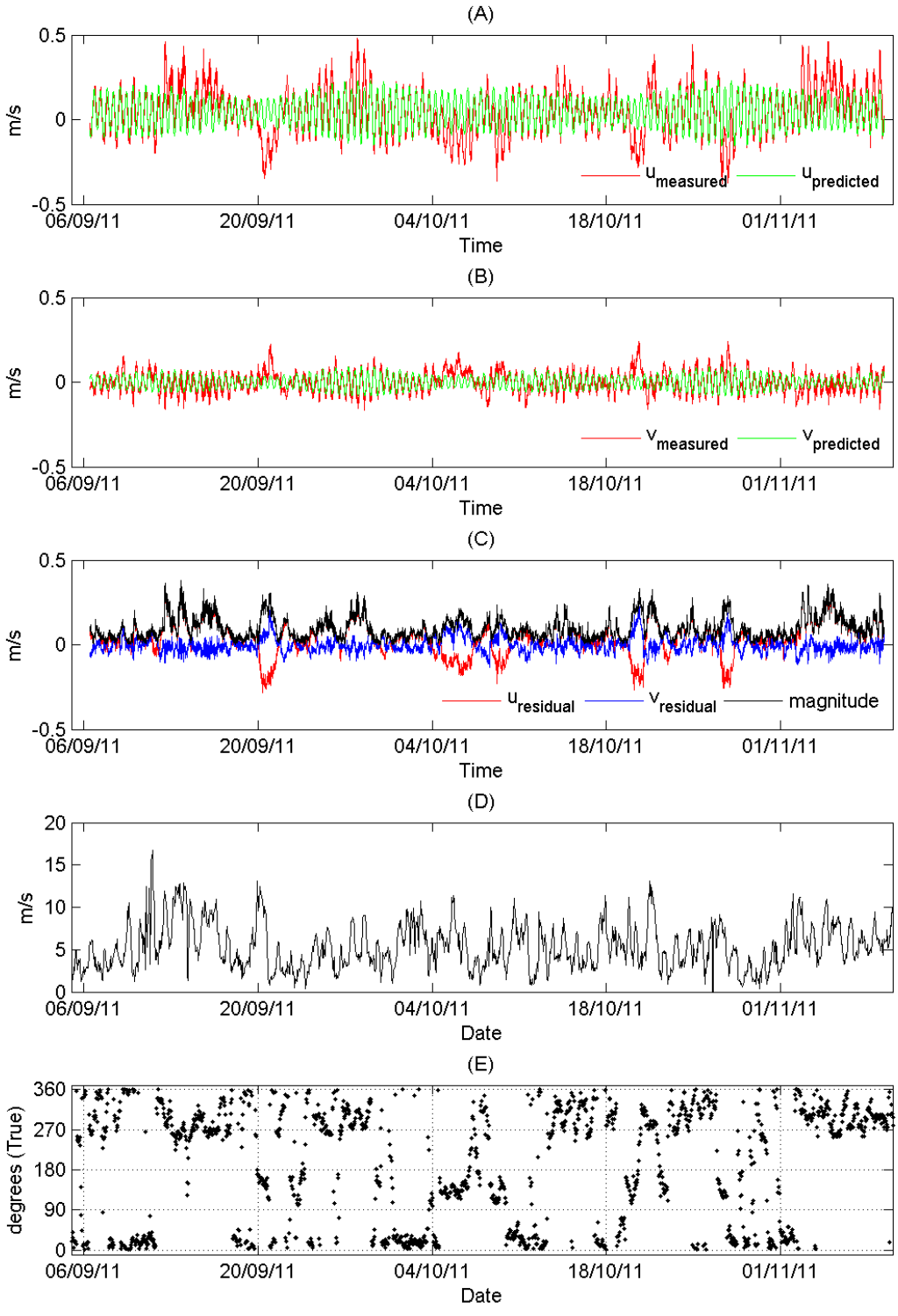

Figure 3-6: Tidal analysis of near-bed currents at S5/D1. Panels: (A) *u* velocity component, (B) *v* velocity component, (C) residual currents, (D) wind speed, and (E) wind direction (in meteorological convention "blowing from").

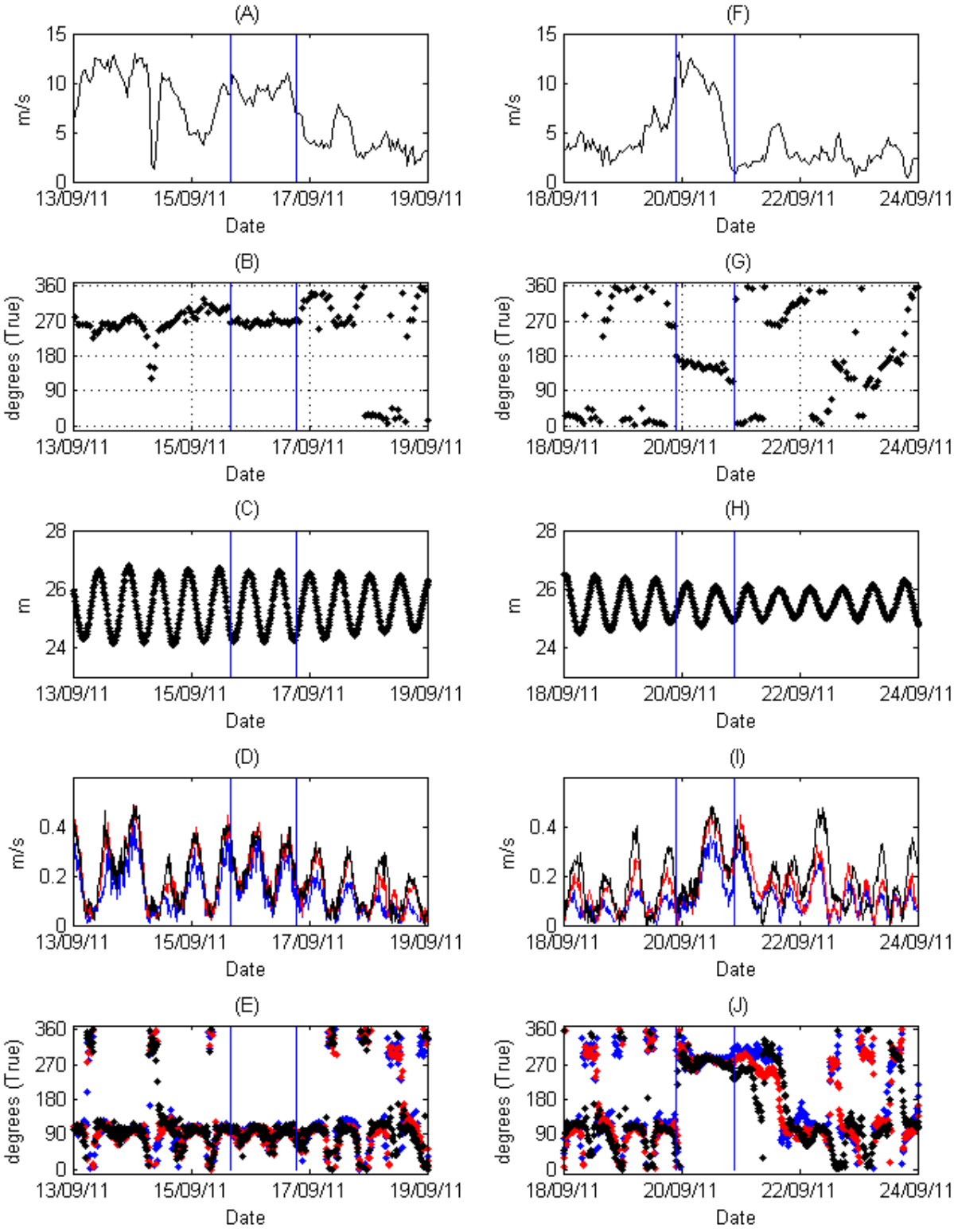

Figure 3-7: Current and wind time series for a W and SE event at S5/D1. Panels A to E relate to the W wind, while panels F to J relate to the SE wind.. (A and F) wind speed, (B and G) wind direction (in meteorological convention "blowing from"), (C and H) water depth, (D and I) current speed at three elevations above the bed, and (E and J) current direction (in oceanographic convention "flowing to").

Unlike the scatter plots, progressive vector diagrams (PVD) show the time sequence of currents. Figure 3-8 shows the PVD for deployment S5/D1 at three elevations above the bed. At all three elevations, aside from the occasional circular meanders, there was a consistent drift towards the E–ESE. Reflecting the increase in current velocities with distance above the bed, the drift distances also increased with elevation above the bed and turned somewhat more clockwise up through the water column. The overall net drift speeds and directions are listed in Table 3-4.

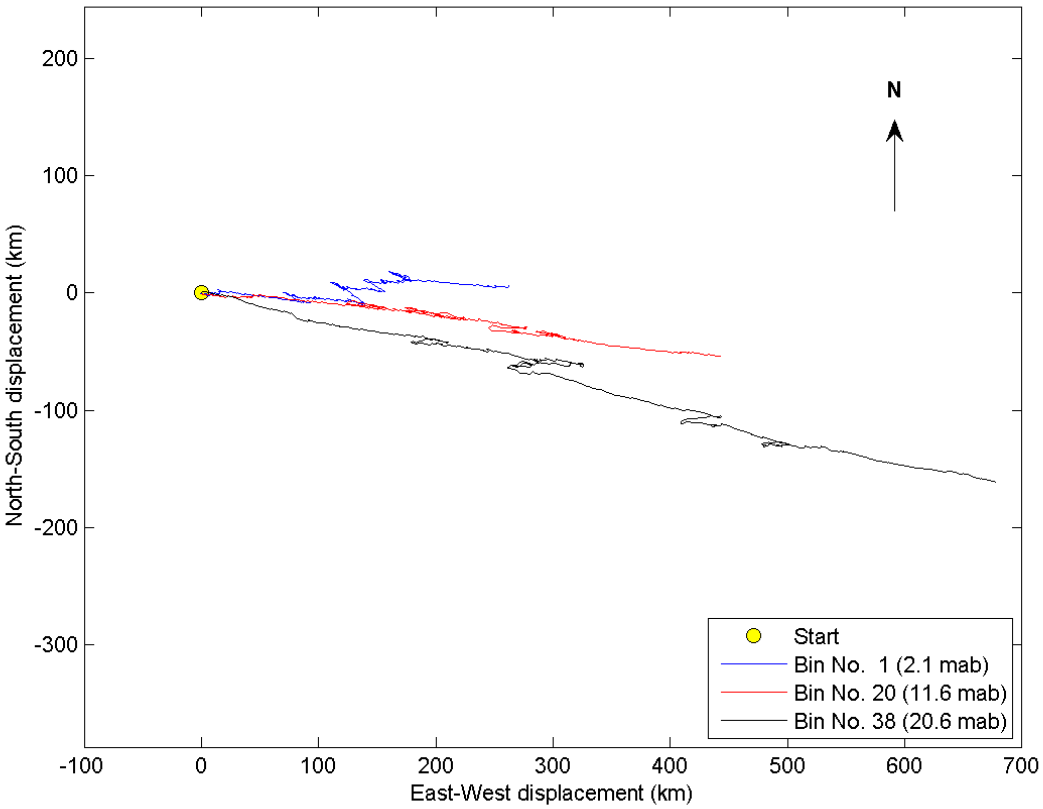

Figure 3-8: Progressive current drift at three elevations above the sea bed for deployment S5/D1 starting 06/09/2011 11:30 (yellow dot) through to 09/11/2011 08:45 (~64 days).

Bin No.	Depth (mab)	Net drift speed (m/s)	Net drift speed (km/day)	Mean drift direction (˚ True North)
1	2.1	0.047	4.10	89
20	11.6	0.081	6.99	97
38	20.6	0.126	10.90	103

Table 3-4: Summary of the overall current drift during deployment S5/D1 (~64 days).

Deployment S5/D2

Time-series plots for S5 deployment 2 (D2) are shown in Figure 3-9.

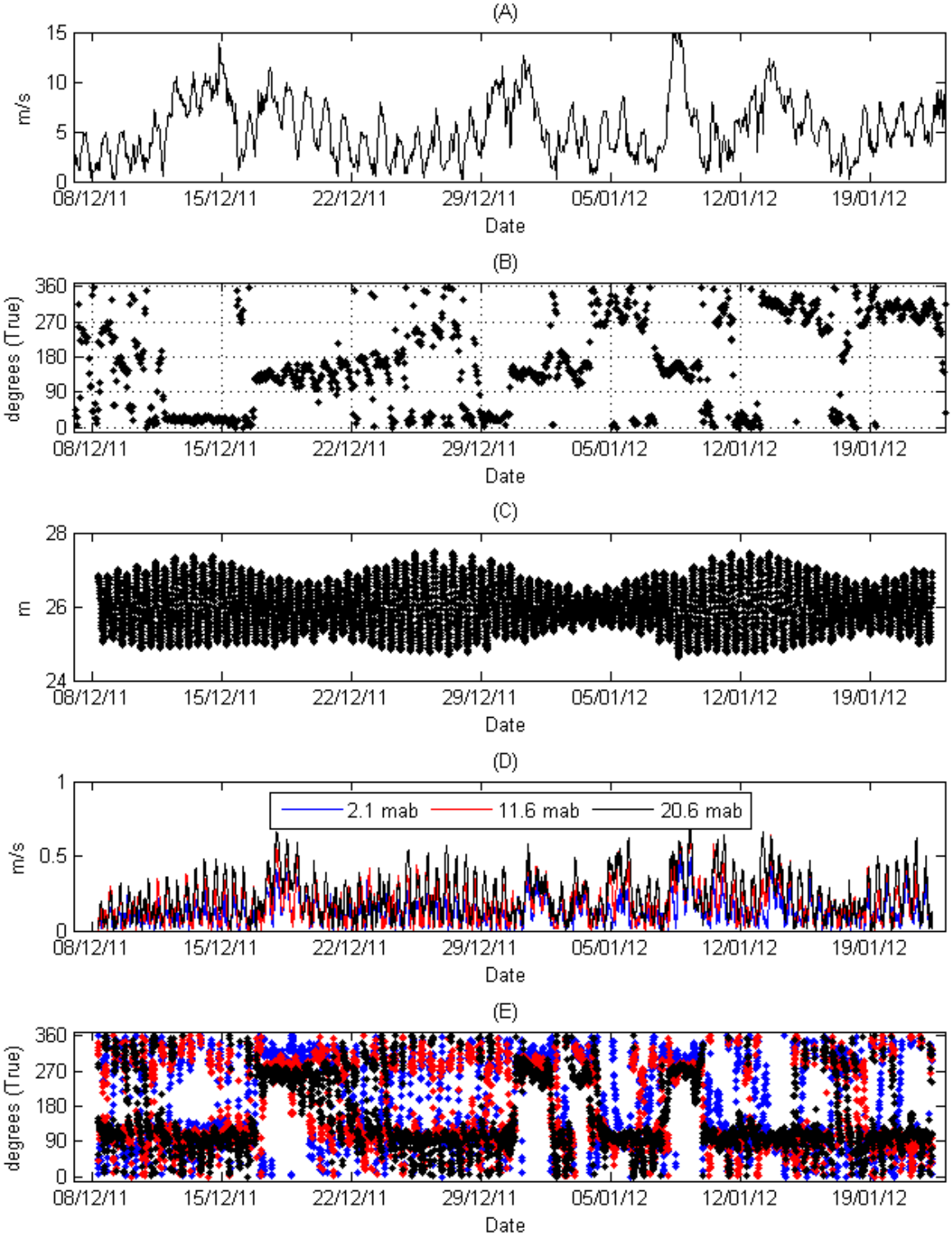

Figure 3-9: Current and wind time series for deployment S5/D2. Panels: (A) wind speed, (B) wind direction (in meteorological convention "blowing from"), (C) water depth, (D) current speed at three elevations above the bed, and (E) current direction (in oceanographic convention "flowing to").

For deployment S5/D2, Figure 3-9D shows that currents were typically less than 0.5 m/s. Near the sea bed, the maximum recorded current speed of 0.55 m/s was measured on 13/01/2012 at 15:00. In the 12-hour period prior, wind speeds range between 4.7 and 12.4 m/s (mean 9.9 m/s) with direction from the NW. Higher in the water column, at 20.6 mab the maximum recorded current speed of 0.68 m/s was measured on 09/01/2011 at 07:15. In the 12-hour period prior, wind speeds range between 6.0 and 14.2 m/s (mean 9.7 m/s) with direction from the SE.

Scatter plots of the velocity data from the three elevations above the sea bed are shown in Figure 3-10. The results of the PCA are summarised in Table 3-5. Currents measured during the S5/D2 deployment had a principal orientation of ESE–WNW, which is the same as that for deployment S5/D1. As before, Figure 3-10 also shows that current speeds increased with elevation above the sea bed.

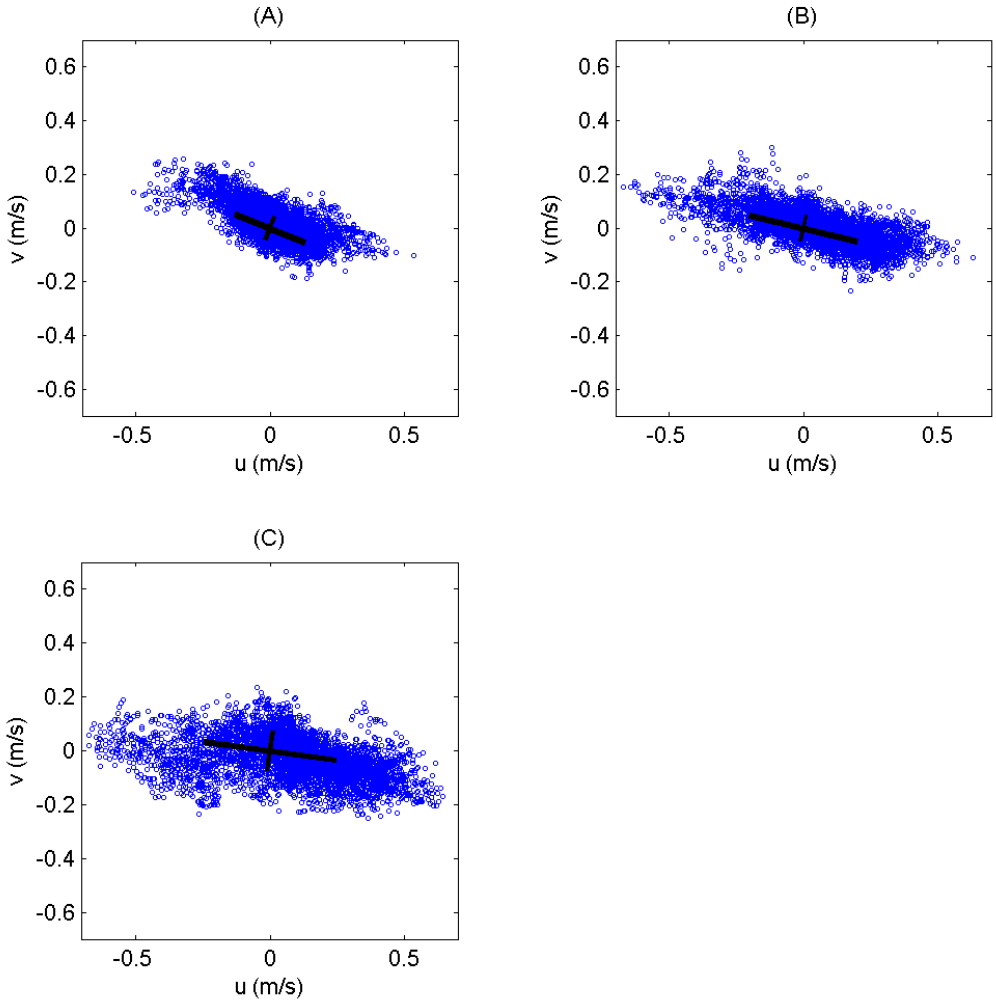

Figure 3-10: Scatter plots of currents at three elevations above the bed from deployment S5/D2: Panels: (A) data from 2.1 mab, (B) data from 11.6 mab, and (C) data from 20.6 mab. Note: the *u* and *v* velocity components relate to the east–west and north–south directions, respectively. The thick line is the major axis and the thin line is the minor axis (both lines span ± standard deviation).

Bin No.	Depth (mab)	Major axis orientation (˚True North)	Minor axis orientation (˚True North)	Major axis std dev. (m/s)	Minor axis std dev. (m/s)
1	2.1	112	22	±0.141	±0.045
20	11.6	104	14	±0.205	±0.049
38	20.6	98	8	±0.247	±0.07

Table 3-5: Summary of principal component analysis for currents during deployment S5/D2.

Based on tidal analysis of the near-bed currents (2.1 mab) over the ~45-day record for the S5/D2 deployment (Appendix B and Figure 3-11), the fitted constituents explain 40% of the total variability in the current velocities (43% and 27% in the *u* and *v* directions, respectively). The amplitude (maximum speed) of the main twice-daily lunar (M2) or average tide is 0.12 m/s and is oriented in the SE–NW direction. As with deployment S5/D1, the largest residuals were associated with winds from the W and the SE. Again, winds from the W were associated with a large positive residual in the *u* component, while winds from the SE were associated with a large negative residual in the *u* component.

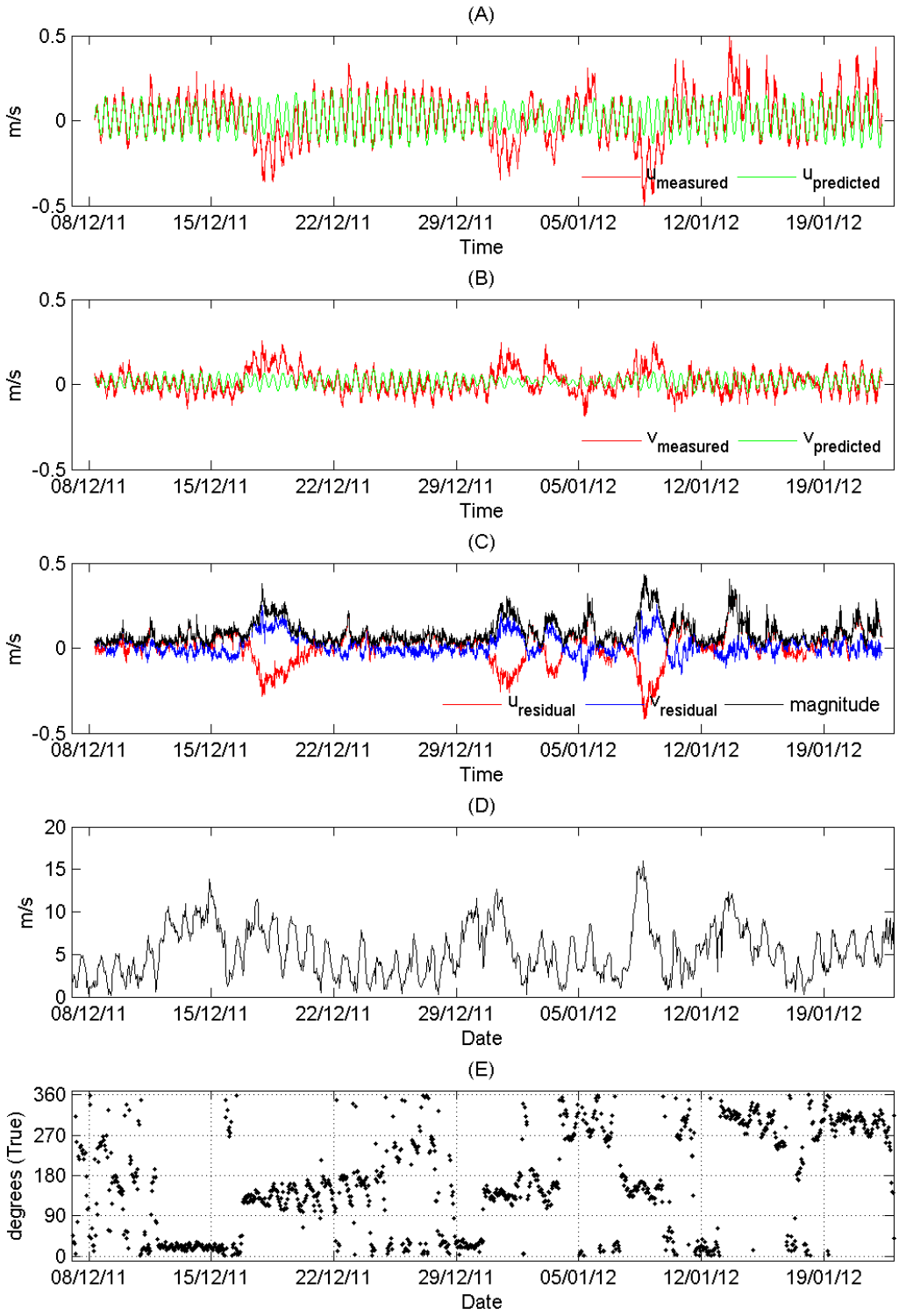

Figure 3-11: Tidal analysis of near-bed currents at S5/D2. Panels: (A) *u* velocity component, (B) *v* velocity component, (C) residual currents, (D) wind speed, and (E) wind direction (in meteorological convention "blowing from").

Figure 3-12 shows the PVD for deployment S5/D2 at three elevations above the bed. For this deployment, the three elevations have quite different net drift directions, which indicate a complicated water-column structure, with different current directions at different depths. The sawtooth patterns in the tracks are due to the passage through the region of weather systems. The period of SE winds that occurred between 17/12/11 and 22/12/11 (Figure 3-11) resulted in a NW drift near the sea bed, while closer to the surface the drift direction was towards the WSW. After this event, during a period of light winds (22/12/11 to 31/12/11), the drift direction was back towards the SE. Following this period of light winds, another SE weather system produced drift directions similar to that encountered during the previous SE event. The drift patterns associated with periods of calm and stormy conditions are consistent throughout the record. The net drift speeds and directions are listed in Table 3-6.

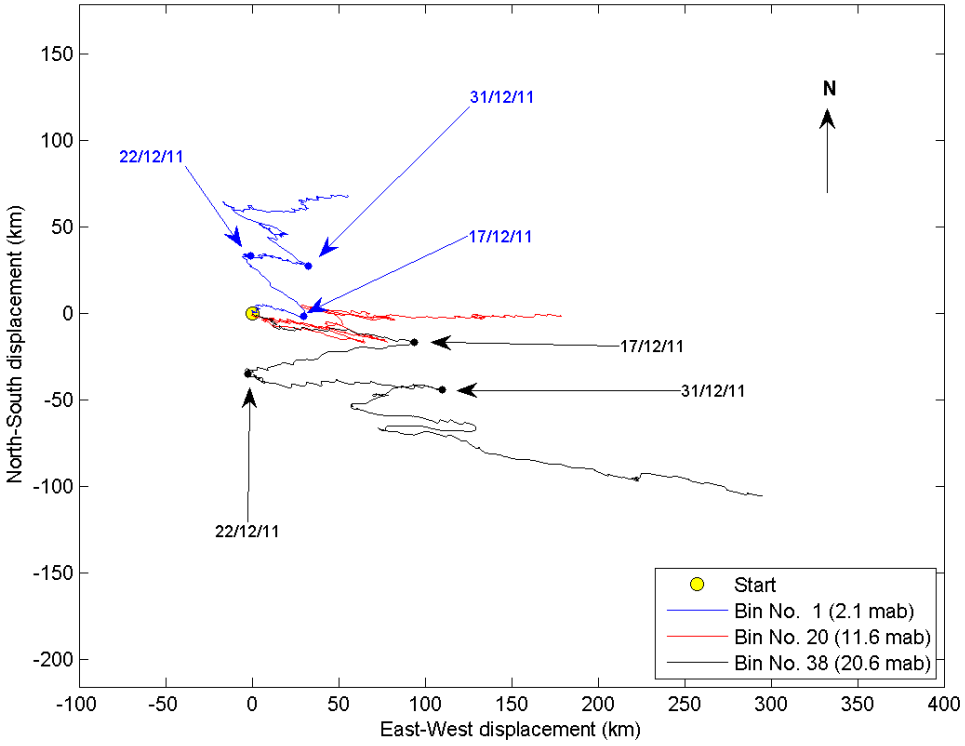

Figure 3-12: Progressive current drift at three elevations above the sea bed for deployment S5/D2 starting 08/12/2011 07:45 (yellow dot) through to 22/01/2012 08:00 (~45 days).

Bin No.	Depth (mab)	Net drift speed(m/s)	Net drift speed(km/day)	Mean drift direction (˚ True North)
1	2.1	0.023	1.94	39
20	11.6	0.046	3.96	90
38	20.6	0.080	6.94	110

Table 3-6: Summary of the overall current drift during deployment S5/D2 (~45 days).

3.3.2 Site 6 (inshore of the PPL)

Two separate ADCP deployments were carried out at site 6 (S6), the details of the location and deployment periods are listed in Table 3-2 and Table A-1 (Appendix A).

Deployment S6/D1

Time-series plots for S6 deployment 1 (D1) are shown in Figure 3-13.

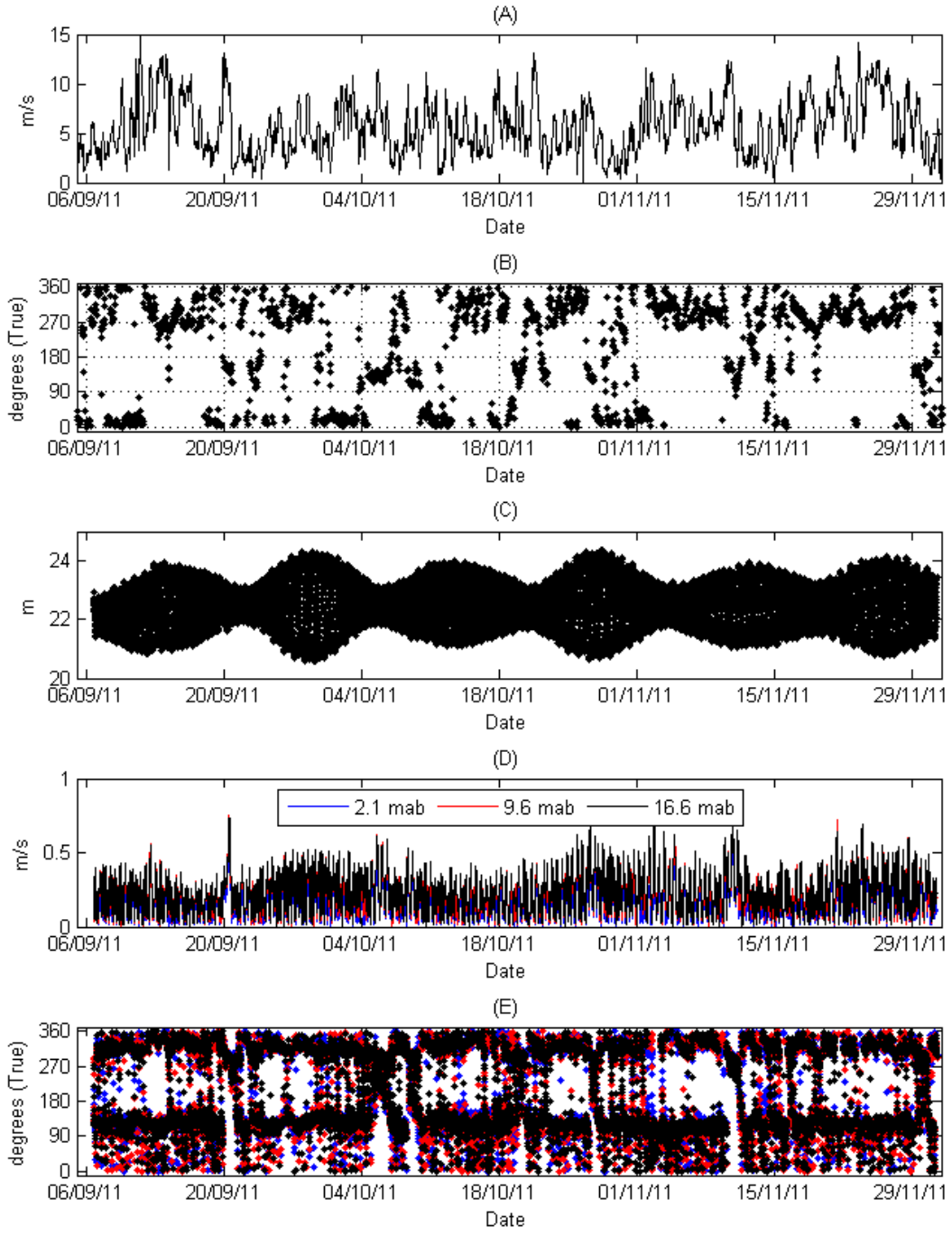

Figure 3-13: Current and wind time series for deployment S6/D1. Panels: (A) wind speed, (B) wind direction (in meteorological convention "blowing from"), (C) water depth, (D) current speed at three elevations above the bed, and (E) current direction (in oceanographic convention "flowing to").

For deployment S6/D1, Figure 3-13D shows that currents were typically less than 0.5 m/s. Near the sea bed, the maximum recorded current speed of 0.65 m/s was measured on 10/11/2011 at 17:15. In the 12-hour period prior, wind speeds ranged between 10.0 and 12.3 m/s (mean 11.2 m/s) with direction from the SE. Higher in the water column, at 16.6 mab, the maximum recorded current speed of 0.73 m/s was measured on 10/11/2011 at 17:00 (roughly the same time as the maximum near-bed current). In the 12-hour period prior, wind speeds ranged between 10.0 and 12.3 m/s (mean 11.2 m/s) blowing from the SE.

Scatter plots of the velocity data from the three elevations above the sea bed are shown in Figure 3-14. The results of the PCA are summarised in Table 3-7. Currents measured during the S6/D1 deployment had a principal orientation of SE–NW, but are directed slightly more towards the S than those measured at the inshore coastal site 5. As expected, Figure 3-14 also shows that current speeds increased with elevation above the sea bed.

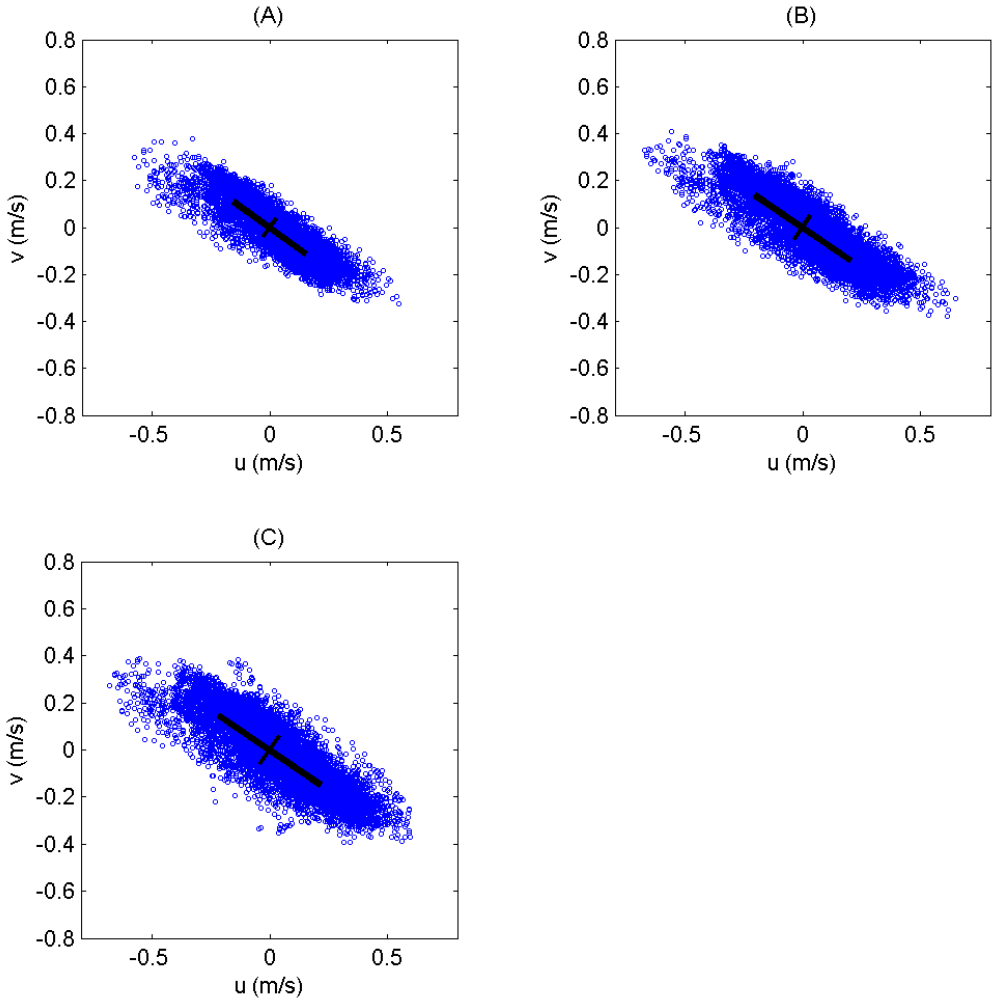

Figure 3-14: Scatter plots of currents at three elevations above the bed from deployment S6/D1. Panels: (A) data from 2.1 mab, (B) data from 9.6 mab, and (C) data from 16.6 mab. Note: the *u* and *v* velocity components relate to the east–west and north–south directions, respectively. The thick line is the major axis and the thin line is the minor axis (both lines span ± standard deviation).

Bin No.	Depth (mab)	Major axis orientation (˚True North)	Minor axis orientation (˚True North)	Major axis std dev. (m/s)	Minor axis std dev. (m/s)
1	2.1	126	36	±0.190	±0.040
16	9.6	124	34	±0.240	±0.060
30	16.6	124	34	±0.262	±0.071

Table 3-7: Summary of principal component analysis for currents during deployment S6/D1.

Based on tidal analysis of the near-bed currents (2.1 mab) over the ~86-day record for the S6/D1 deployment (Appendix B and Figure 3-15), the fitted tidal constituents explain 73% of the total variability in the current velocities (66% and 87% in the *u* and *v* directions, respectively). In comparison with site 5, the tides at site 6 account for substantially more of the energy (variance) exhibited by the measured currents. The amplitude (maximum speed) of the main twice-daily lunar (M2) tide is 0.22 m/s and is oriented in the SE–NW direction. As at site 5, the largest residuals were associated with winds from the W and the SE.

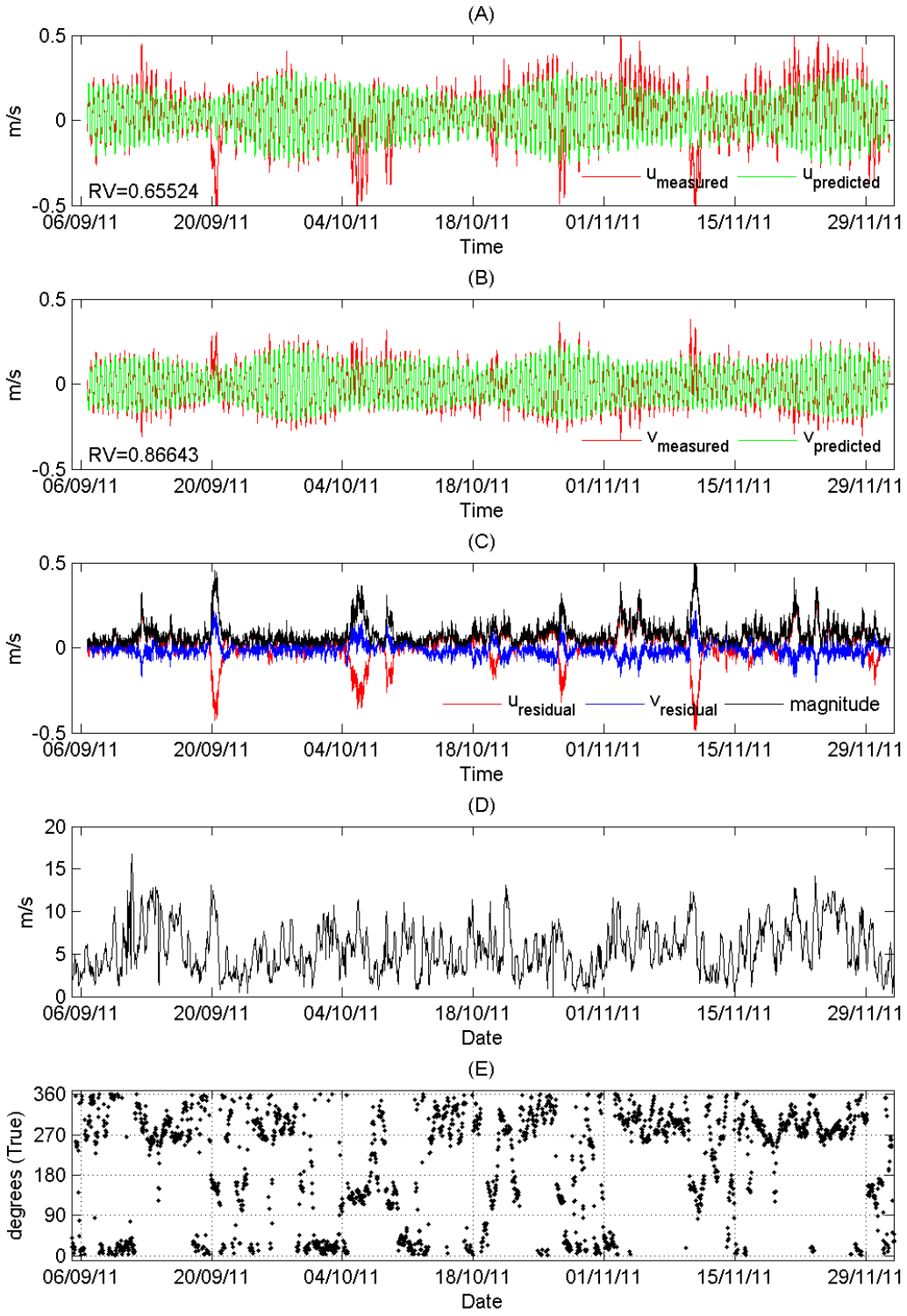

Figure 3-15: Tidal analysis of near-bed currents at S6/D1. Panels: (A) *u* velocity component, (B) *v* velocity component, (C) residual currents, (D) wind speed, and (E) wind direction (in meteorological convention "blowing from").

Figure 3-16 shows the PVD for deployment S6/D1 at three elevations above the bed. At all three elevations, aside from the occasional circular meanders, there was a consistent drift in the E–ESE direction. Reflecting the increase in current velocities with distance above the bed, drift distances also increased with elevation above the bed. The finer saw-tooth pattern reflects the regular tidal-cycle pattern. The net drift speeds and directions are listed in Table 3-8.

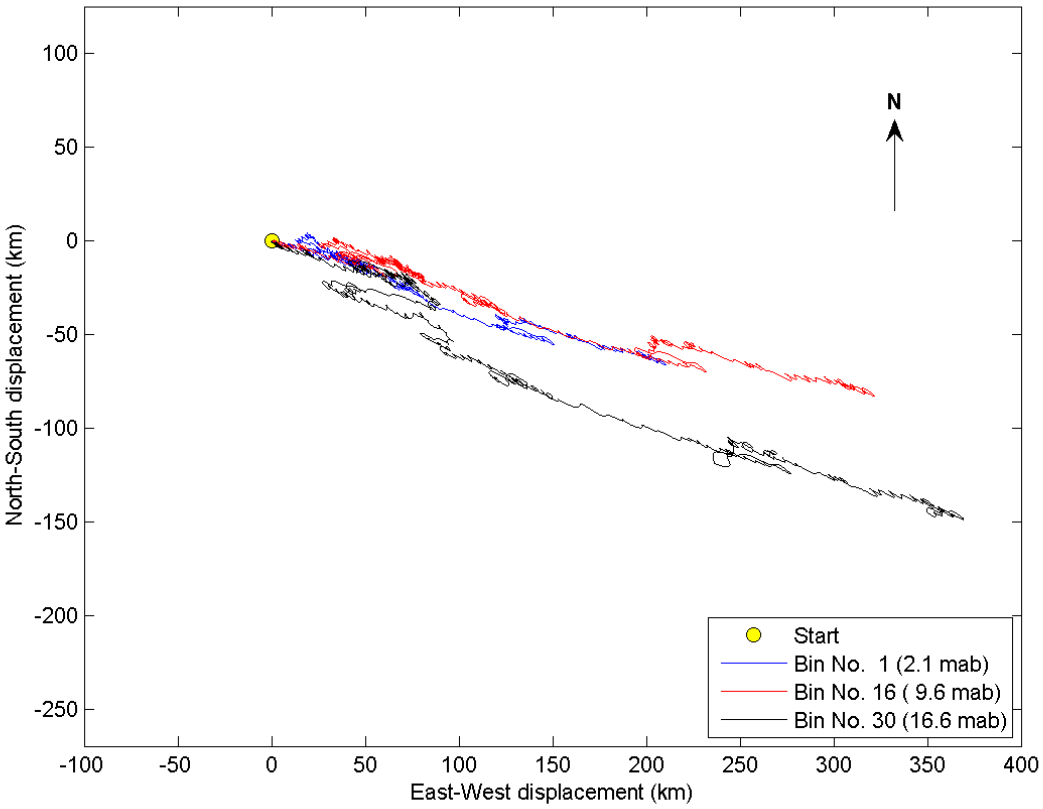

Figure 3-16: Progressive current drift at three elevations above the sea bed for deployment S6/D1 starting 06/09/2011 16:30 (yellow dot) through to 01/12/2011 13:15 (~86 days).

Bin No.	Depth (mab)	Net drift speed(m/s)	Net drift speed(km/day)	Mean drift direction (˚ True North)
1	2.1	0.028	2.44	107
16	9.6	0.043	3.70	104
30	16.6	0.052	4.46	112

Table 3-8: Summary of the overall current drift during deployment S6/D1 (~86 days).

Deployment S6/D2

Time-series plots for S6 deployment 2 (D2) are shown in Figure 3-17.

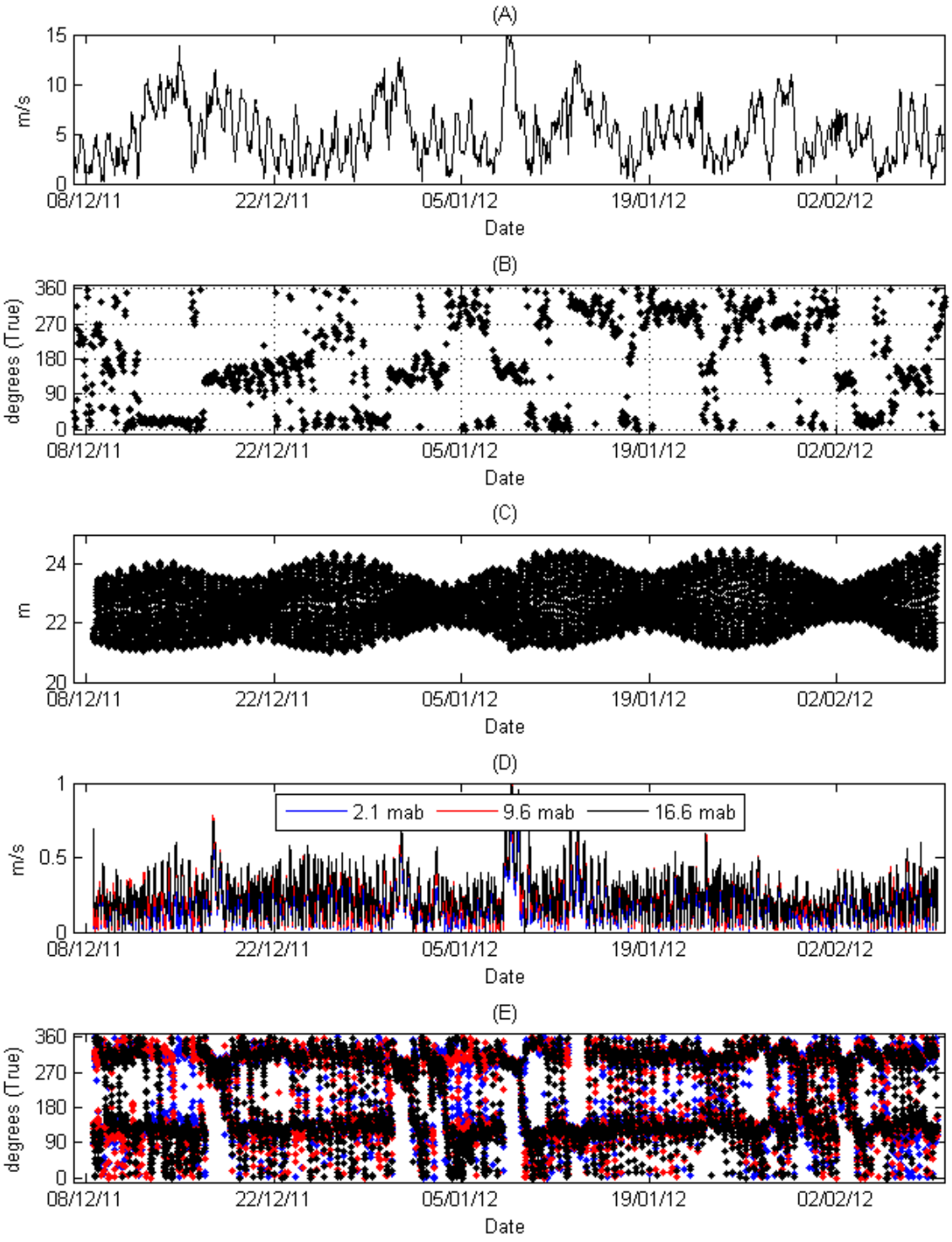

Figure 3-17: Current and wind time series for deployment S6/D2. Panels: (A) wind speed, (B) wind direction (in meteorological convention "blowing from"), (C) water depth, (D) current speed at three elevations above the bed, and (E) current direction (in oceanographic convention "flowing to").

For deployment S6/D2, Figure 3-17D shows that currents were typically less than 0.5 m/s. Near the sea bed, the maximum recorded current speed of 0.93 m/s was measured on 08/01/2012 at 17:45. In the 12-hour period prior, wind speeds ranged between 11.0 and 16 m/s (mean 14.2 m/s) with direction from the SE. Higher in the water column, at 16.6 mab, the maximum recorded current speed of 0.98 m/s was measured on 08/01/2012 at 16:30 (roughly the same time as the maximum near-bed current). In the 12-hour period prior, wind speeds ranged between 11.0 and 16 m/s (mean 14.2 m/s) with a direction from the SE.

Scatter plots of the velocity data from the three elevations above the sea bed are shown in Figure 3-18. The results of the PCA are summarised in Table 3-9. Currents measured during the S6/D2 deployment had a principal orientation of SE–NW, which is the same as deployment S6/D1. As expected, Figure 3-18 also shows that current speeds increased with elevation above the sea bed.

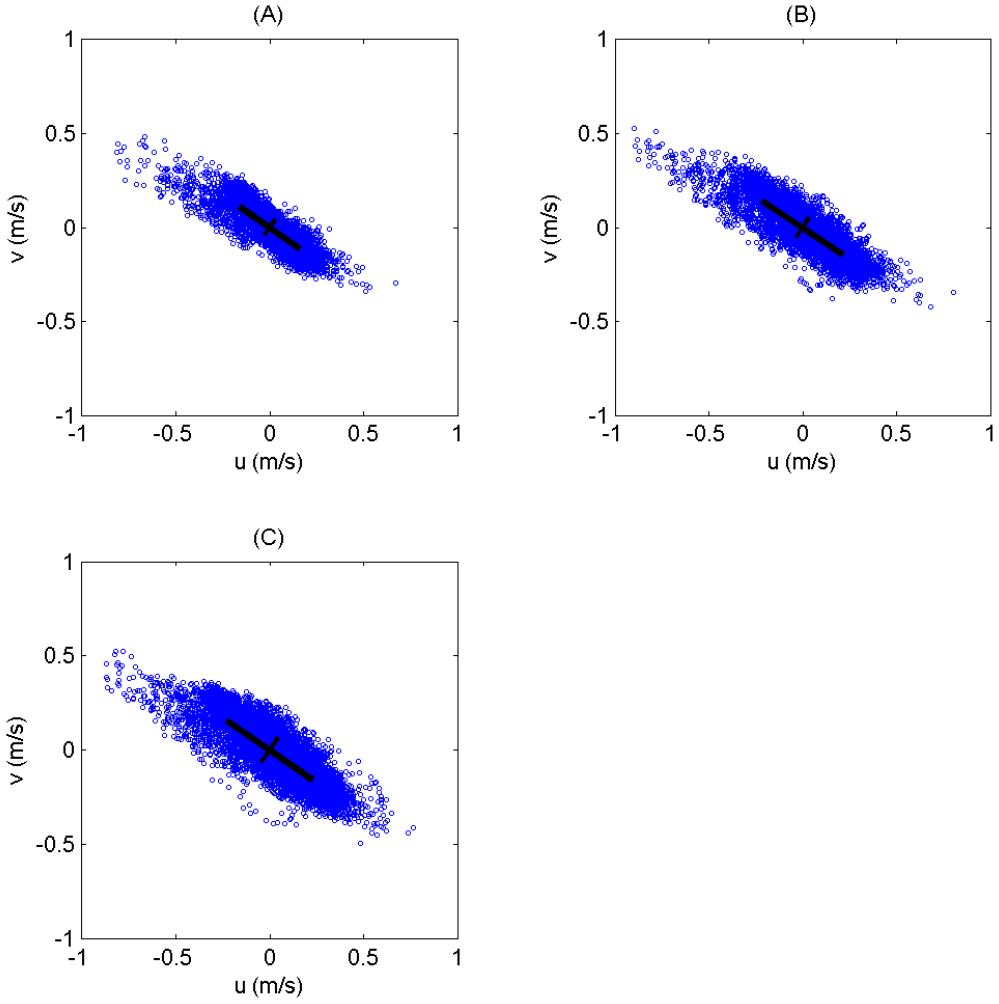

Figure 3-18: Scatter plots of currents at three elevations above the bed from deployment S6/D2. Panels: (A) data from 2.1 mab, (B) data from 9.6 mab, and (C) data from 16.6 mab. Note: the *u* and *v* velocity components relate to the east–west and north–south directions, respectively. The thick line is the major axis and the thin line is the minor axis (both lines span ± standard deviation).

Bin No.	Depth (mab)	Major axis orientation (˚True North)	Minor axis orientation (˚True North)	Major axis std dev. (m/s)	Minor axis std dev. (m/s)
1	2.1	125	35	±0.194	±0.049
16	9.6	124	34	±0.256	±0.063
30	16.6	125	35	±0.274	±0.080

Table 3-9: Summary of principal component analysis for currents during deployment S6/D2.

Based on tidal analysis of the near-bed currents (2.1 mab) over the ~63-day record for the S6/D2 deployment (Appendix B and Figure 3-19), the fitted constituents explain 63% of the total variability in the current velocities (54% and 79% in the *u* and *v* directions, respectively). The amplitude (maximum speed) of the main twice-daily lunar (M2) tide is 0.21 m/s and is oriented in the SE–NW direction. The largest residuals were again associated with winds from the W and the SE.

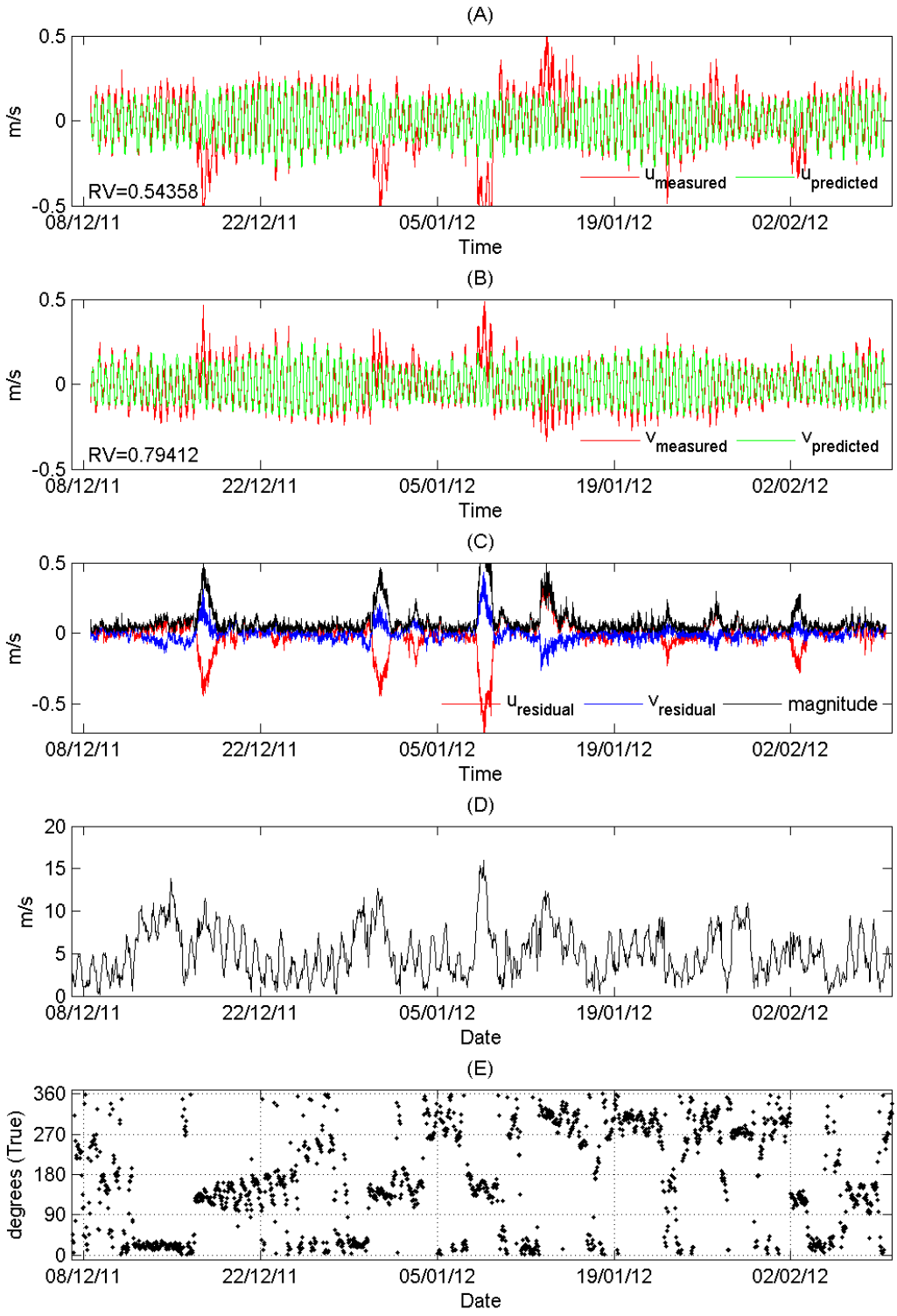

Figure 3-19:Tidal analysis of near-bed currents at S6/D2. (Panels: (A) *u* velocity component, (B) *v* velocity component, (C) residual currents, (D) wind speed, and (E) wind direction (in meteorological convention "blowing from").

Figure 3-20 shows the PVD for deployment S6/D2 at three elevations above the bed. The drift tracks underwent a series of to-and-fro movements in a SE–NW direction, which were driven by strong alternating SE and NW winds. The period of SE winds that occurred between 07/01/12 and 10/01/12 (see Figure 3-19) resulted in a NW drift throughout the water column. In contrast to the SE winds, the winds from the NW that occurred between 12/01/12 and 16/01/12 (see Figure 3-19) resulted in a SE drift throughout the water column. The drift distances associated with these weather systems are significant and therefore have implications for the transport of suspended sediments in the STB (compared with the much smaller net tidal drift). The net drift speeds and directions are listed in Table 3-10.

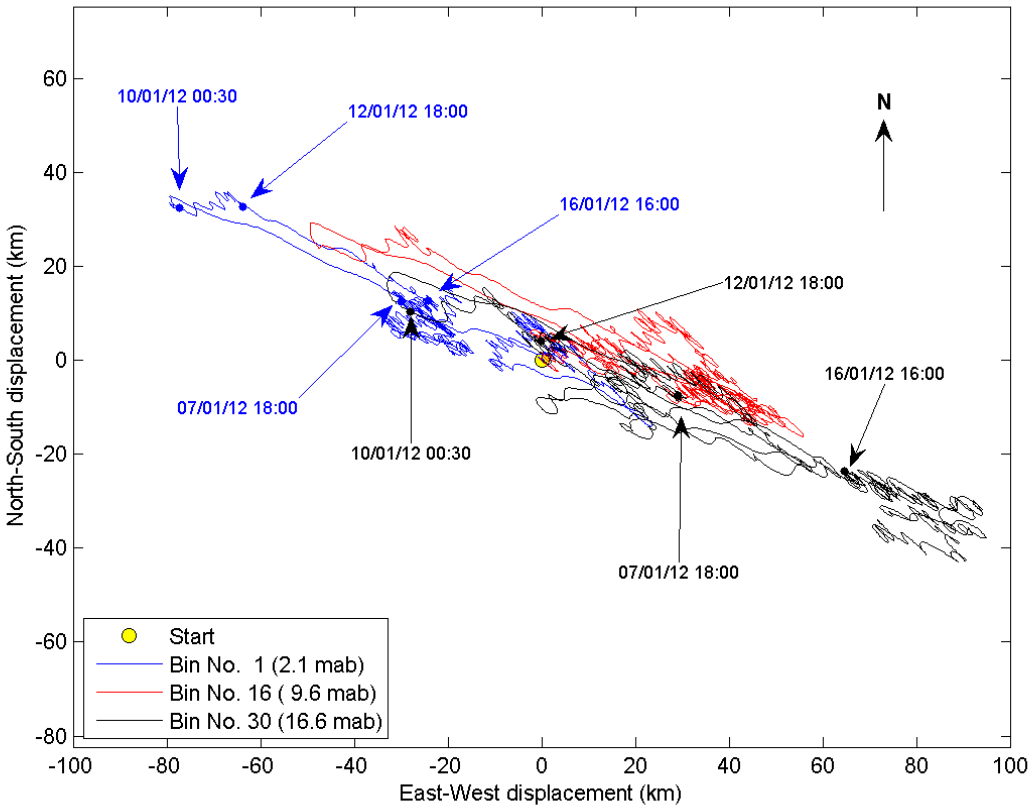

Figure 3-20:Progressive current drift at three elevations above the sea bed for deployment S6/D2 starting 08/12/2011 12:30 (yellow dot) through to 09/02/2012 12:15 (~63 days).

Bin No.	Depth (mab)	Net drift speed (m/s)	Net drift speed (km/day)	Mean drift direction (˚True North)
1	2.1	0.004	0.38	308
16	9.6	0.006	0.55	92
30	16.6	0.015	1.28	116

Table 3-10: Summary of the overall current drift during deployment S6/D2 (~63 days).

3.3.3 Site 7 (inshore end of the PPL)

Two separate ADCP deployments were carried out at site 7 (S7), the details of the location and deployment periods are listed in Table 3-2 and Table A-1 (Appendix A).

Deployment S7/D1

Time-series plots for S7 deployment 1 (D1) are shown in Figure 3-21.

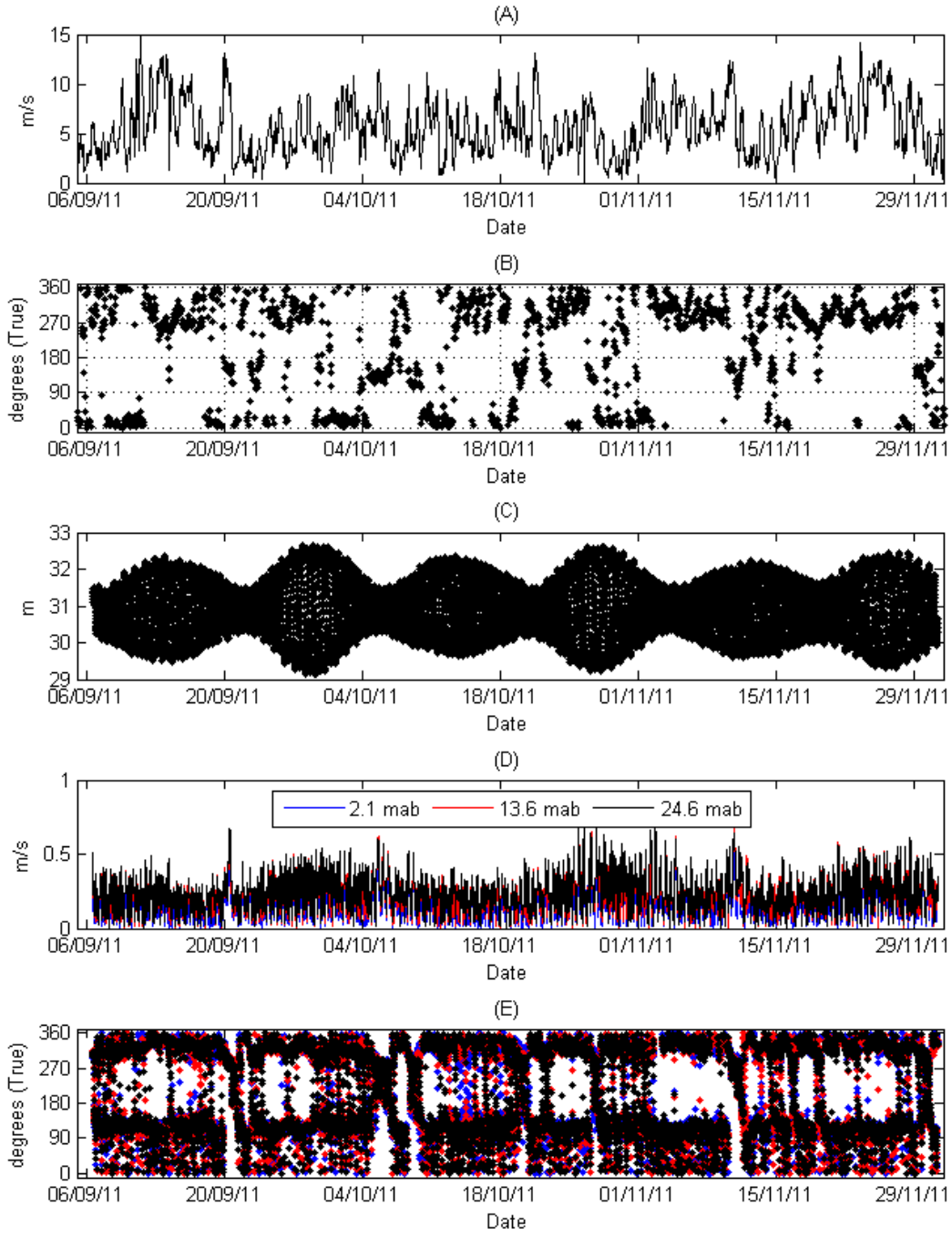

Figure 3-21:Current and wind time series for deployment S7/D1. Panels: (A) wind speed, (B) wind direction (in meteorological convention "blowing from"), (C) water depth, (D) current speed at three elevations above the bed, and (E) current direction (in oceanographic convention "flowing to").

For deployment S7/D1, Figure 3-21D shows that currents were typically less than 0.5 m/s. Near the sea bed, the maximum recorded current speed of 0.60 m/s was measured on 10/11/2011 at 19:00. In the 12-hour period prior, wind speeds ranged between 10.0 and 12.2 m/s (mean 10.9 m/s) with direction from the SE. Higher in the water column, at 24.6 mab, the maximum recorded current speed of 0.75 m/s was measured on 02/11/2011 at 17:45. In the 12-hour period prior, wind speeds ranged between 4.4 and 11.2 m/s (mean 9.3 m/s) blowing from the N.

Scatter plots of the velocity data from the three elevations above the sea bed are shown in Figure 3-22. The results of the PCA are summarised in Table 3-11. Currents measured during the S7/D1 deployment had a principal orientation of SE–NW. As expected, Figure 3-22 also shows that current speeds increased with elevation above the sea bed.

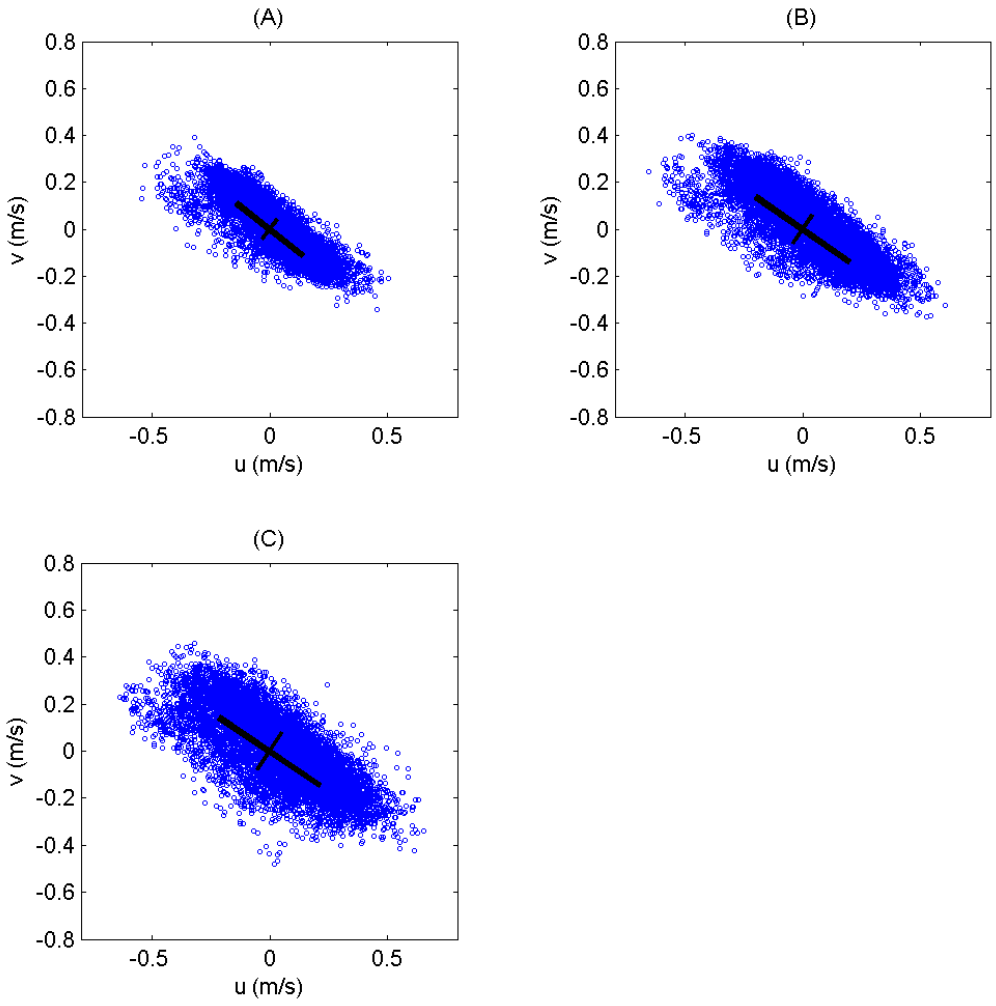

Figure 3-22: Scatter plots of currents at three elevations above the bed from deployment S7/D1.
Panels: (A) data from 2.1 mab, (B) data from 13.6 mab, and (C) data from 24.6 mab. Note: the *u* and *v* velocity components relate to the east–west and north–south directions, respectively. The thick line is the major axis and the thin line is the minor axis (both lines span ± standard deviation).

Bin No.	Depth (mab)	Major axis orientation (˚True North)	Minor axis orientation (˚True North)	Major axis std dev. (m/s)	Minor axis std dev. (m/s)
1	2.1	128	38	±0.181	±0.052
24	13.6	124	34	±0.243	±0.073
46	24.6	124	34	±0.259	±0.094

Table 3-11: Summary of principal component analysis for currents during deployment S7/D1.

Based on tidal analysis of the near-bed currents (2.1 mab) over the ~86-day record for the S7/D1 deployment (Appendix B and Figure 3-23), the fitted constituents explain 78% of the total variability in the current velocities (72% and 88% in the *u* and *v* directions, respectively). The amplitude (maximum speed) of the main twice-daily lunar (M2) or average tide is 0.22 m/s and is oriented in the SE–NW direction. The largest residuals were again associated with winds from the W and the SE.

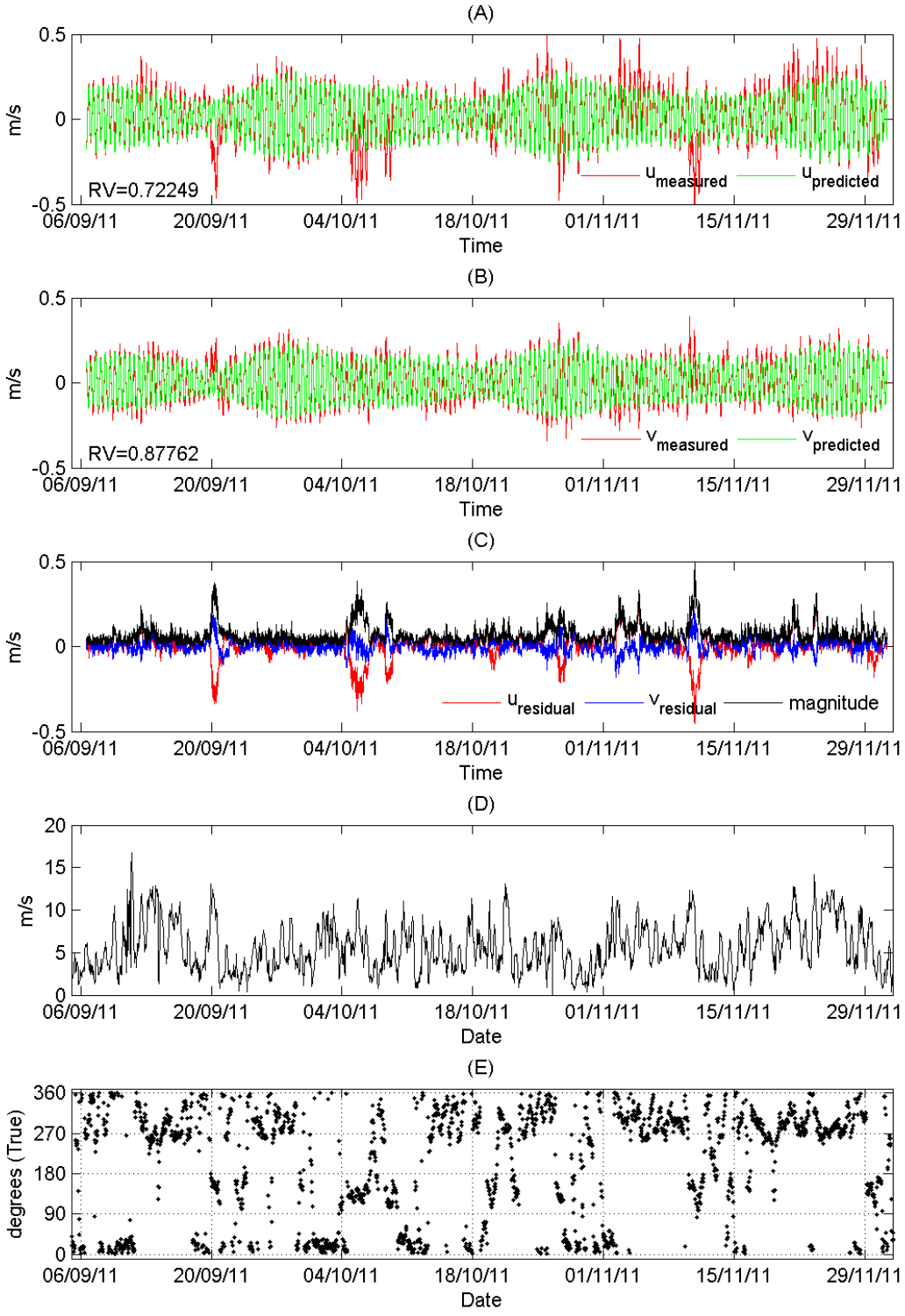

Figure 3-23: Tidal analysis of near-bed currents at S7/D1. Panels: (A) *u* velocity component, (B) *v* velocity component, (C) residual currents, (D) wind speed, and (E) wind direction (in meteorological convention "blowing from").

Figure 3-24 shows the PVD for deployment S7/D1 at three elevations above the bed. At all three elevations there was an overall drift onshore towards ENE. The period of SE winds that occurred between 09/11/11 and 12/11/12 (see Figure 3-23) resulted in a pronounced drift towards the NW. During light winds, such as the conditions experienced towards the end of the deployment (see Figure 3-23), the drift direction at all heights was towards the NE. The net drift speeds and directions are listed in Table 3-12.

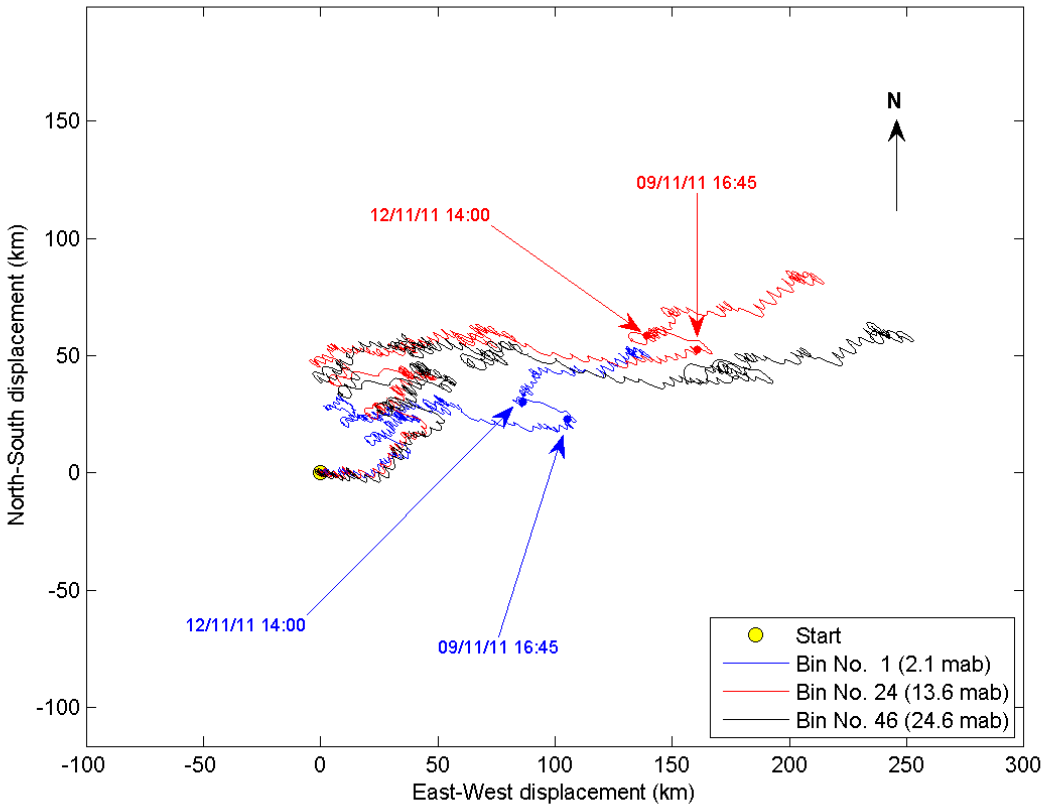

Figure 3-24: Progressive current drift at three elevations above the sea bed for deployment S7/D1 starting 06/09/2011 14:15 (yellow dot) through to 01/12/2011 10:15 (~86 days).

Bin No.	Depth (mab)	Net drift speed (m/s)	Net drift speed (km/day)	Mean drift direction (˚True North)
1	2.1	0.019	1.68	69
24	13.6	0.030	2.61	68
46	24.6	0.034	2.90	76

Table 3-12: Summary of the overall current drift during deployment S7/D1 (~86 days)

Deployment S7/D2

Time-series plots for S7 deployment 2 (D2) are shown in Figure 3-25.

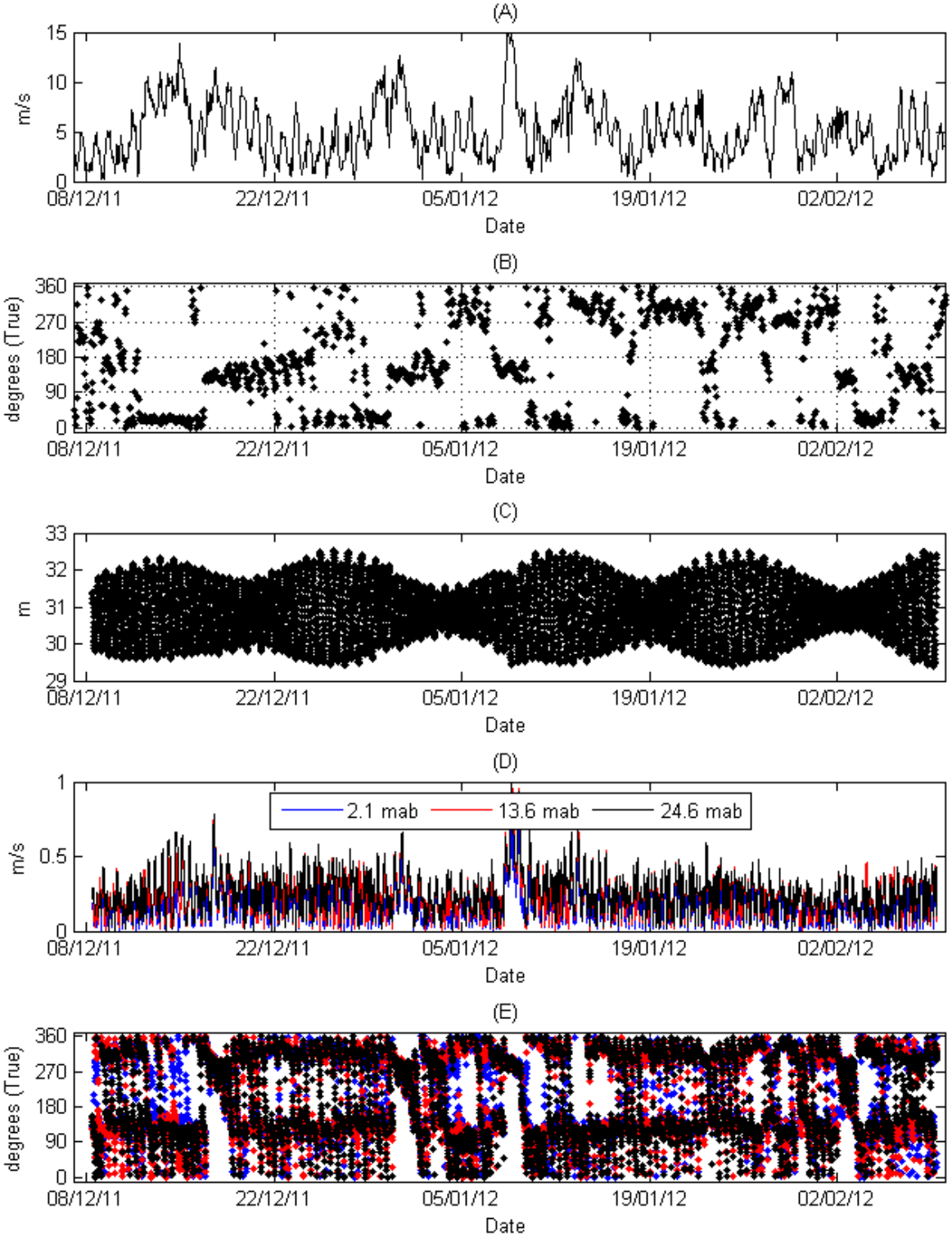

Figure 3-25:Current and wind time series for deployment S7/D2. Panels: (A) wind speed, (B) wind direction (in meteorological convention "blowing from"), (C) water depth, (D) current speed at three elevations above the bed, and (E) current direction (in oceanographic convention "flowing to").

For deployment S7/D2, Figure 3-25D shows that currents were typically less than 0.5 m/s. Near the sea bed, the maximum recorded current speed of 0.87 m/s was measured on 08/01/2012 at 16:15. In the 12-hour period prior, wind speeds ranged between 10.1 and 16.0 m/s (mean 13.6 m/s) with direction from the SE. Higher in the water column, at 24.6 mab, the maximum recorded current speed of 1.0 m/s was measured on 08/01/2012 at 17:15 (roughly the same time as the maximum near-bed current). In the 12-hour period prior, wind speeds ranged between 10.6 and 16.0 m/s (mean 14.0 m/s) blowing from a SE direction.

Scatter plots of the velocity data from the three elevations above the sea bed are shown in Figure 3-26. The results of the PCA are summarised in Table 3-13. Currents measured during the S7/D2 deployment had a principal orientation of SE–NW. As expected, Figure 3-26 also shows that current speeds increased with elevation above the sea bed.

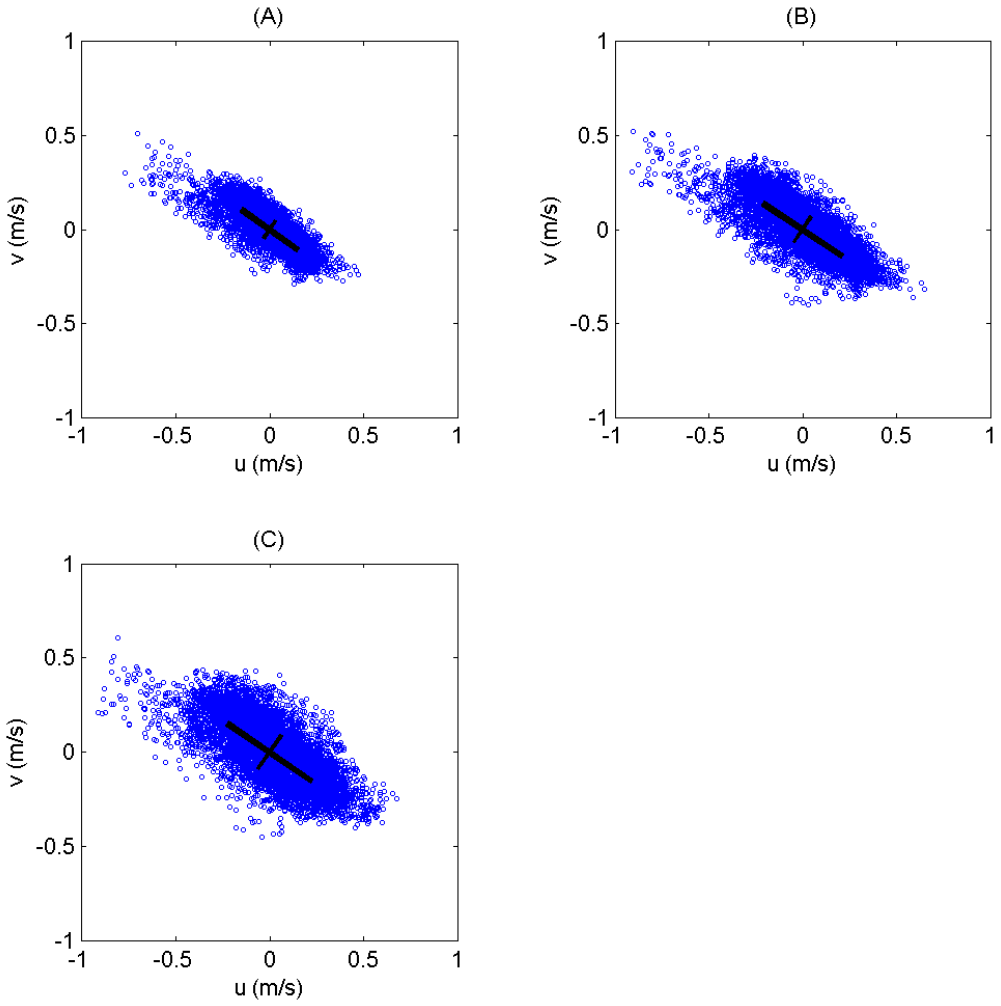

Figure 3-26: Scatter plots of currents at three elevations above the bed from deployment S7/D2.
Panels: (A) data from 2.1 mab, (B) data from 13.6 mab, and (C) data from 24.6 mab. Note: the *u* and *v* velocity components relate to the east–west and north–south directions, respectively. The thick line is the major axis and the thin line is the minor axis (both lines span ± standard deviation).

Bin No.	Depth (mab)	Major axis orientation (˚True North)	Minor axis orientation (˚True North)	Major axis std dev. (m/s)	Minor axis std dev. (m/s)
1	2.1	125	35	±0.184	±0.055
24	13.6	124	34	±0.253	±0.080
46	24.6	125	35	±0.271	±0.108

Table 3-13: Summary of principal component analysis for currents during deployment S7/D2.

Based on tidal analysis of the near-bed currents (2.1 mab) over the ~63-day record for the S7/D2 deployment (Appendix B and Figure 3-27), the fitted tidal constituents explain 65% of the total variability in the current velocities (58% and 79% in the *u* and *v* directions, respectively). The amplitude of the main twice-daily lunar (M2) or average tide is 0.21 m/s and is oriented in the SE–NW direction. The largest residuals were again associated with winds from the W and the SE.

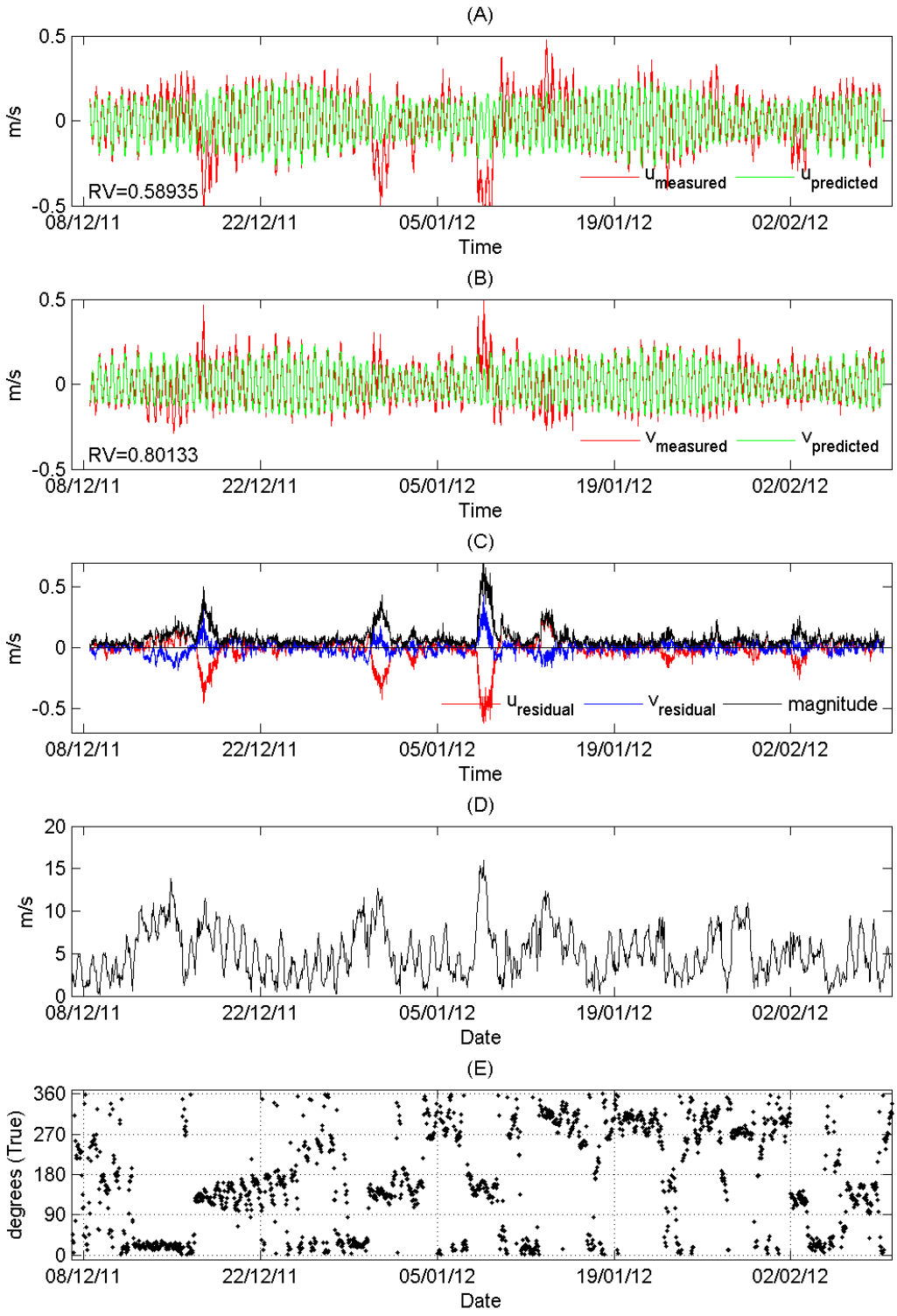

Figure 3-27: Tidal analysis of near-bed currents at S7/D2. Panels: (A) *u* velocity component, (B) *v* velocity component, (C) residual currents, (D) wind speed, and (E) wind direction (in meteorological convention "blowing from").

Figure 3-28 shows the PVD for deployment S7/D2 at three elevations above the bed. The drift tracks underwent a series of to-and-fro movements. As with S6/D2, this to-and-fro motion was associated with alternating strong SE and NW winds. The period of SE winds that occurred between 07/01/12 and 10/01/12 (see Figure 3-27) resulted in a NW drift throughout the water column. In contrast to the SE winds, a period of NW winds that occurred between 12/01/12 and 15/01/12 (see Figure 3-27) resulted in a SE drift throughout the water column. As with S7/D1, during periods of light winds there was a drift towards NE. The net drift speeds and directions are listed in Table 3-14.

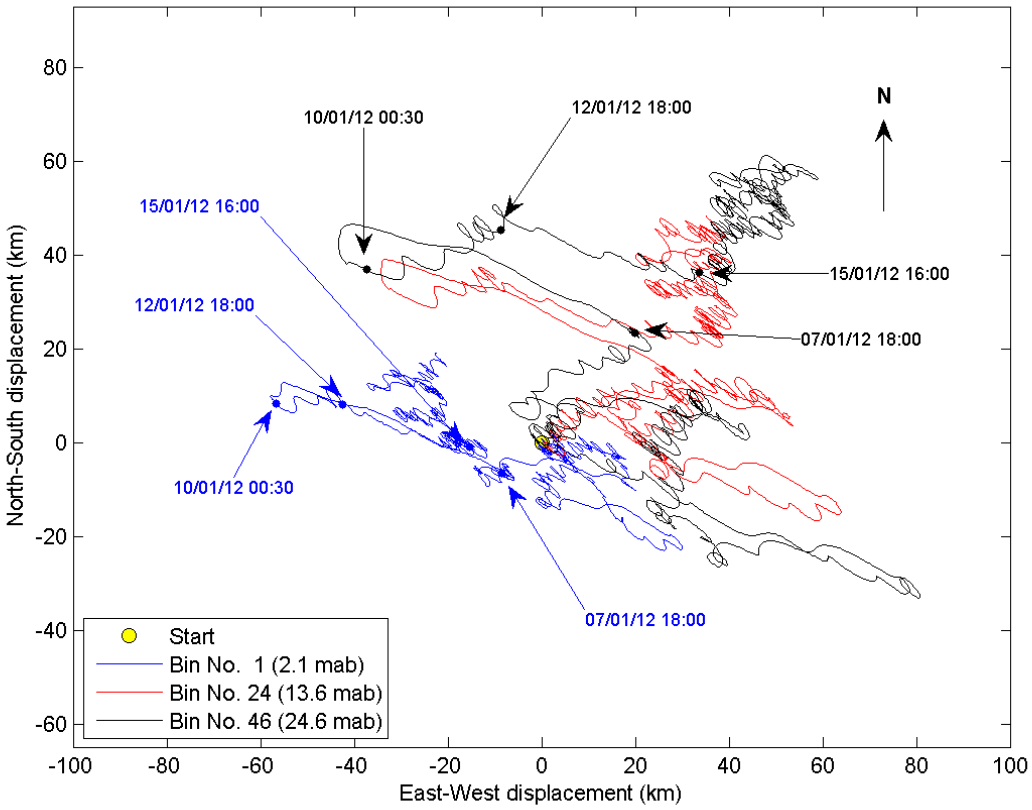

Figure 3-28: Progressive current drift at three elevations above the sea bed for deployment S7/D2 starting 08/12/2011 10:15 (yellow dot) through to 09/02/2012 10:00 (~63 days).

Bin No.	Depth (mab)	Net drift speed (m/s)	Net drift speed (km/day)	Mean drift direction (˚True North)
1	2.1	0.005	0.47	310
24	13.6	0.011	0.95	36
46	24.6	0.011	0.96	39

Table 3-14: Summary of the overall current drift during deployment S7/D2 (~63 days).

3.3.4 Site 8 (SSE of the PPL)

A single ADCP deployment was carried out at site 8 (S8) during Deployment 3. The details of the location and deployment period are listed in Table 3-2 and Table A-1 (Appendix A).

Time-series plots for S8 deployment (D3) are shown in Figure 3-29.

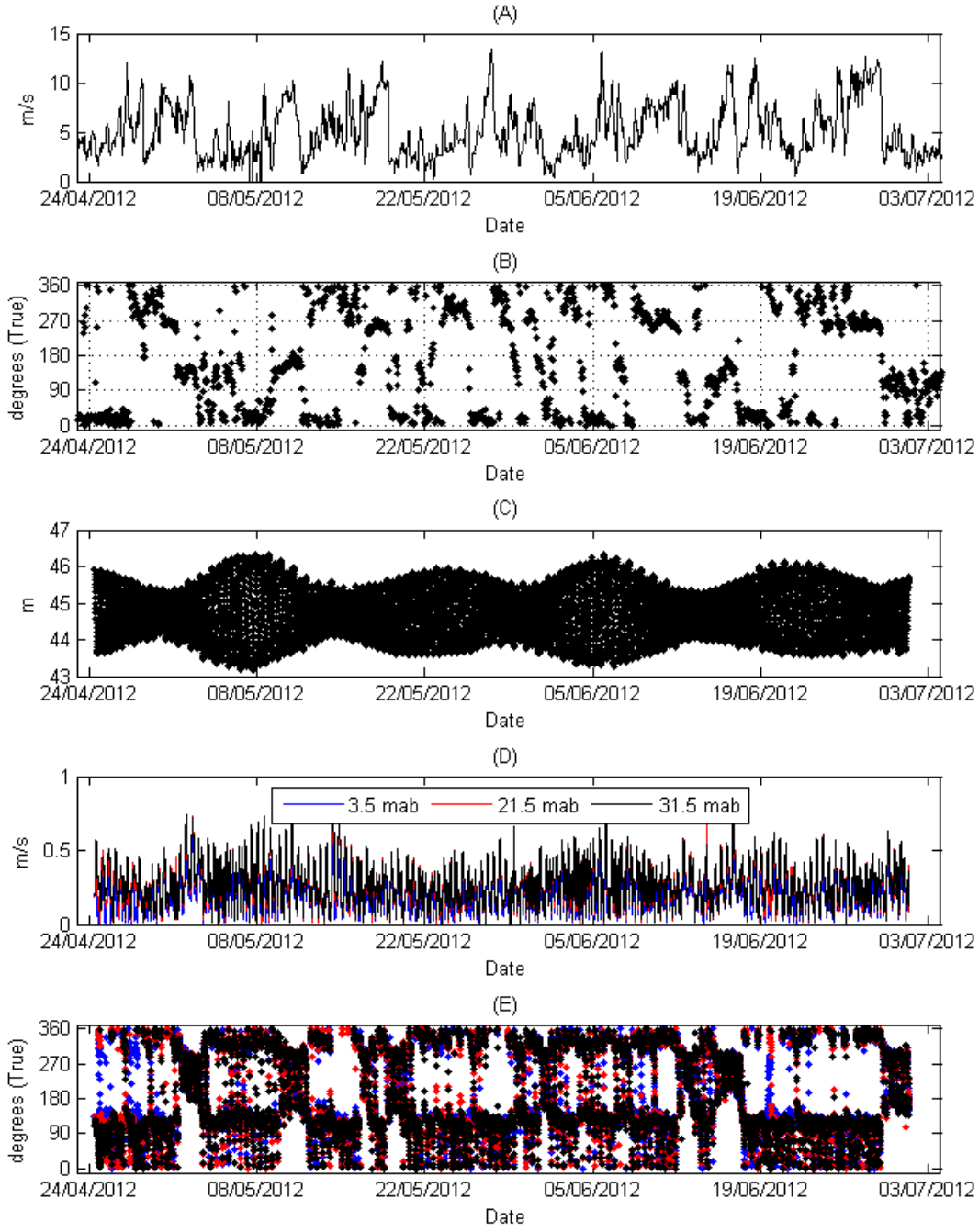

Figure 3-29: Current and wind time series for deployment S8/D3. Panels: (A) wind speed, (B) wind direction (in meteorological convention "blowing from"), (C) water depth, (D) current speed at three elevations above the bed, and (E) current direction (in oceanographic convention "flowing to").

For deployment S8/D3, Figure 3-29D shows that currents were typically less than 0.5 m/s. Near the sea bed, the maximum recorded current speed of 0.65 m/s was measured on 02/05/2012 at 03:00. In the 12-hour period prior, wind speeds ranged between 3.8 and 7.3 m/s (mean 6.2 m/s) with direction from the ESE. Higher in the water column, at 31.5 mab, the maximum recorded current speed of 0.78 m/s was measured on 10/05/2012 at 22:15. In the 12-hour period prior, wind speeds ranged between 8.1 and 9.6 m/s (mean 8.6 m/s) blowing from a SSE direction.

Scatter plots of the velocity data from the three elevations above the sea bed are shown in Figure 3-30. The results of the PCA are summarised in Table 3-15. Currents measured during the S8/D3 deployment had a principal orientation of SE–NW. As expected, Figure 3-30 also shows that current speeds increased with elevation above the sea bed.

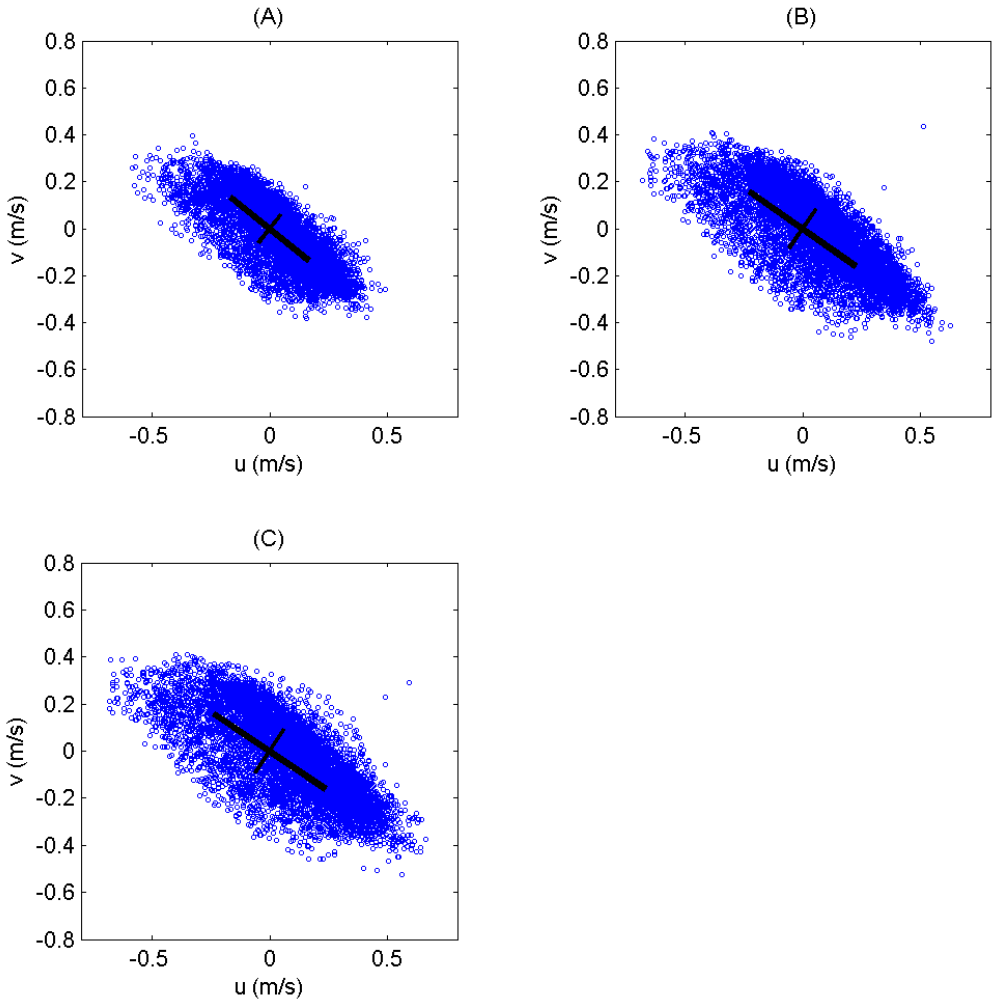

Figure 3-30: Scatter plots of currents at three elevations above the bed from deployment S8/D3. Panels: (A) data from 3.5 mab, (B) data from 21.5 mab, and (C) data from 31.5 mab. Note: the *u* and *v* velocity components relate to the east–west and north–south directions, respectively. The thick line is the major axis and the thin line is the minor axis (both lines span ± standard deviation).

Bin No.	Depth	Major axis orientation (˚True North)	Minor axis orientation (˚True North)	Major axis std dev. (m/s)	Minor axis std dev. (m/s)
1	3.5	129	39	±0.213	±0.077
10	21.5	125	35	±0.277	±0.100
15	31.5	124	34	±0.287	±0.109

Table 3-15: Summary of principal component analysis for currents during deployment S8/D3.

Based on tidal analysis of the near-bed currents (3.5 mab) over the ~68-day record for the S8/D3 deployment (Appendix B and Figure 3-31), the fitted constituents explain 70% of the total variability in the current velocities (57% and 87% in the *u* and *v* directions, respectively). The amplitude (maximum speed) of the main twice-daily lunar (M2) or average tide is 0.25 m/s and is oriented in the SE–NW direction. The largest residuals were again associated with winds from the W and the SE.

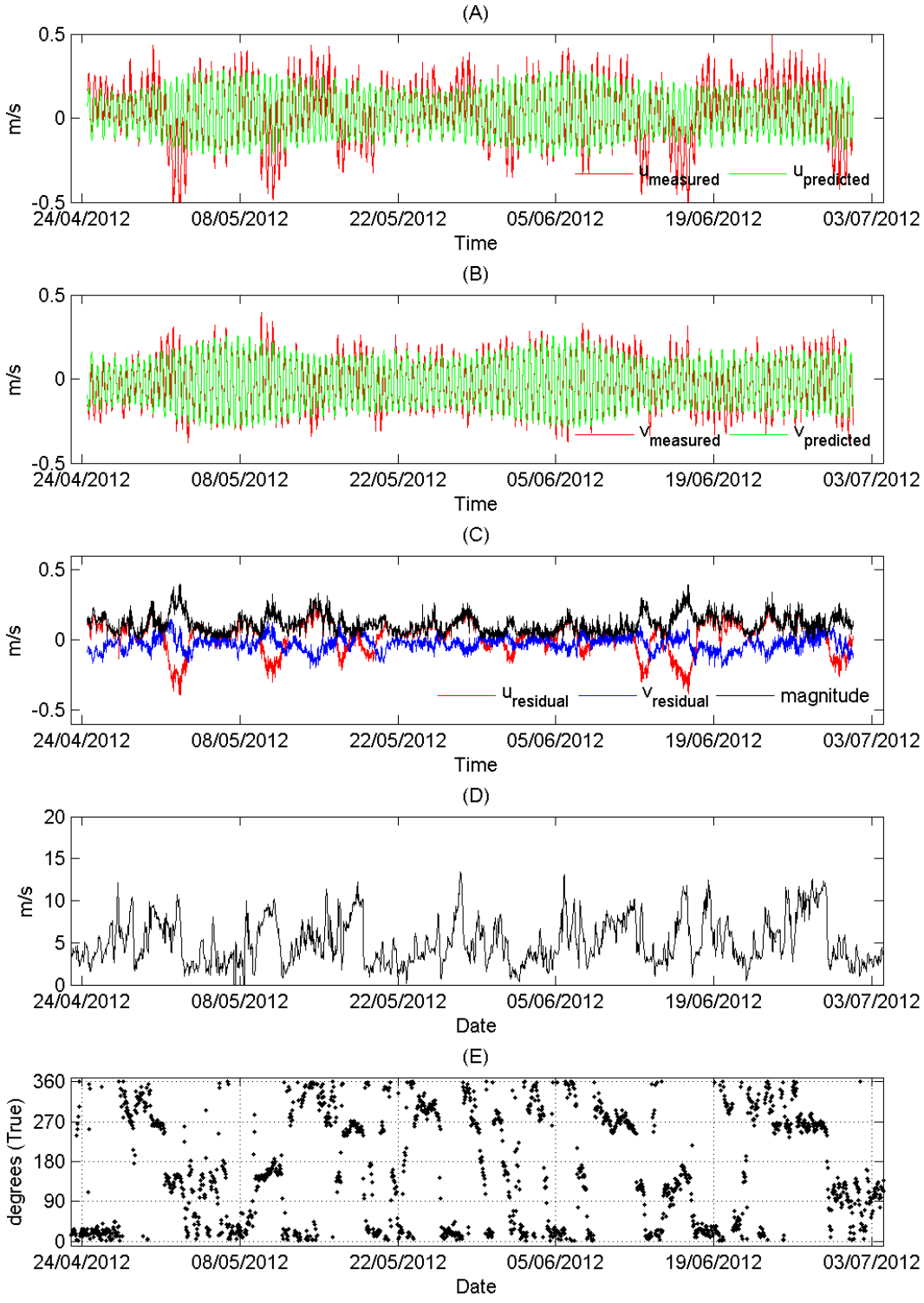

Figure 3-31: Tidal analysis of near-bed currents at S8/D3. Panels: (A) *u* velocity component, (B) *v* velocity component, (C) residual currents, (D) wind speed, and (E) wind direction (in meteorological convention "blowing from").

Figure 3-32 shows the PVD for deployment S8/D3 at three elevations above the bed. There was a general net drift towards the SE. The tracks also show that the current drift rotated anticlockwise towards the east with increasing elevation above the sea bed. The period of SE winds that occurred between 15/06/12 and 17/06/12 (see Figure 3-31) resulted in a drift towards the W. During periods of light winds there was a persistent drift towards the SE. Towards the end of the deployment period the drift tracks looped back on themselves. This was the result of a W wind (26/06/12 to 28/06/20:00) which drove the drift towards the NE, which was was then followed by a SW drift driven by winds from the SE. The small-scale saw-tooth pattern is due to the tidal cycle residual. The net drift speeds and directions are listed in Table 3-16.

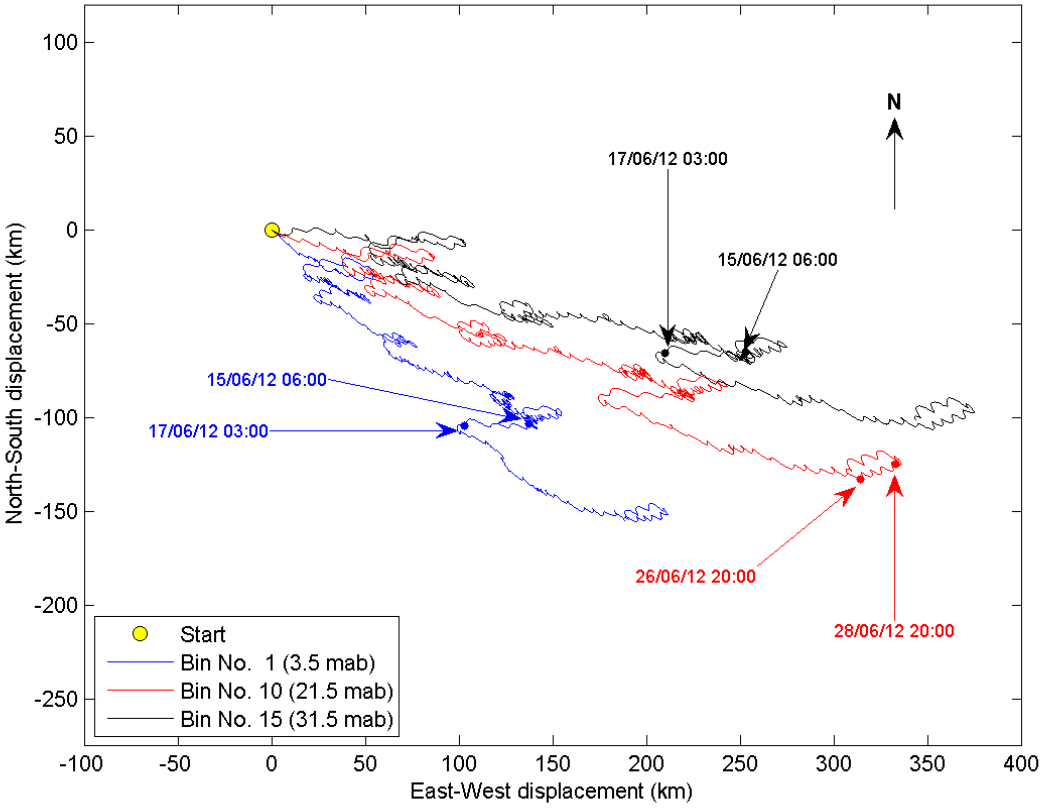

Figure 3-32: Progressive current drift at three elevations above the sea bed for deployment S8/D3 starting 24/04/2012 11:45 (yellow dot) through to 01/06/2012 08:30 (~68 days).

Bin No.	Depth (mab)	Net drift speed (m/s)	Net drift speed (km/day)	Mean drift direction (˚True North)
1	3.5	0.042	3.59	130
10	21.5	0.057	4.90	113
15	31.5	0.061	5.28	106

Table 3-16: Summary of the overall current drift during deployment S8/D3 (~68 days).

3.3.5 Site 10 (offshore end of the PPL)

A single ADCP deployment was carried out at site 10 (S10) during Deployment 3. The details of the location and deployment period listed in Table 3-2 and Table A-1 (Appendix A).

Time-series plots for S10 deployment 3 (D3) are shown in Figure 3-33.

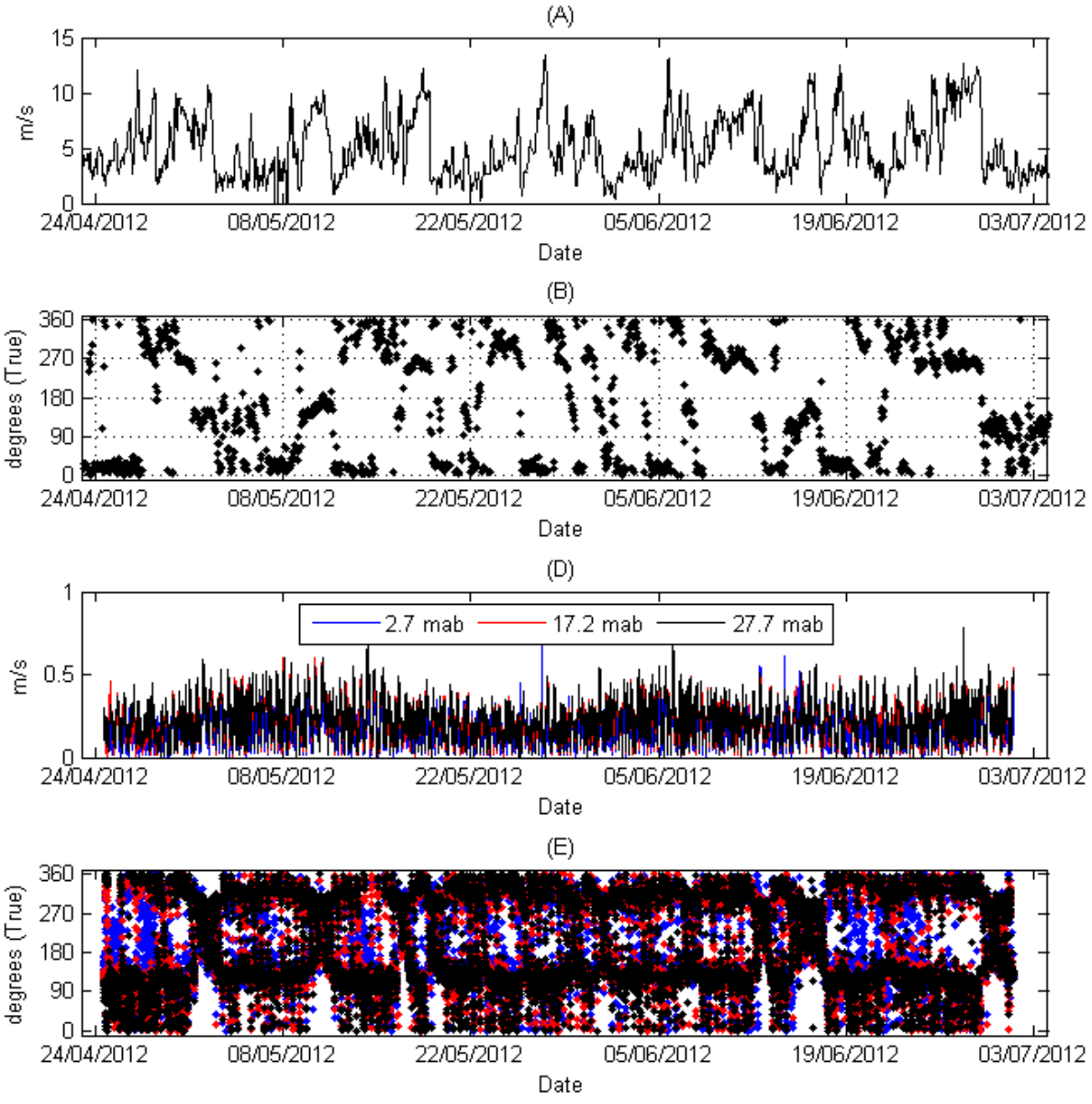

Figure 3-33: Current and wind time series for deployment S10/D3. Panels: (A) wind speed, (B) wind direction (in meteorological convention "blowing from"), (C) water depth, (D) current speed at three elevations above the bed, and (E) current direction (in oceanographic convention "flowing to").

For deployment S10/D3, Figure 3-33D shows that currents were typically less than 0.5 m/s. Near the sea bed, the maximum recorded current speed of 0.69 m/s was measured on 27/05/2012 at 07:30. In the 12-hour period prior, wind speeds ranged between 4.7 and 9.4 m/s (mean 7.5 m/s) from a N to NE direction. Higher in the water column, at 27.7 mab, the maximum recorded current speed of 0.79 m/s was measured on 27/06/2012 15:40. In the 12-

hour period prior, wind speeds ranged between 7.8 and 12.3 m/s (mean 10.0 m/s) blowing from the W.

Scatter plots of the velocity data from the three elevations above the sea bed are shown in Figure 3-34. The results of the PCA are summarised in Table 3-17. Currents measured during the S10/D3 deployment had a principal orientation of SE–NW. As expected, Figure 3-34 also shows that current speeds increased with elevation above the sea bed.

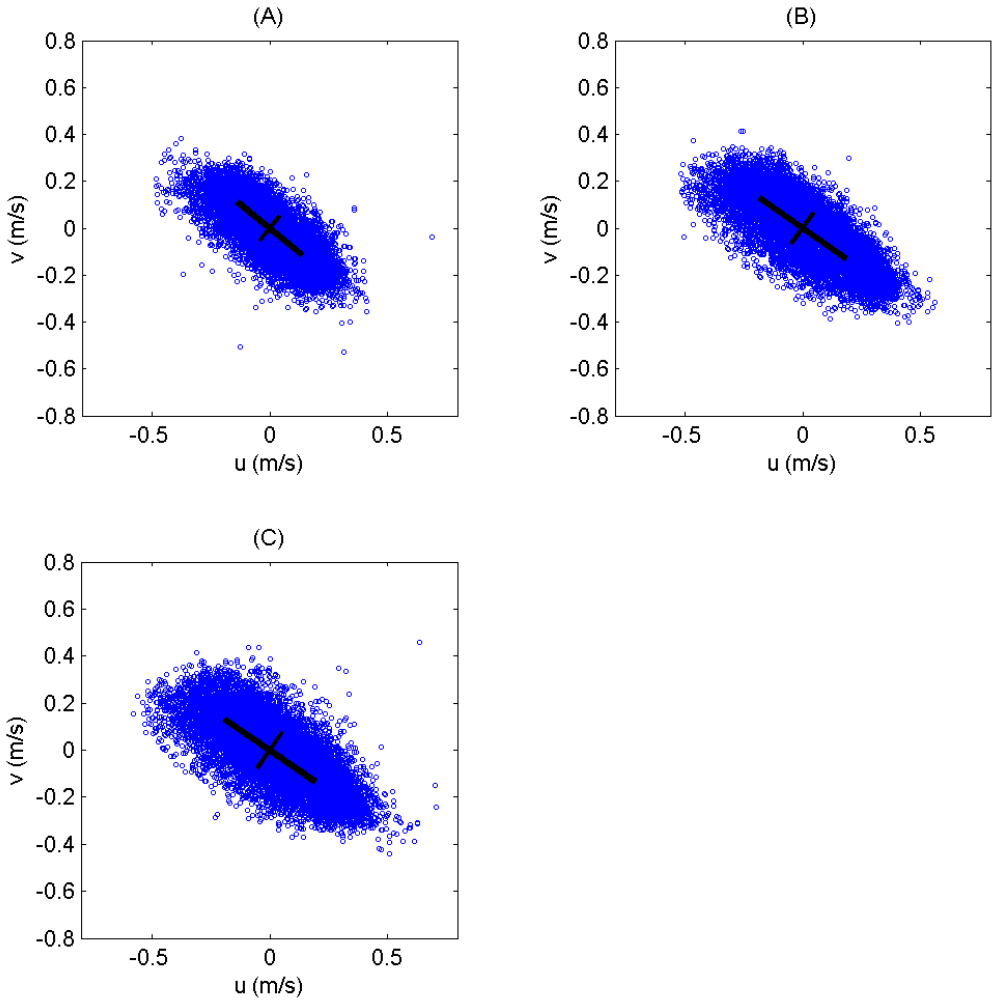

Figure 3-34: Scatter plots of currents at three elevations above the bed from deployment S10/D3. Panels: (A) data from 2.7 mab, (B) data from 17.2 mab, and (C) data from 27.7 mab. Note: the *u* and *v* velocity components relate to the east-west and north-south direction respectively. The thick line is the major axis and the thin line is the minor axis (both lines span ± standard deviation).

Bin No.	Depth	Major axis orientation (˚True North)	Minor axis orientation (˚True North)	Major axis std dev. (m/s)	Minor axis std dev. (m/s)
1	2.7	129	39	±0.178	±0.067
30	17.2	125	35	±0.227	±0.080
51	27.7	125	35	±0.235	±0.092

Table 3-17: Summary of principal component analysis for currents during deployment S10/D3.

Based on tidal analysis of the near-bed currents (2.7 mab) over the ~68 day record for the S10/D3 deployment (Appendix B and Figure 3-35), the fitted constituents explain 66% of the total variability in the current velocities (64% and 67% in the *u* and *v* directions, respectively). The amplitude (maximum speed) of the main twice-daily lunar (M2) tide is 0.2 m/s and is oriented in the SE–NW direction. While the largest residuals were again associated with winds from the W and the SE, they were typically smaller in magnitude than the residuals at the other sites discussed previously.

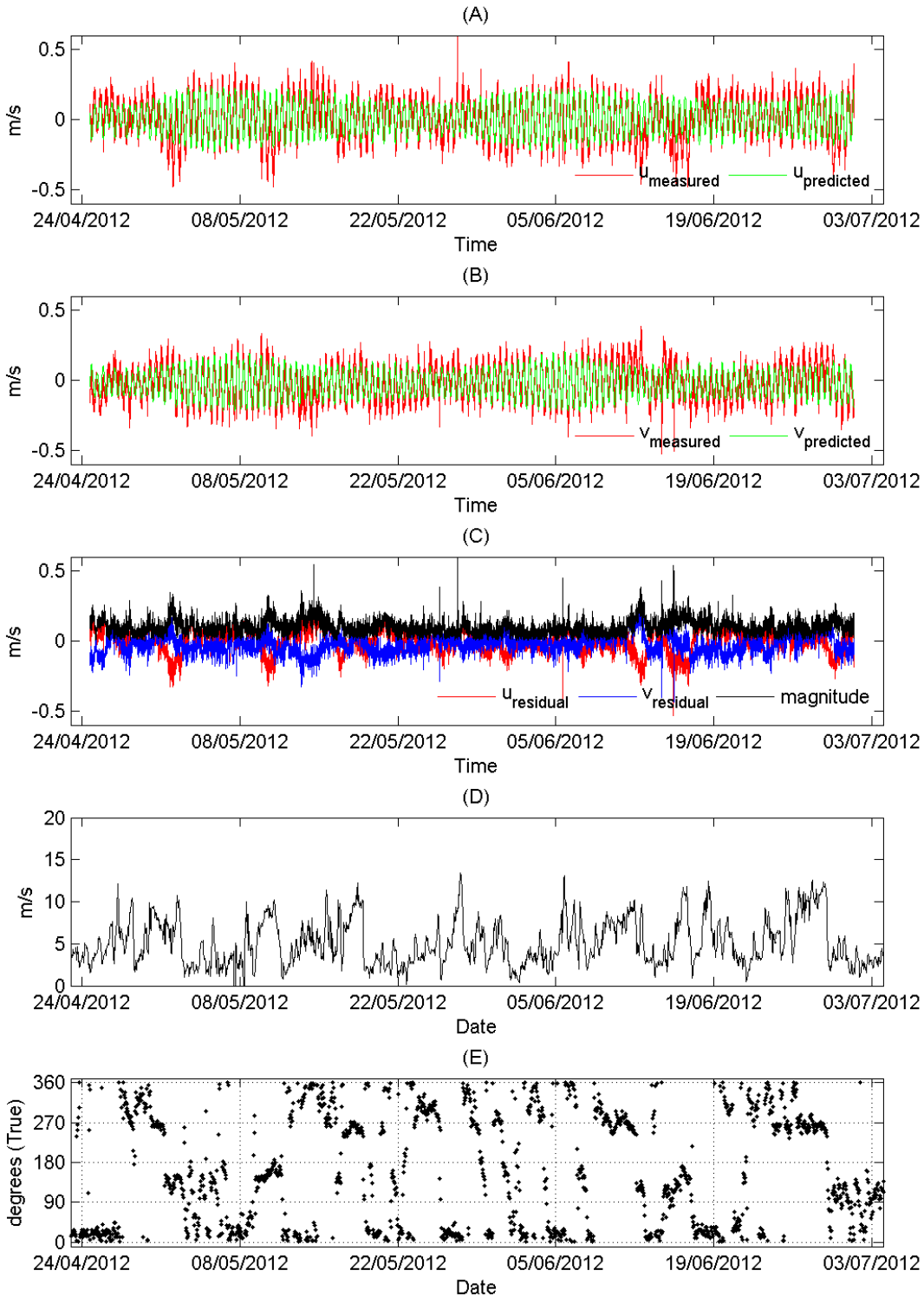

Figure 3-35: Tidal analysis of near-bed currents at S10/D3. Panels: (A) *u* velocity component, (B) *v* velocity component, (C) residual currents, (D) wind speed, and (E) wind direction (in meteorological convention "blowing from").

Figure 3-36 shows the PVD for deployment S10/D3 at three elevations above the bed. There was a general net drift towards the SE. The tracks also show that the current drift rotated anticlockwise towards the E with increasing elevation above the sea bed. The drift patterns for S10/D3 are very similar to S8/D3 covering the same period. The period of SE winds that occurred between 15/06/12 and 17/06/12 (see Figure 3-35) resulted in a drift towards the west. Westerly winds such as those that occurred during the period between 26/06/12 and 28/06/12 resulted in current drifts towards the NNE. During periods of light winds there was a persistent drift towards the SE. An interaction between SE, light and W winds drove the larger loops that can be observed in the current drifts. The smaller saw-tooth pattern is the drift produced by the tides. The net drift speeds and directions are listed in Table 3-18.

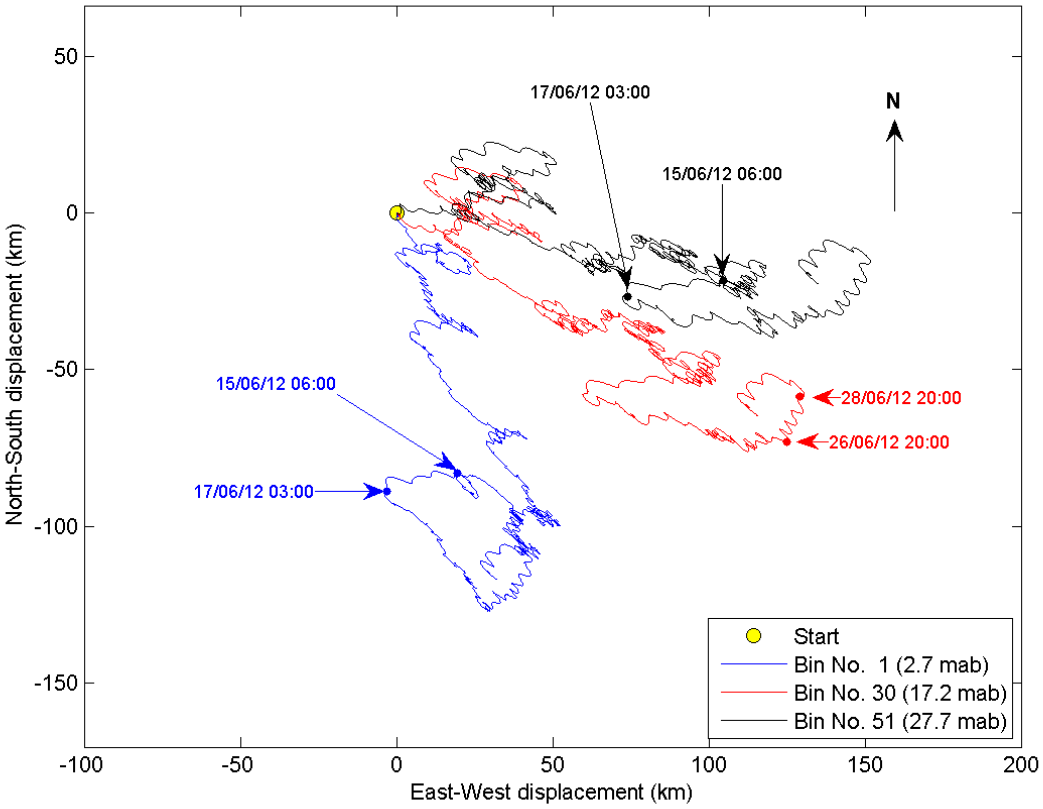

Figure 3-36: Progressive current drift at three elevations above the sea bed for deployment S10/D3 starting 24/04/2012 16:20 (yellow dot) through to 01/07/2012 10:20 (~68 days).

Bin No.	Depth (mab)	Net drift speed (m/s)	Net drift speed (km/day)	Mean drift direction (˚True North)
1	2.7	0.021	1.79	165
30	17.2	0.023	1.95	119
51	27.7	0.023	2.02	100

Table 3-18: Summary of the overall current drift during deployment S10/D3 (~68 days).

3.4 Waves

Measurements of waves are shown in this section in the form of:

- Time series plots of significant wave height (H_s), mean spectral period (T_m), mean direction of wave propagation (D_p)[5], wind speed and wind direction.
- Wave rose diagrams, which illustrate the relationship between wave height and direction.

3.4.1 Sites 1, 2, 3 and 4 (coastal sites from Hawera to south of Waverley)

Time series of the wave parameters derived from the DWG measurements at sites 1 to 4 (Figure 3-1) for deployments D1and D2 are shown in Figure 3-37.

The mean spectral wave period (T_m) is reported here as the DWG "sees it", that is, it is not adjusted for depth attenuation (see section 2.1.2). In this case, T_m can be interpreted as the mean spectral period of the wave-orbital motions at the level of the DWG (i.e., at the sea bed). The estimates of H_s have however been adjusted for the depth-attenuation of pressure so it is more representative of surface waves.

[5] From ADCP and wave rider deployments only.

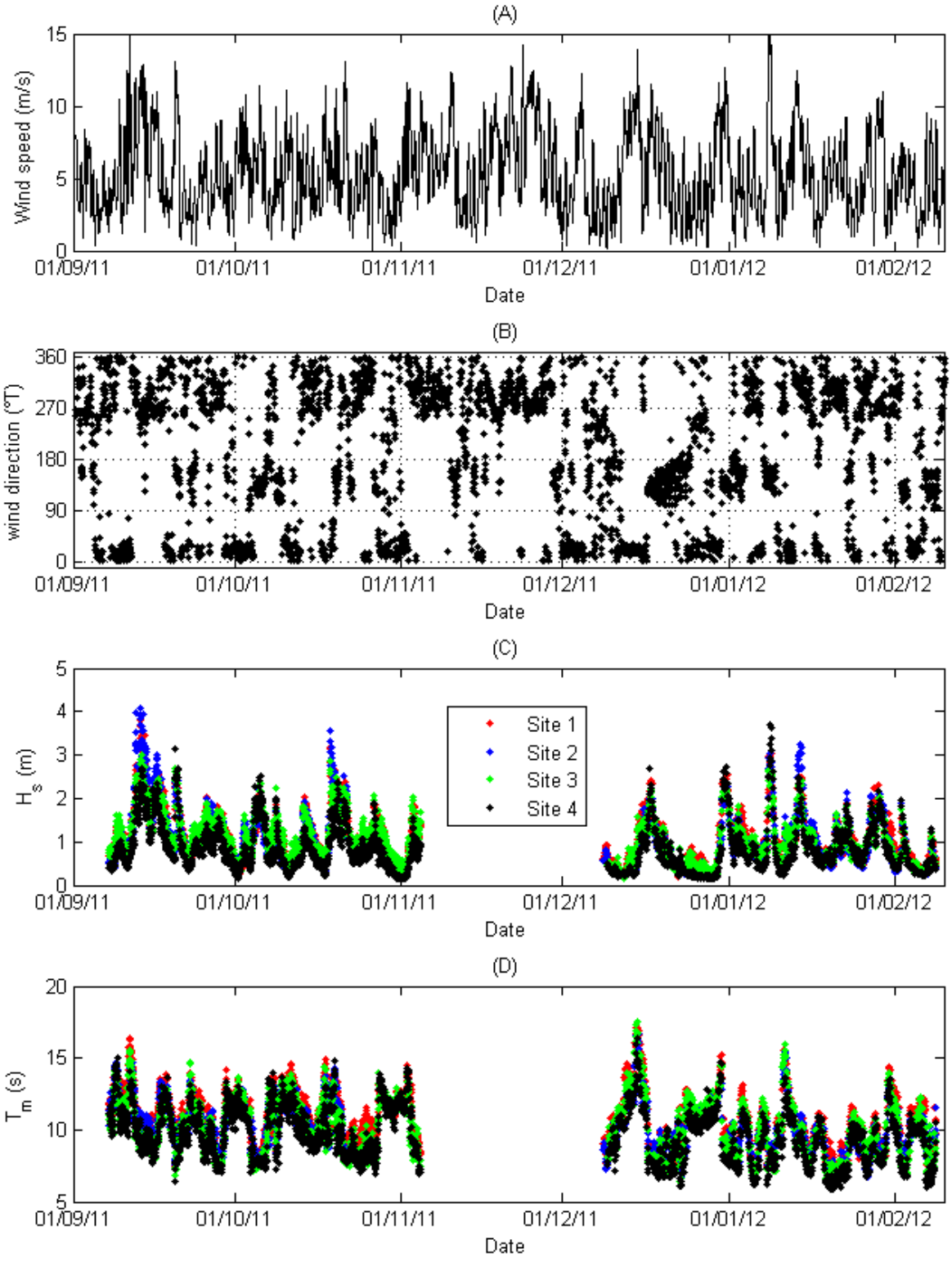

Figure 3-37: Wave parameters measured at sites 1 to 4 for deployments D1 and D2. Panels: (A) wind speed, (B) wind direction (in meteorological convention "blowing from"), (C) significant wave height (H_s), (D) mean spectral period at the sea bed(T_m).

Waves varied similarly at all 4 sites throughout the deployment. At sites 1, 2 and 3 the largest measured H_s was 3.8, 4.1 and 3.0 m, respectively. The maxima in H_s were recorded on the 13/09/2011 at all three sites. The mean spectral period T_m corresponding to the maximum H_s was 10.7, 11.1 and 8.2 seconds at sites 1, 2 and 3, respectively. The winds at Hawera preceding this time were strong (~12 m/s) and blew from the W. At Site 4, the largest H_s of 3.7 m was reached on 08/01/2012 at 18:00, at which time T_m was 8.4 seconds. The winds at Hawera preceding this time were strong (~15 m/s) from a SSE direction.

3.4.2 Sites 5, 6 and 7 (off Kai iwi and in the PPL)

Time series of the wave parameters measured by the ADCPs at sites 5, 6 and 7 for deployments D1and D2 are shown in Figure 3-38.

Waves varied similarly at all 3 sites throughout the deployment, but the maximum H_s at each site occurred at different times (Table 3-19). The three days in which the maximum significant wave heights occurred correspond to the three largest wave events measured during the field campaign.

Site	Date and Time	H_s (m)	T_m (s)	D_p (dir)	Wind speed (m/s)	Wind Direction
5	08/01/2012 19:00	4.03	7.2	175 (S)	15	SSE
6	13/09/2011 10:00	4.87	9.5	272 (W)	12	W
7	13/01/2012 22:00	5.22	8.7	282 (W)	12	WNW

Table 3-19: Wave parameters and wind conditions associated with the largest measured significant wave heights at sites 5, 6 and 7 during deployments D1 and D2. The mean spectral period is at the surface.

From Figure 3-38 it is also evident that at times the wave heights measured at the inshore site 5 were slightly smaller than those measured offshore at sites 6 and 7. Presumably, this was caused by sheltering of the prevailing swell by the tip of the South Island. This reduction in wave height is also reflected in the maximum wave heights shown in Table 3-19.

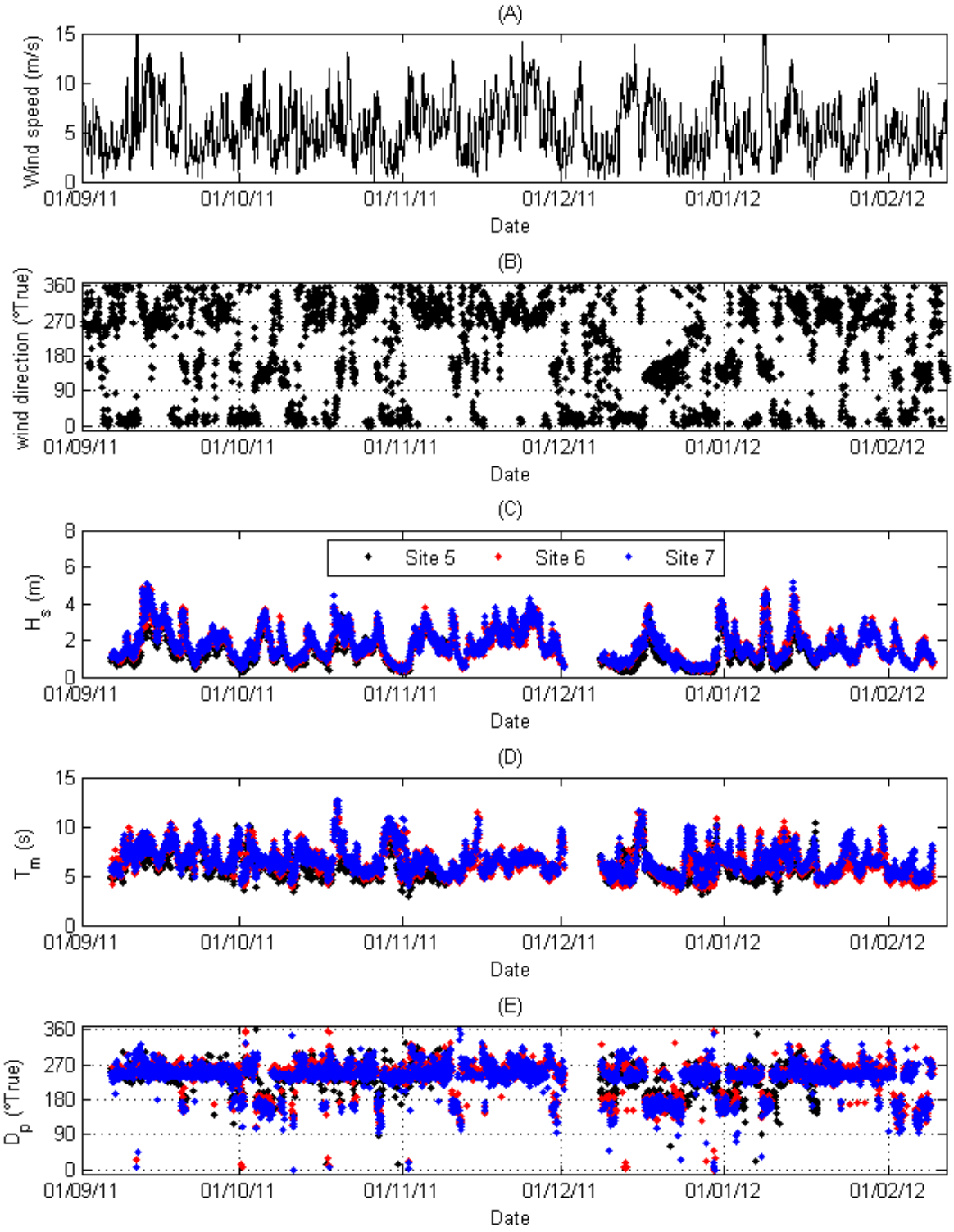

Figure 3-38: Wave parameters at sites 5, 6 and 7 for deployments D1 and D2. Panels: (A) wind speed, (B) wind direction (in meteorological convention "blowing from"), (C) significant wave height (H_s), (D) mean spectral period (T_m) at the sea surface, and (E) peak wave direction (D_p) (wave direction is the direction that the waves are coming from).

The wave roses for significant wave heights greater than 2 m for sites 5, 6 and 7 are shown in Figure 3-39, Figure 3-40 and Figure 3-41, respectively. By removing the wave heights less than 2 m from the wave rose plots we are able to identify the wave directions associated with larger-wave events.

Figure 3-39 shows that the wave directions associated with wave heights greater than 2 m at site 5 exhibit a strong bimodal distribution, dominated by waves from either the S to SSE or from the SW to WSW directions.

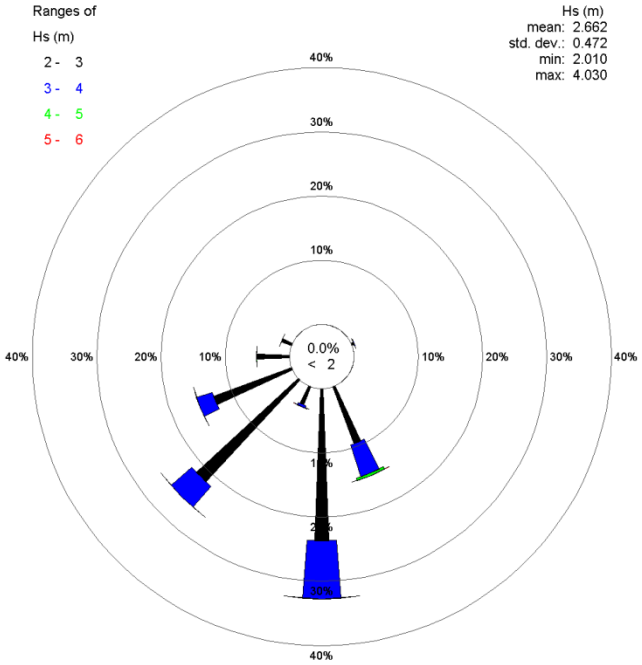

Figure 3-39: Wave rose for inshore site 5 for H_s greater than 2 m. (wave direction is the direction that the waves come from).

Figure 3-40 shows that the wave directions associated with wave heights greater than 2 m at site 6 also exhibit a strong bimodal distribution, dominated by waves from either the S to SE or from the W to SW directions. The wave direction at site 6 is dominated by waves from the WSW direction, which account for over 40% of the waves.

Figure 3-41 shows that the wave directions associated with wave heights greater than 2 m at site 7 are similar those at site 6, dominated by waves from either the S to SE or from the W to SW direction. However, at site 7 there are more SW and fewer WSW wave directions compared to site 6.

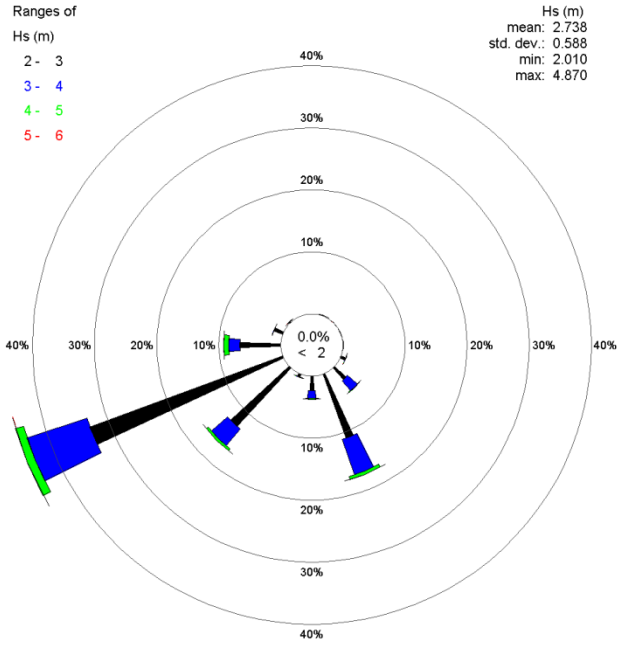

Figure 3-40: Wave rose for site 6 for H_s greater than 2 m. (wave direction is the direction that the waves come from).

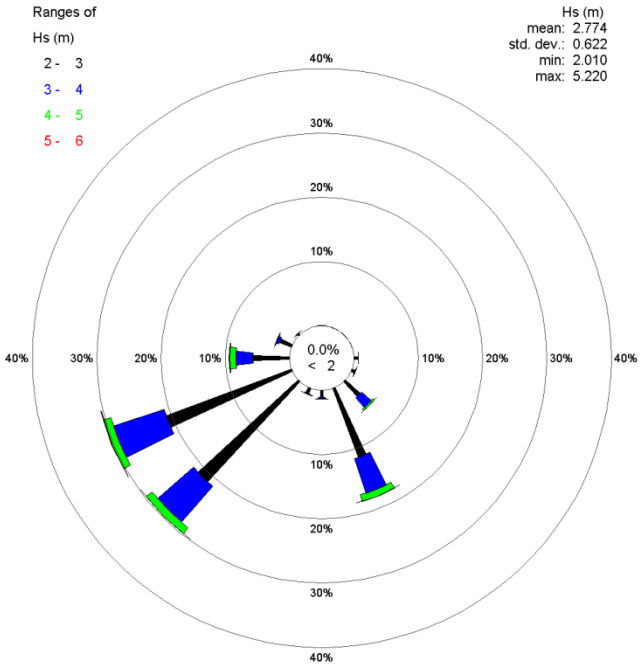

Figure 3-41: Wave rose for site 7 for H_s greater than 2 m. (wave direction is the direction that the waves come from).

3.4.3 Site 9 (furthest offshore site on the 50 m depth contour)

Time series of wave parameters measured by the wave rider buoy at site 9 are shown in Figure 3-42. The largest H_s recorded during the deployment period was 7.1 m, which had T_m of 8.4 seconds and which arrived from the south. The maximum H_s was recorded on 03/03/2012 at 05:40, and the wind speed measured at Whanganui during this period was ~17 m/s (61 km/hr) from the SSW with gusts up to 102 km/hr. No wind speed or direction data were available from the Hawera wind station during this time, presumably as a result of damage sustained during this strong weather-bomb event.

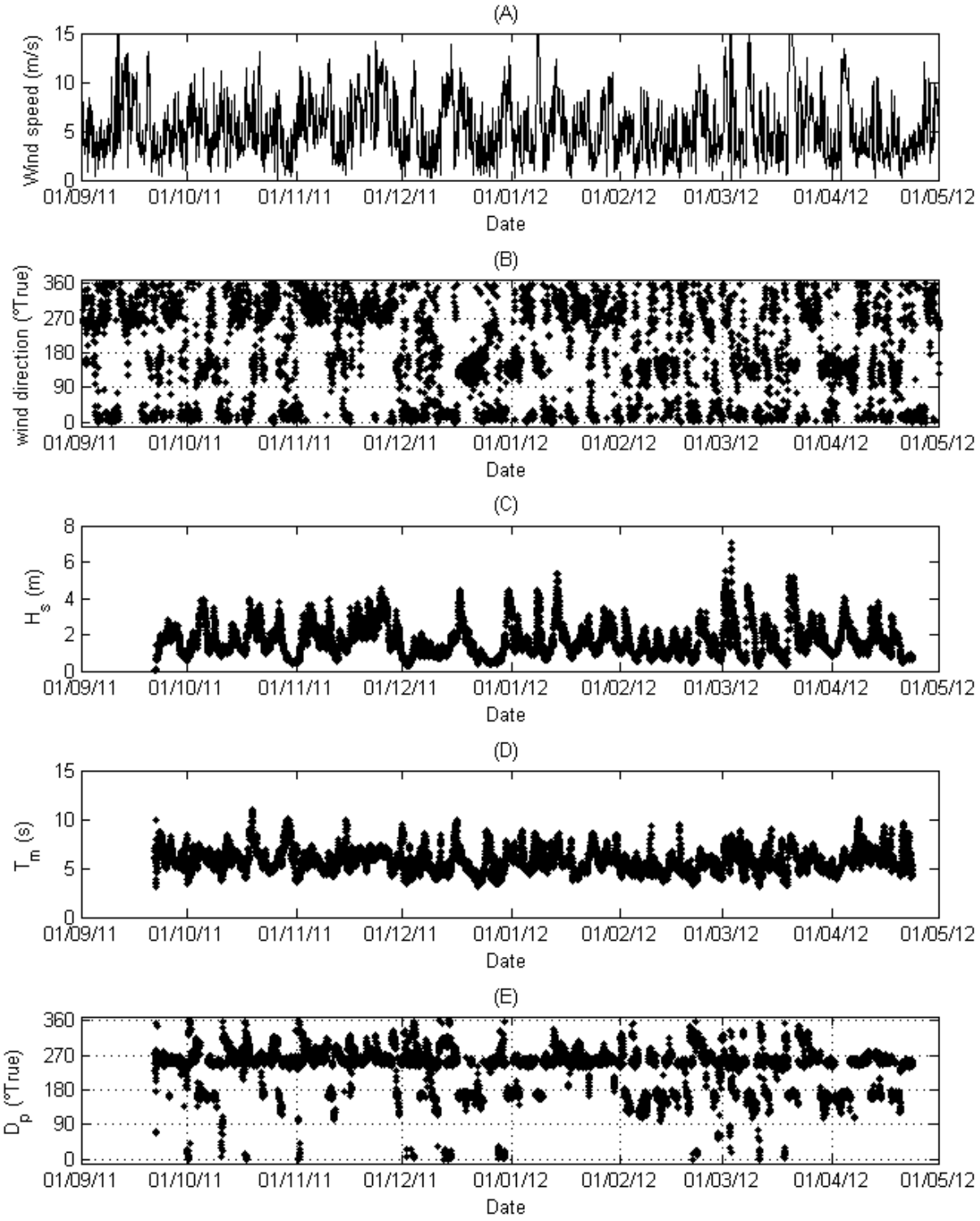

Figure 3-42: Wave parameters measured at site 9. Panels: (A) wind speed, (B) wind direction (in meteorological convention "blowing from"), (C) significant wave height (H_s), (D) mean spectral period at the sea surface (T_m), and (E) peak wave direction (D_p) (wave direction is the direction that the waves come from).

Figure 3-43 shows that the wave directions associated with wave heights greater than 2 m at site 9 exhibit a strong bimodal distribution, dominated by waves from either the SSE or from the WSW. Over 70% of the waves with wave heights greater than 2 m approached from these two directions.

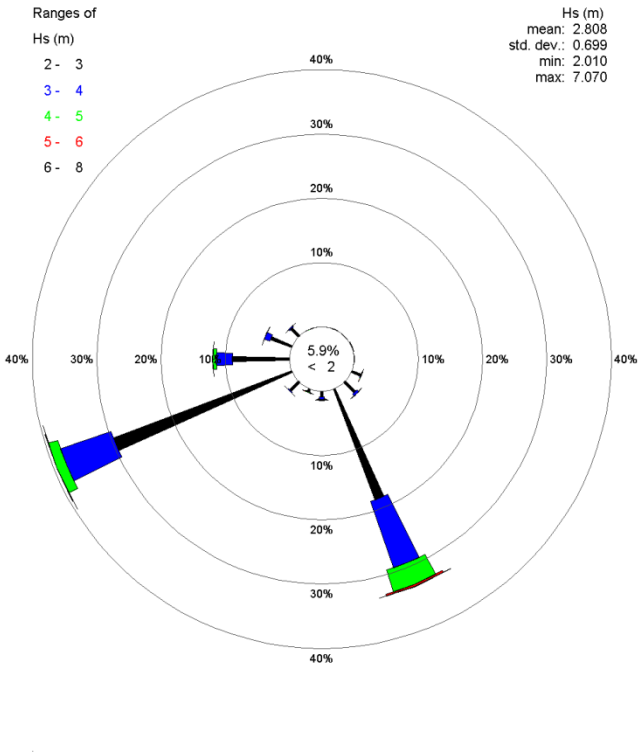

Figure 3-43: Wave rose for site 9 for H_s greater than 2 m. (wave direction is the direction that the waves come from).

3.4.4 Wave height comparison

Figure 3-44 shows a comparison of H_s measured at sites 1, 7 and 9, which is an approximate transect from nearshore to offshore off Hawera. Temporal changes in H_s are consistent at the three sites. Furthermore, H_s measured at site 7 is very similar to H_s measured at site 9, as the two time series from these offshore site closely overlap. There is also a reduction in H_s at the nearshore site 1 compared to sites 7 and 9.

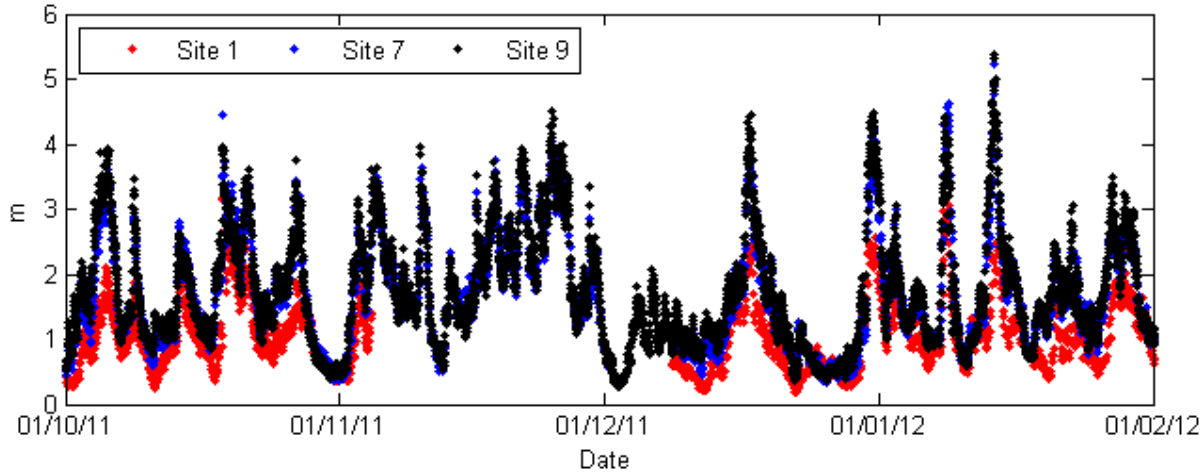

Figure 3-44: Comparison of H_s at sites1 (nearshore), 7 and 9.

3.5 Temperature and Salinity

3.5.1 Site 7 (inshore end of the PPL)

Time series of temperature and salinity measured at site 7 during deployments D1 and D2 are shown in Figure 3-45. Temperature at the various depths displayed very similar temporal patterns. There were only small vertical differences in temperature, with the surface waters being slightly warmer than the water further down in the water column. The temperature ranged from below 13˚C at the beginning of September 2011 to just over 19˚C towards the end of March 2012.

The salinity measurements from deployment D2, taken near the bed (2 mab) and around mid-depth (22 mab), display similar temporal patterns, with only small vertical differences in salinity. The salinity was typically around 35 psu, ranging in a narrow band from 34.51 psu to 35.17 psu over the deployment period. Lower salinity water is likely to be found in the vicinity of major rivers in the STB (e.g., Patea, Waitotara and Whanganui).

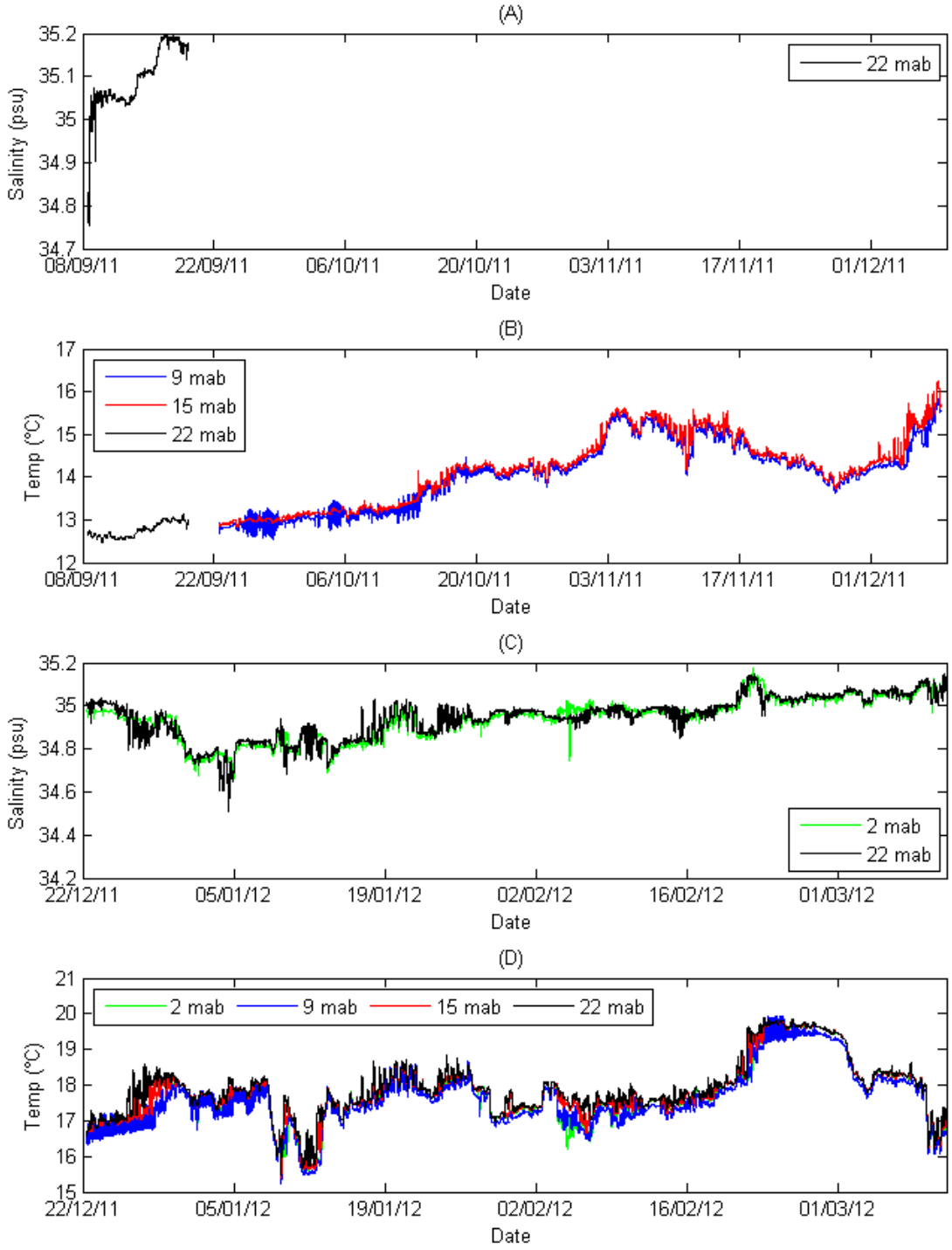

Figure 3-45: Salinity and temperature measurements at site 7. Panels: (A) salinity measured during deployment D1, (B) temperature measured during deployment D1, (C) salinity measured during deployment D2, and (D) temperature measured during deployment D2.

3.5.2 Site 9 (furthest offshore site on the 50 m depth contour)

Time series of near-bed temperature and salinity measured at site 9 during D1 are shown in Figure 3-46. At site 9, the temperature was around 12.5˚C at the beginning of September 2011 and reached a maximum of 14.5˚C near 4 November 2011. The variation in water temperature at site 9 is similar to that observed at site 7.

The near-bed salinity at site 9 was typically around 35 psu. The major feature in the salinity record is the large drop in salinity between 4/11/11 and 11/11/11, which is unlikely to be real (we suspect it was caused by a temporary blockage of the conductivity cell). Ignoring that period, salinity ranged from 34.96 to 35.19 psu over the deployment period, which is smaller than the range of salinities encountered at site 7.

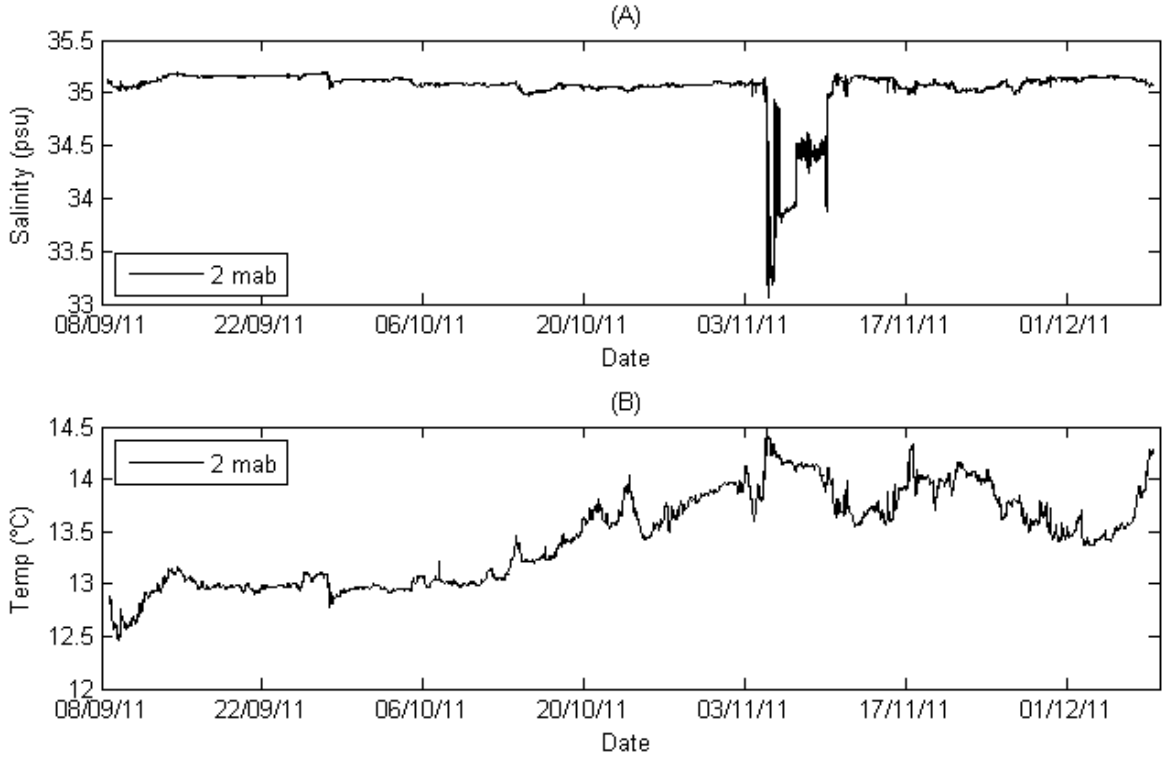

Figure 3-46: Salinity and temperature measurements at site 9. Panels: (A) salinity measured during deployment D1, and (B) temperature measured during deployment D1.

3.5.3 Site 10 (offshore end of the PPL)

Time series of temperature and salinity measured at site 10 during deployment D3 are shown in Figure 3-47. The temperature time series measured at the two depths are virtually identical. Temperature ranged between 15.8˚C at the beginning of the record and 14.1˚C at the end of the record.

The salinity measurements taken near the bed (2 mab) and around mid-depth (22 mab) follow very similar temporal patterns. A notable feature is the small and constant salinity offset of ~ 0.02 psu between the two records. Given how consistent (and small) this offset is, it probably relates to slight errors in the instrument calibration coefficients. Salinity at site 10

ranged between 35.13 and 35.30 psu, which is smaller than the range encountered at site 7 (during a different period).

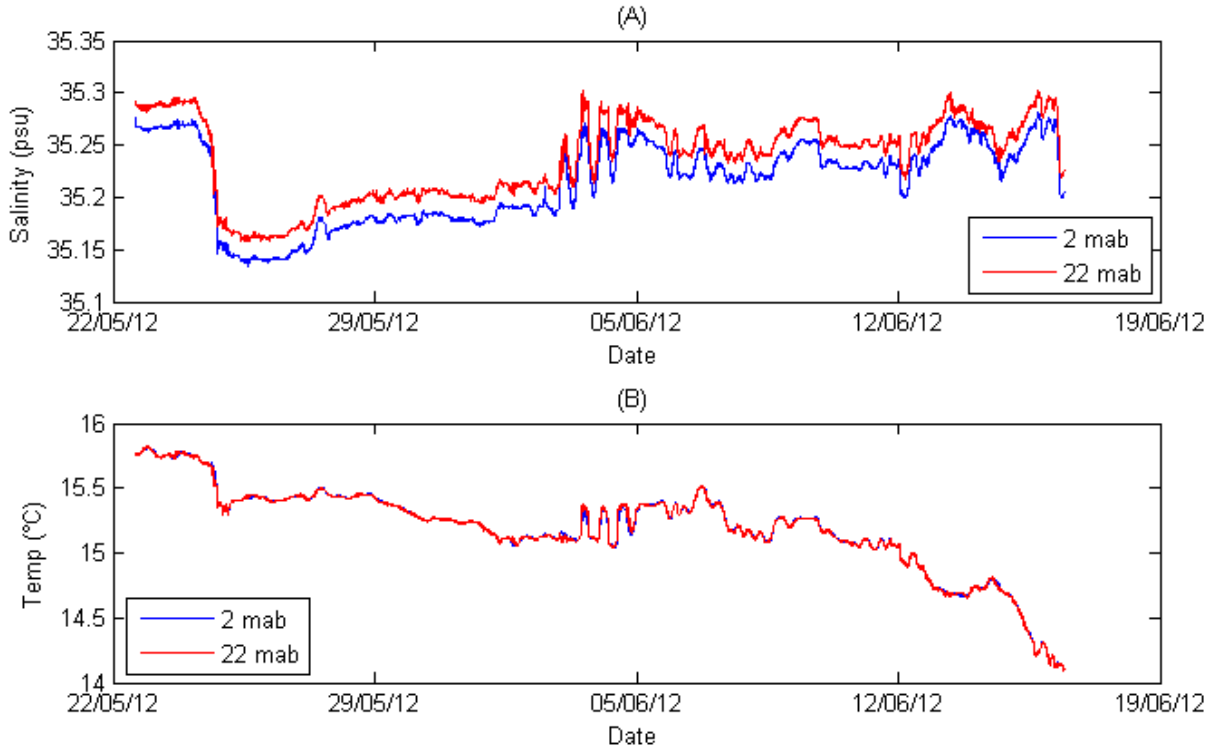

Figure 3-47: Salinity and temperature measurements at site 10. Panels: (A) salinity measured during deployment D1, and (B) temperature measured during deployment D1.

3.6 Suspended Sediment Concentration (SSC)

In this section the SSC results are presented. Details about the location, periods and sampling schemes relating to the SSC measurements can be found in Table 3-2 and in Table A-4 (Appendix A).

In this section all SSC data are presented as burst (time) averages rather than instantaneous values.

3.6.1 Instrument calibrations

Gains and offsets derived from the calibration of the OBS sensors are shown in Table 3-20. Recall that the voltage output by the optical backscatter sensor (*V*) is related to *SSCm* (suspended-mud concentration) by a linear relationship:

$$SSCm = G*V + O$$

where *G* is the sensor gain (unit of g/l per volt) and *O* is the sensor offset (units of g/l).

The results shown in Table 3-20 were derived from the calibration data shown in Figure C-1 (Appendix C).

Site	Deployment	Water column position	OBS serial #	OBS Gain (*G*)	OBS Offset (*O*)
5	D1 and D2	near-surface	10295	0.151	0.004
6	D1 and D2	near-surface	10600	0.192	-0.004
6	D1 and D2	near bed	11871	0.999	-0.004
7	D1 and D2	near-surface	10597	0.148	0.001
7	D1 and D2	near bed	11870	0.670	-0.003
8	D3	near-surface	10600	0.192	-0.004
8	D3	near bed	11870	0.670	-0.003
10	D3	near-surface	10295	0.151	0.004
10	D3	near bed	11871	0.999	-0.004

Table 3-20: OBS gains and offsets used in deriving estimates of *SSCm*.

The values for K_t derived from the ABS calibrations are shown in Table 3-21 and in Figure C-2 (Appendix C). The sediments used in the calibration of ABS#1 came from site 7 (ABS#1 was deployed there during D1 and D2). Sediments used in the calibration of ABS#2 came from site 6 (ABS#2 was deployed there during D1 and D2). All ABS data were inverted using the K_t values shown in Table 3-21.

ABS	Frequencies used in inversion	K_t values
ABS#1	2 and 3 MHz	0.00646 (2 MHz) and 0.0115 (3 MHz)
ABS#2	1 and 2 MHZ	453.94 (1 MHz) and 130.59 (2 MHz)

Table 3-21: K_t values derived from ABS calibration.

The inversion method also requires information about the size distribution of the particles in suspension; this information was obtained from grainsize analysis of bed sediments that were collected near the ABS deployment sites. The particle size distributions (PSDs) obtained from the analysis of bed sediment samples at the four ABS deployment sites are shown in Figure 3-48. The median particle size (*D50*) of the PSDs shown in Figure 3-48 are listed in Table 3-22.

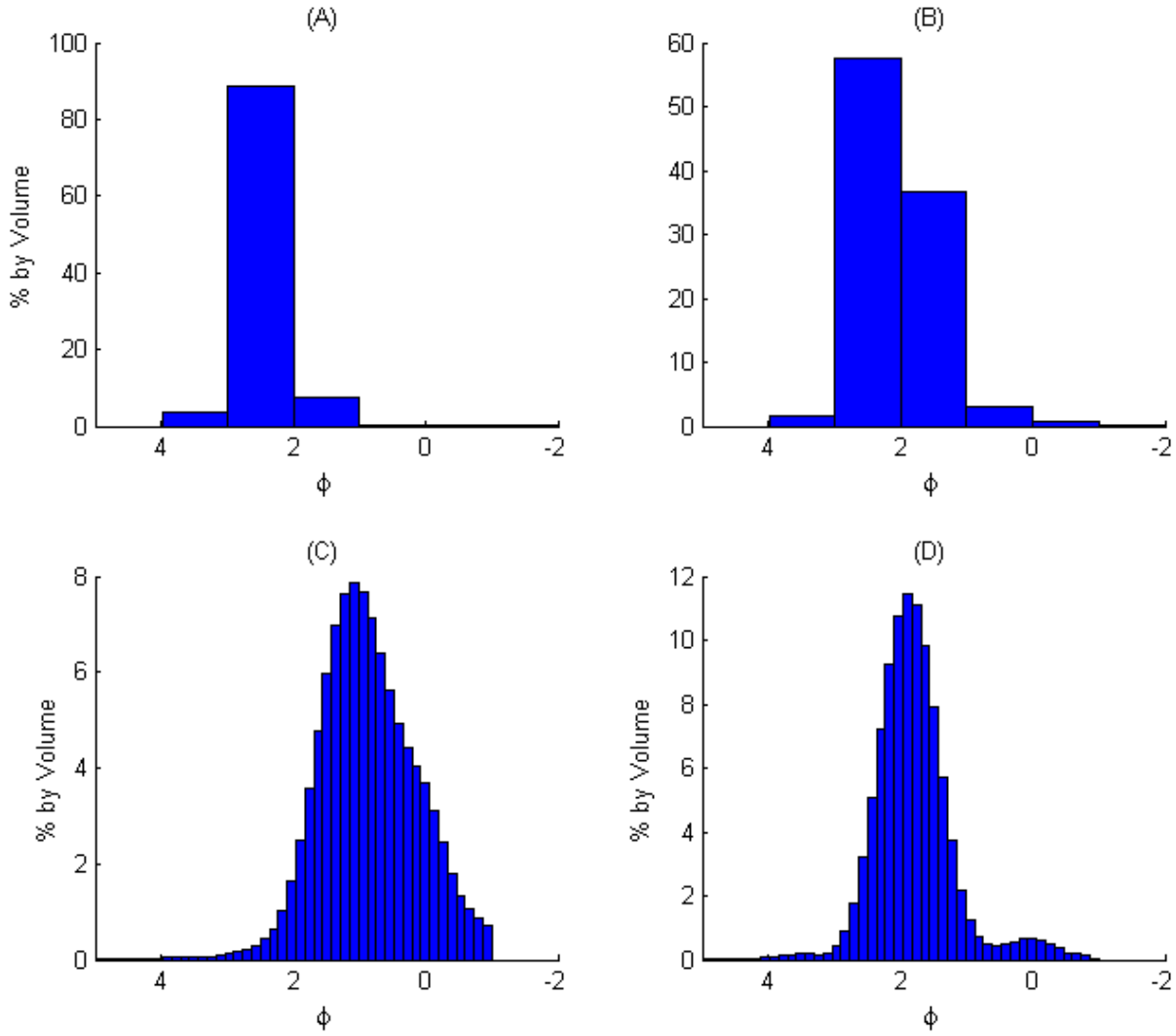

Figure 3-48: Particle size distribution of the bed sediments at the four ABS deployments sites. Panels: (A) site 6, (B) site 7, (C) site 8 and (D) site 10. Note $\phi = -\log_2(d)$, with I the particle diameter in millimetres.

	Site 6	Site 7	Site 8	Site 10
***D50* (µm)**	199	285	664.0	349.1
Sediment group	Fine sand	Medium sand	Coarse sand	Medium sand

Table 3-22: Median particle sizes at the four ABS deployment sites.

3.6.2 *SSCm* in the near-surface region

Site 5 (near-shore site off Kai iwi)

Time series of near-surface *SSCm* measured at site 5 are shown in Figure 3-49.

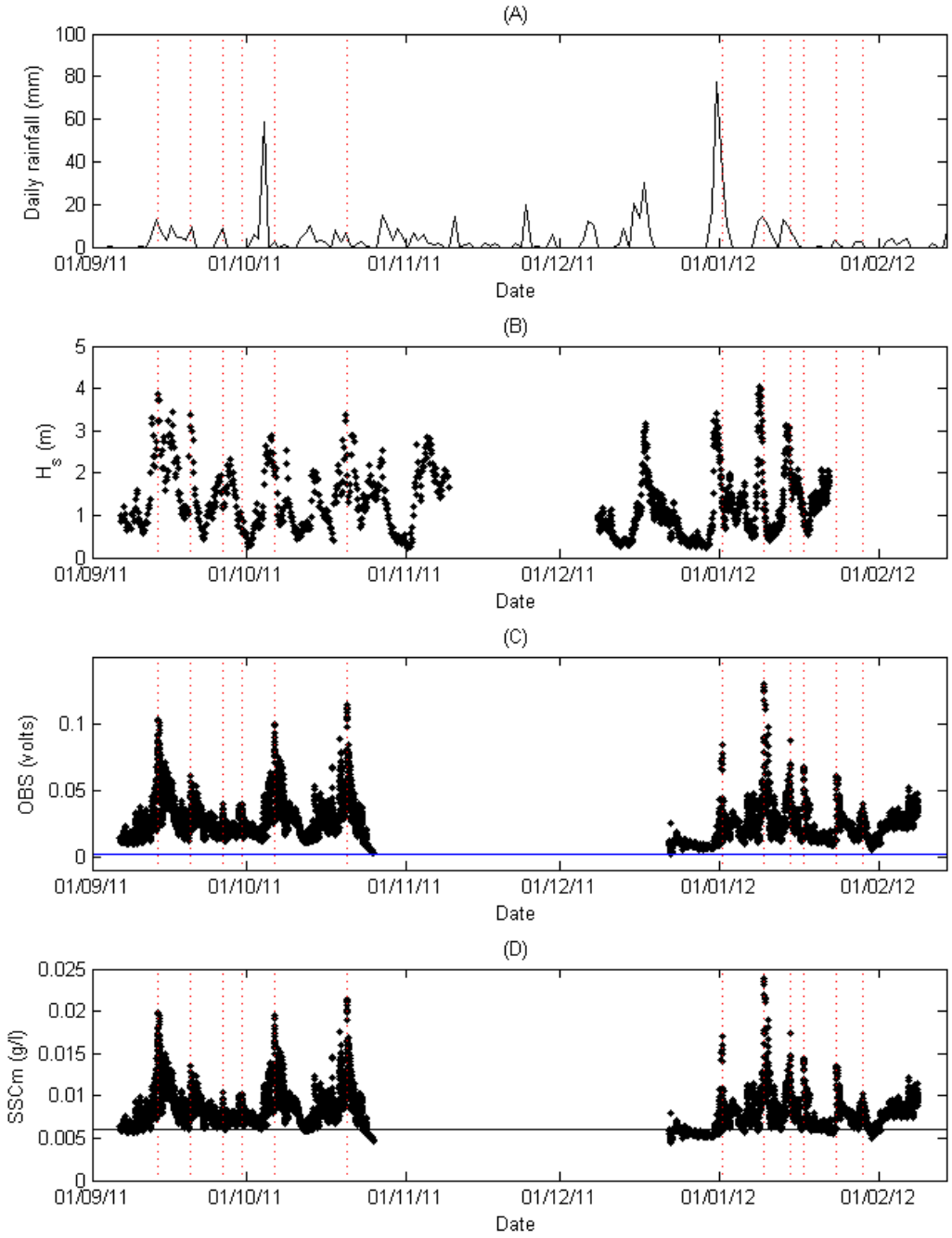

Figure 3-49: *SSCm* in the near-surface region at site 5 for deployments D1 and D2. Panels: (A) daily rainfall measured at Hawera (mm), (B) H_s, (C) OBS voltage (blue line shows OBS voltage recorded in particle-free tap water), and (D) *SSCm* (black line shows background *SSCm* during calm periods).

The maximum *SSCm* measured in the near-surface region at site 5 was ~0.025 g/l. During calm periods background *SSCm* was around 0.006 g/l (black line in Figure 3-49D), which is close to the lower detection limit of the OBS. Figure 3-49C shows that the voltages recorded during calm periods were only slightly greater (~8 mV) than the voltage recorded by the OBS in particle-free tap water (blue line). (Note that the OBS operates over a 0–5 V range.)

At site 5, *SSCm* showed considerable temporal variability, with peaks in *SSCm*, as indicated by the vertical dashed-red lines, tending to occur during or just after periods of significant rainfall. At these times it is likely that rivers were discharging fine sediments into the STB, which were then being transported in suspension through the measurement site.

Some of the peaks in *SSCm* also coincided with times of large H_s While it is possible that large waves resuspended fine sediments from the sea bed and increased *SSCm* near the surface, it is also possible that the increase resulted from an increase in optical backscatter generated by the entrainment of air bubbles into the water column by an energetic sea.

Site 6 (inshore of the PPL)

Time series of near-surface *SSCm* measured at site 6 are shown in Figure 3-50.

Figure 3-50D shows that the linear relationship used to convert optical backscatter to *SSCm* at times generated very small negative values for *SSCm*. During calm periods, the negative concentration was constant around -0.002 g/l (black line in Figure 3-50D). From a practical point of view, the *SSCm* as estimated by the OBS during these periods was essentially zero. In order to correct for the negative offset, 0.002 g/l was added to the *SSCm* estimates to produce the offset-adjusted time series (blue dots in Figure 3-50D).

Apart from a few outliers, the maximum *SSCm* measured in the near-surface region at site 6 was ~0.003 g/l, which is about an order of magnitude less than that measured at site 5.

At site 6, *SSCm* did vary throughout the deployment period, but the variation was much reduced compared to site 5. Peaks in *SSCm*, as indicated by the vertical dashed-red lines, tended to occur during or just after periods of significant rainfall, which is indicative of river inputs of suspended-fine sediments. Some of the peaks in *SSCm* also coincided with times of large H_s As noted above, this could have been due to wave resuspension of fine sediments from the bed and/or an increase in the optical backscatter generated by the entrainment of air bubbles.

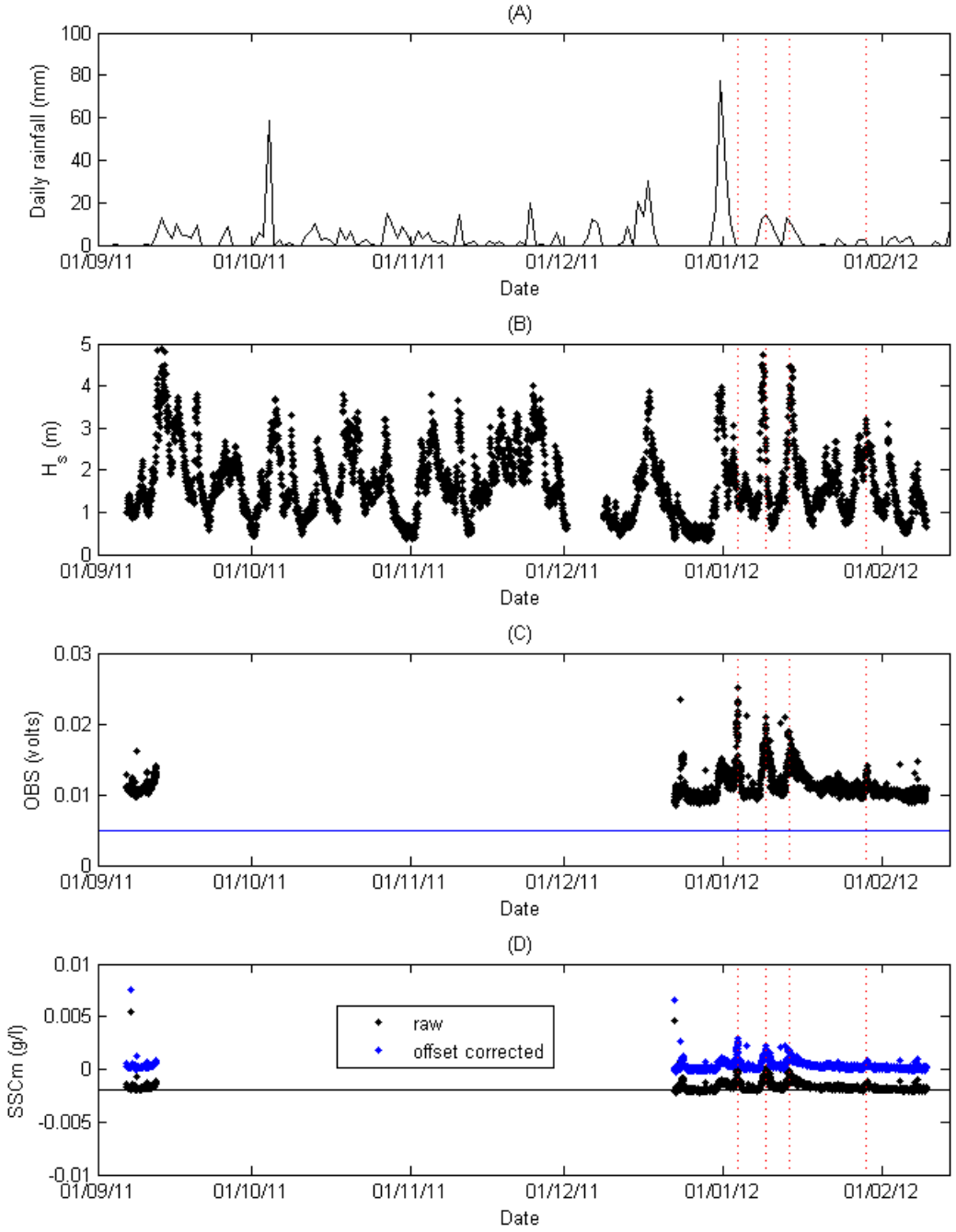

Figure 3-50: *SSCm* in the near-surface region at site 6 for deployments D1 and D2. Panels: (A) daily rainfall measured at Hawera (mm), (B) H_s, (C) OBS voltage (blue line shows OBS voltage recorded in particle-free tap water), and (D) *SSCm* (black line shows background *SSCm* during calm periods), Refer to text for explanation of the symbols in panel (D).

Site 7 (inshore end of the PPL)

Time series of near-surface *SSCm* measured at site 7 are shown in Figure 3-51.

The maximum *SSCm* measured in the near-surface region at site 7 was ~0.025 g/l. The event that generated this peak was not recorded at site 6 as the OBS at site 6 was no longer running by that time. During calm periods, background *SSCm* was around 0.02 g/l (blue line in Figure 3-51D), which is close to the lower detection limit of the OBS.

At site 7, *SSCm* varied considerably throughout the deployment. Peaks in *SSCm*, as indicated by the vertical dashed-red lines, tended to occur during or just after periods of significant rainfall, which is indicative of river inputs of suspended-fine sediments..

Some of the peaks in *SSCm* also coincided with times of large H_s. As noted above, this could have been due to wave resuspension of fine sediments from the bed and/or an increase in the optical backscatter generated by the entrainment of air bubbles.

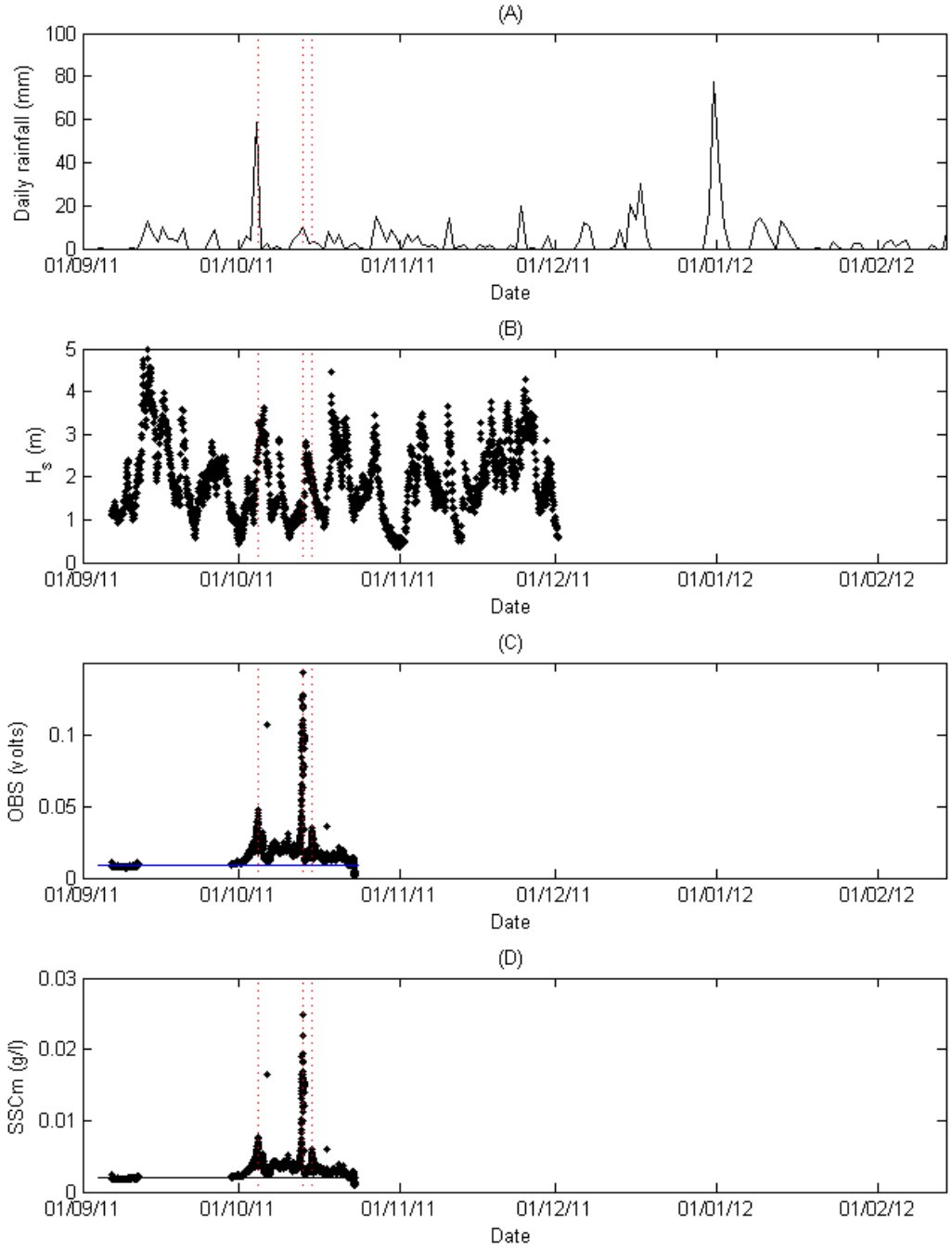

Figure 3-51: *SSCm* in the near-surface region at site 7 for deployment D1 (no D2 data due to lost OBS).Panels: (A) daily rainfall measured at Hawera (mm), (B) H_s, (C) OBS voltage (blue line shows OBS voltage recorded in particle-free tap water), and (D) *SSCm* (black line shows background *SSCm* during calm periods).

Site 8 (SSE of the PPL)

Time series of near-surface *SSCm* measured at site 8 are shown in Figure 3-52.

Figure 3-52C shows that all *SSCm* estimates are negative, which have resulted from very low backscatter voltages and a small error in the calibrated OBS offset. In order to correct for the negative offset, 0.002 g/l was added to the *SSCm* estimates to produce the offset-adjusted time series (blue dots in Figure 3-52C). After correcting for the offset error, the maximum *SSCm* measured at site 8 is found to be around 0.001 g/l. There was very little temporal variability in *SSCm* at site 8. However, very small peaks in *SSCm* (dashed-red lines) tended to occur during or just after periods of significant rainfall, which is indicative of river inputs of suspended-fine sediments.

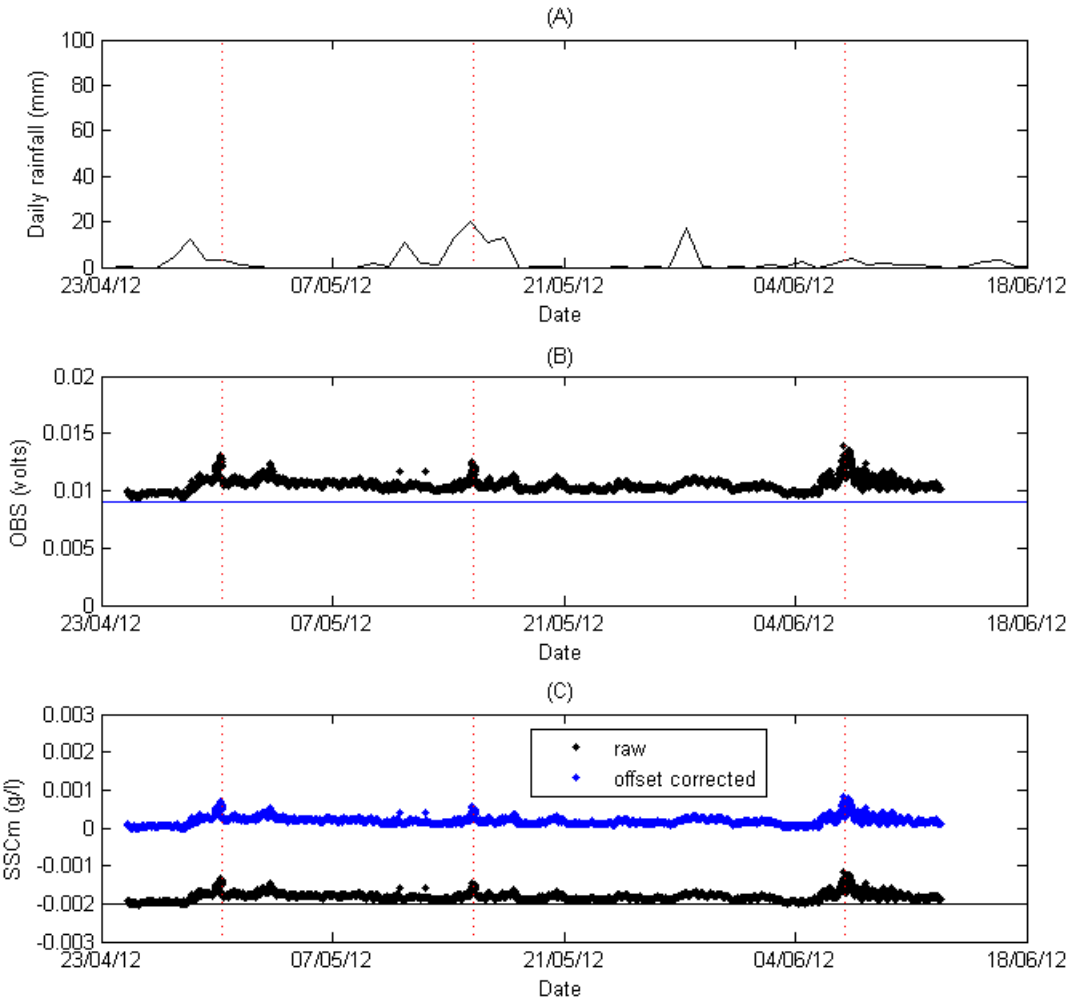

Figure 3-52: *SSCm* in the near-surface region at site 8 for deployment D3.Panels: (A) daily rainfall measured at Hawera (mm), (B) OBS voltage (blue line shows OBS voltage recorded in particle-free tap water), and (C) *SSCm* (black line shows background *SSCm* during calm periods), Refer to text for explanation of the symbols in panel (C).

Site 10 (offshore end of the PPL)

Time series of near-surface *SSCm* measured at site 10 are shown in Figure 3-53.

The maximum *SSCm* measured in the near-surface region at site 10 was ~0.006 g/l. During calm periods background *SSCm* was around 0.0055 g/l (blue line in Figure 3-53C). All the *SSCm* measurements at site 10 are close to the lower detection limit of the OBS.

As at site 8, there was very little temporal variability in *SSCm*. However, very small peaks in *SSCm* (dashed red lines) tended to occur during or just after periods of significant rainfall, which is indicative of river inputs of suspended-fine sediments.

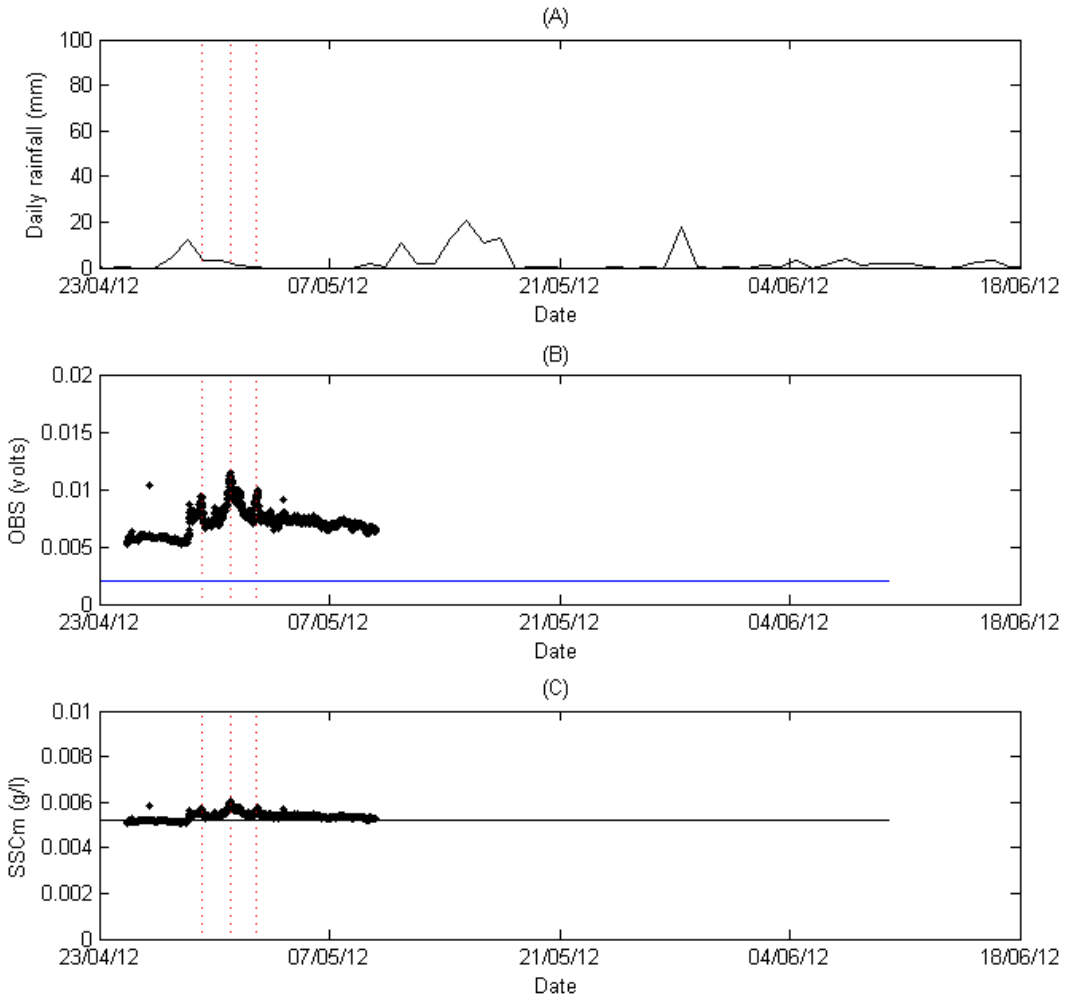

Figure 3-53: *SSCm* in the near-surface region at site 10 for deployment D3. Panels: (A) daily rainfall measured at Hawera (mm), (B) OBS voltage (blue line shows OBS voltage recorded in particle-free tap water), and (C) *SSCm* (black line shows background *SSCm* during calm periods).

The near-surface *SSCm* results imply a reduction in the magnitude and variability of *SSCm* moving in a NW direction (i.e., from site 4 to site 10). This may be because the major sources of fine-sediment input into the coastal zone are likely to come from the Whanganui, Whangaehu and Rangitikei Rivers, which are all located in the southern section of the STB.

3.6.3 SSC in the near-bed region

Site 6 (inshore of the PPL)

Time series plots of near-bed SSC measurements at site 6 for deployments D1 and D2 are shown in Figure 3-54. Figure 3-54C plots C_{ref}, which is the suspended-sand reference concentration. This was evaluated as *SSCs* in the 1-cm-thick bin that is in contact with the sea bed. C_{ref} can be thought of as "scaling" sand transport, since the higher the value of C_{ref} the more sand is in suspension throughout the bounday layer (see, for example, Green and Black, 1999). The time series of C_{ref} show that a number of resuspension events, as indicated by the vertical blue lines, occurred during the deployment periods. Furthermore, these resuspension events coincided with periods of large waves, thus highlighting the importance of waves in resuspending sand from the seabed at this site. The maximim C_{ref} recorded at site 6 was ~ 0.56 g/l. During calm periods no sand was in suspension.

Figure 3-54B shows that the maximum *SSCm* (muds/silts) measured in the near-bed region at site 6 was slightly less than 0.04 g/l. Peaks in *SSCm* did not always coincide with peaks in H_s, which implies that the increase in *SSCm* was not always driven by local resuspension. Instead, fine suspended sediment may have been advected to the measurement site from some "upstream" location. During calm periods, background *SSCm* was typically around 0.014 g/l, which is close to the lower detection limit of the OBS.

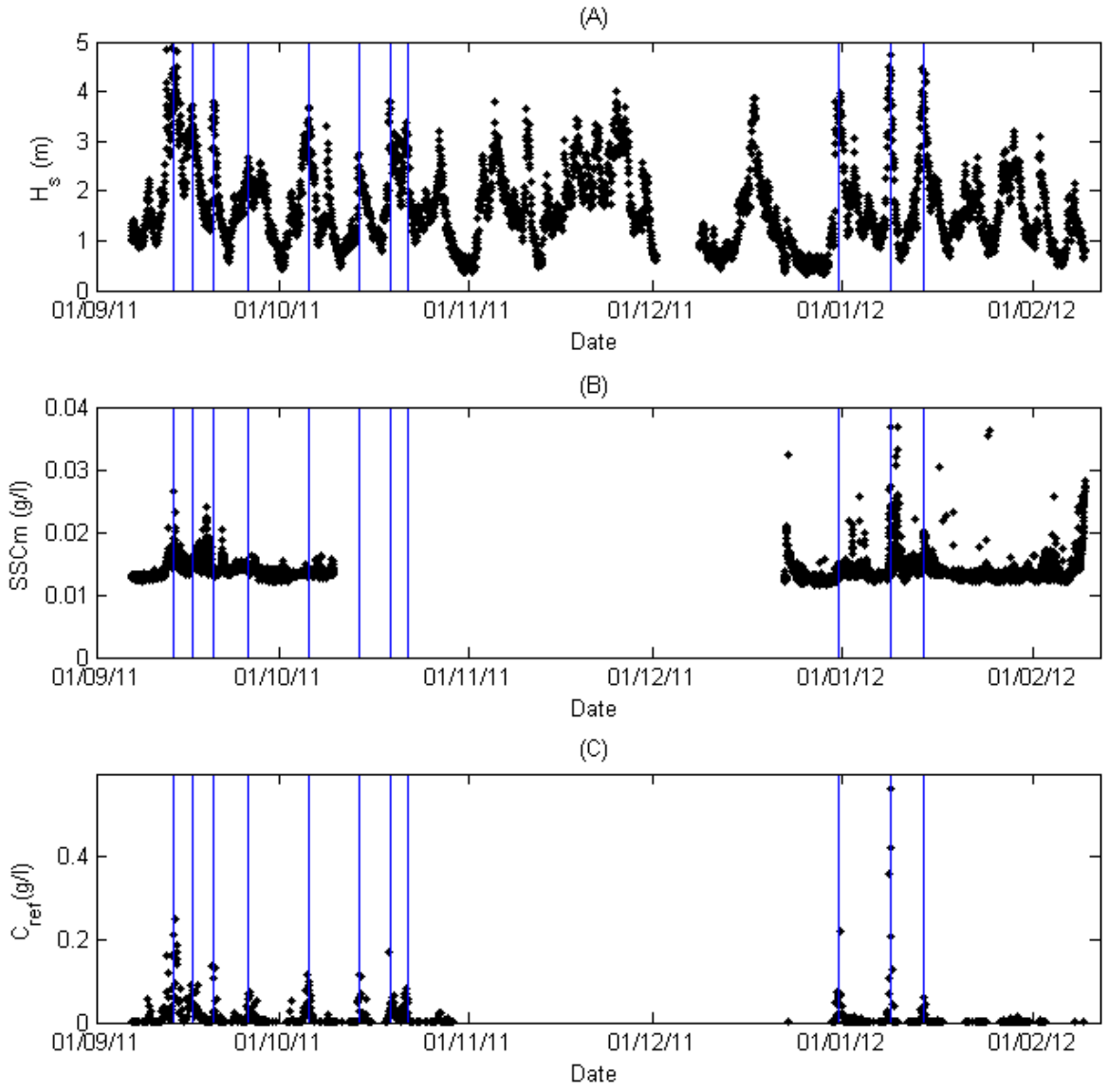

Figure 3-54: Near-bed SSC measurements at site 6 for deployments D1 and D2. Panels (A) significant wave height (H_s), (B) *SSCm*, and (C) C_{ref}.

Site 7 (inshore end of the PPL)

Time series plots of near-bed SSC measurements at site 7 for deployments D1 and D2 are shown in Figure 3-55. The time series of C_{ref} show that a number of resuspension events, as indicated by the vertical blue lines, occurred during the deployment periods. As at site 6, resuspension events coincided with periods of large waves, again highlighting the importance of waves in resuspending sand from the sea bed into the water column. The maximum C_{ref} recorded at site 7 was ~ 1.9 g/l, which was much larger than that measured at site 6. We shall return to this observation shortly, as this requires further discussion. During calm periods no sand was in suspension.

Figure 3-55B shows that the maximum *SSCm* (muds/silts) measured in the near-bed region at site 7 was ~ 0.08 g/l. As at site 6, peaks in *SSCm* did not always coincide with peaks in H_s, which again implies that the increase in *SSCm* was not always driven by local resuspension, and that suspended fine sediment may have been advected through the measurement site

from some “upstream" location. During calm periods, the background *SSCm* was typically around 0.005 g/l, which is close to the lower detection limit of the OBS.

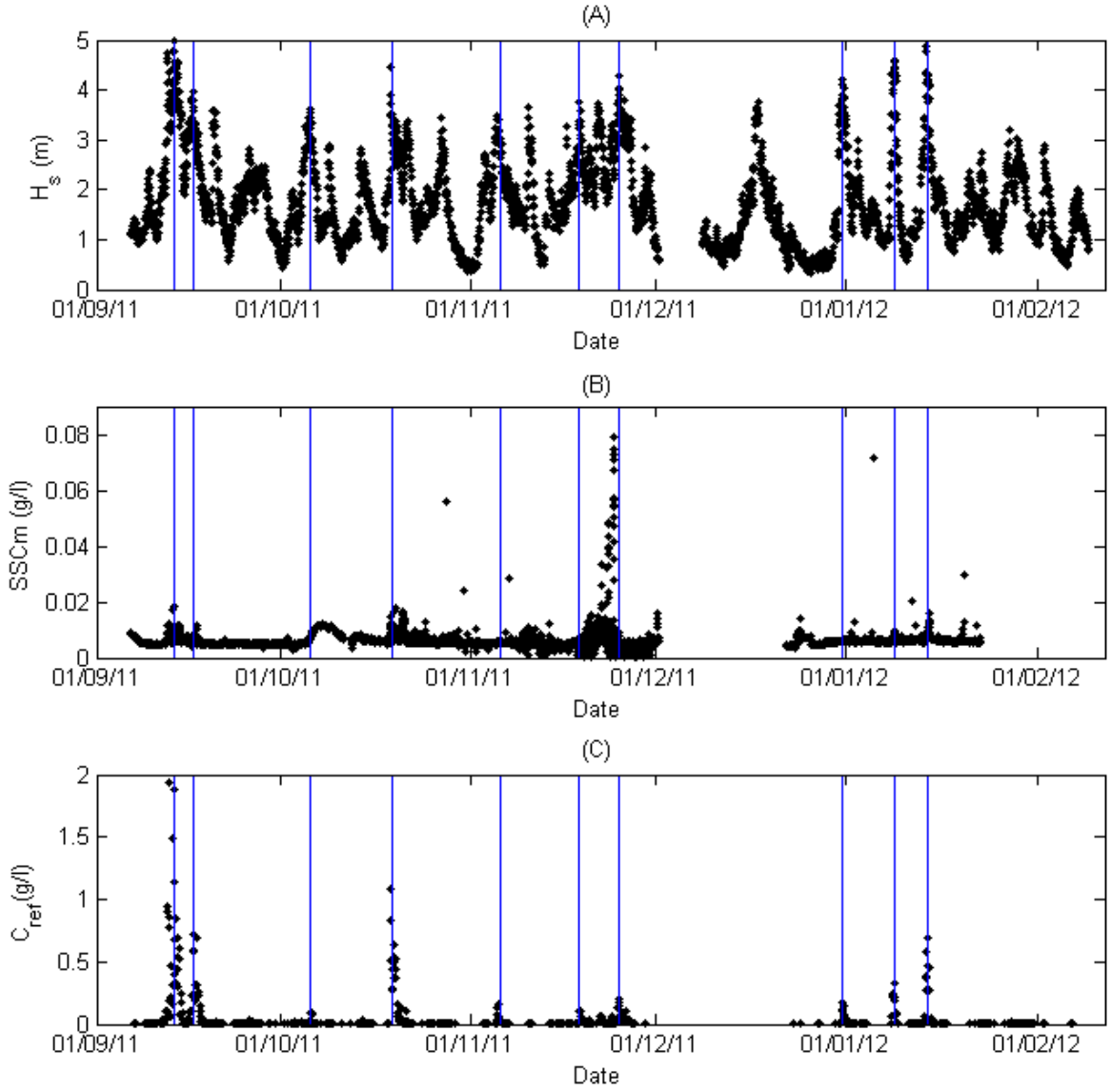

Figure 3-55: Near-bed SSC measurements at site 7 for deployments D1 and D2. Panels: (A) significant wave height (H_s), (B) *SSCm*, and (C) C_{ref}.

The observation that maximum C_{ref} measured at site 7 was larger than maximum C_{ref} measured at site 6 requires explanation. Both sites are subjected to waves of a similar height and period. However, as site 6 is located in shallower water than site 7, the wave-orbital motions that resuspend bed sediments will be greater at site 6 compared to site 7. However, while being an important factor, the magnitude of the wave-orbital motions is only one component that governs the amount of sand in suspension. Another control is the bedform geometry. For instance, Green and Black (1999) showed that given the same (wave) forcing, differences in bedform geometry can produce C_{ref} values that are a factor of 20 times different. Therefore, it is entirely feasible that relatively small differences in bedform geometry are responsible for the differences in maximum values of C_{ref} measured at the two sites.

Figure 3-56 shows an underwater picture of the bedforms at site 7, which clearly shows two distinct regions. The region in the right of the image shows a rippled bed while the region in the left of the image shows a flat bed; there is also an abrupt interface between the rippled and the flat bed. This geological feature is called a sorted-bedform or ripple-scour-depression (Green et al. 2004). A characteristic of this type of feature is that the sediment within the rippled area is coarser than the fine-sands found in the flat-bed region. Complex substrates like this are known to produce complex patterns in sediment resuspension from the seabed.

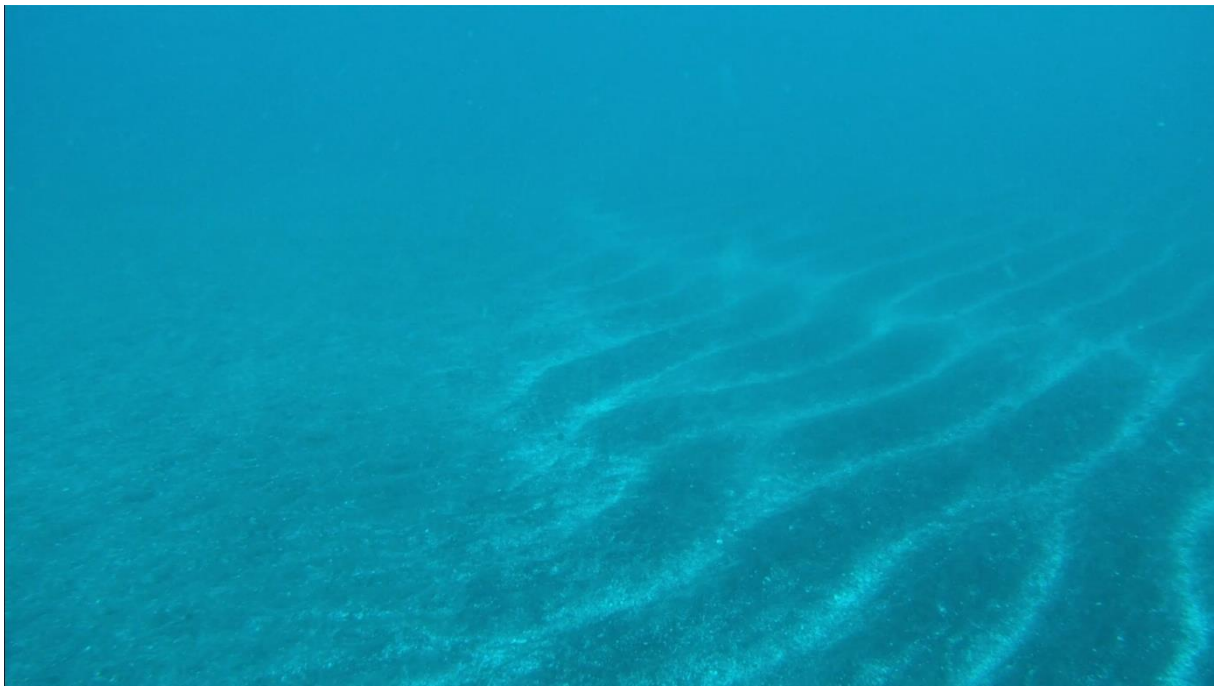

Figure 3-56: Sorted bedforms on seabed at site 7.

Site 8 (SSE of the PPL)

Time series plots of the near-bed SSC measurements at site 8 for deployment D3 are shown in Figure 3-57. The time series of C_{ref} show a number of resuspension events that concide with periods of high winds (proxy for wave height), and thus are most likely to have been driven by waves. The maximim C_{ref} recorded at site 8 was ~ 0.13 g/l, which was much smaller than that measured at sites 6 and 7. During calm periods no sand was in suspension.

Figure 3-57B shows that near-bed *SSCm* at site 8 was generally constant over the entire deployment period. Furthermore, *SSCm* was much less than 0.01 g/l, which is close to the lower detection limit of the OBS.

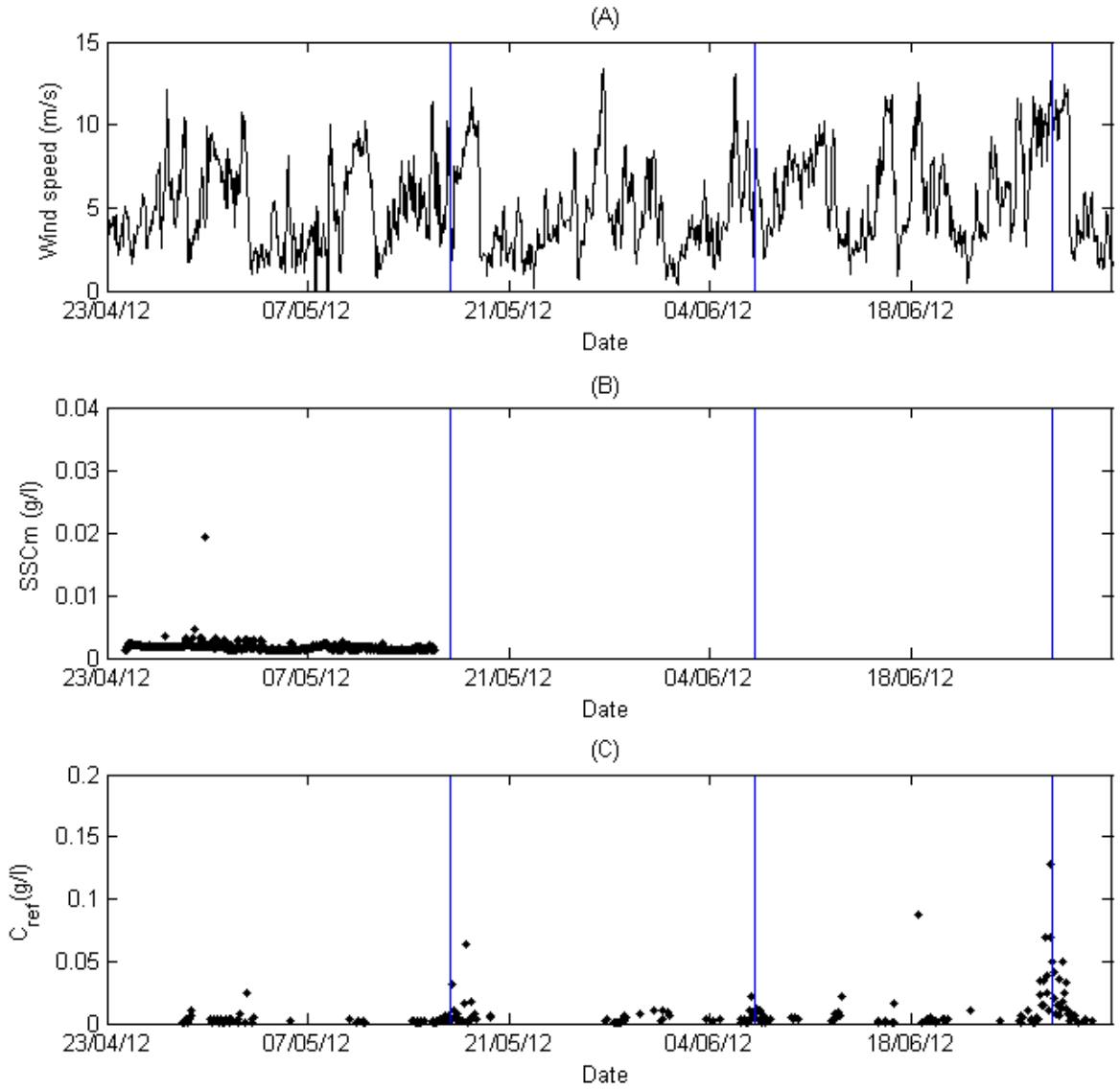

Figure 3-57: Near-bed SSC measurements at site 8 for deployment D3. Panels: (A) wind speed (proxy for H_s as no wave data was collected during D3), (B) *SSCm*, and (C) C_{ref}.

Site 10 (offshore end of the PPL)

Time series plots of the near-bed SSC measurements at site 10 for deployment D3 are shown in Figure 3-58. The time series of C_{ref} show a number of resuspension events that concide with periods of high winds, and thus are most likely to have been driven by waves. The maximim C_{ref} recorded at site 10 was ~0.036 g/l, which was much smaller than that measured at sites 6 and 7. The event that generated a C_{ref} of 0.13 g/l at site 8 was not captured at site 10 as the instrument had stopped logging by the time of the event. During calm periods no sand was in suspension.

Figure 3-58B shows that near-bed *SSCm* at site 10 varied temporally. However, the peaks in *SSCm* typically coincided with peaks in C_{ref}, which suggests that during these periods the OBS may have been responding to the increased *SSCs* and not to any increase in *SSCm*. During calm periods, the background *SSCm* was typically around 0.002 g/l, which is close to the lower detection limit of the OBS.

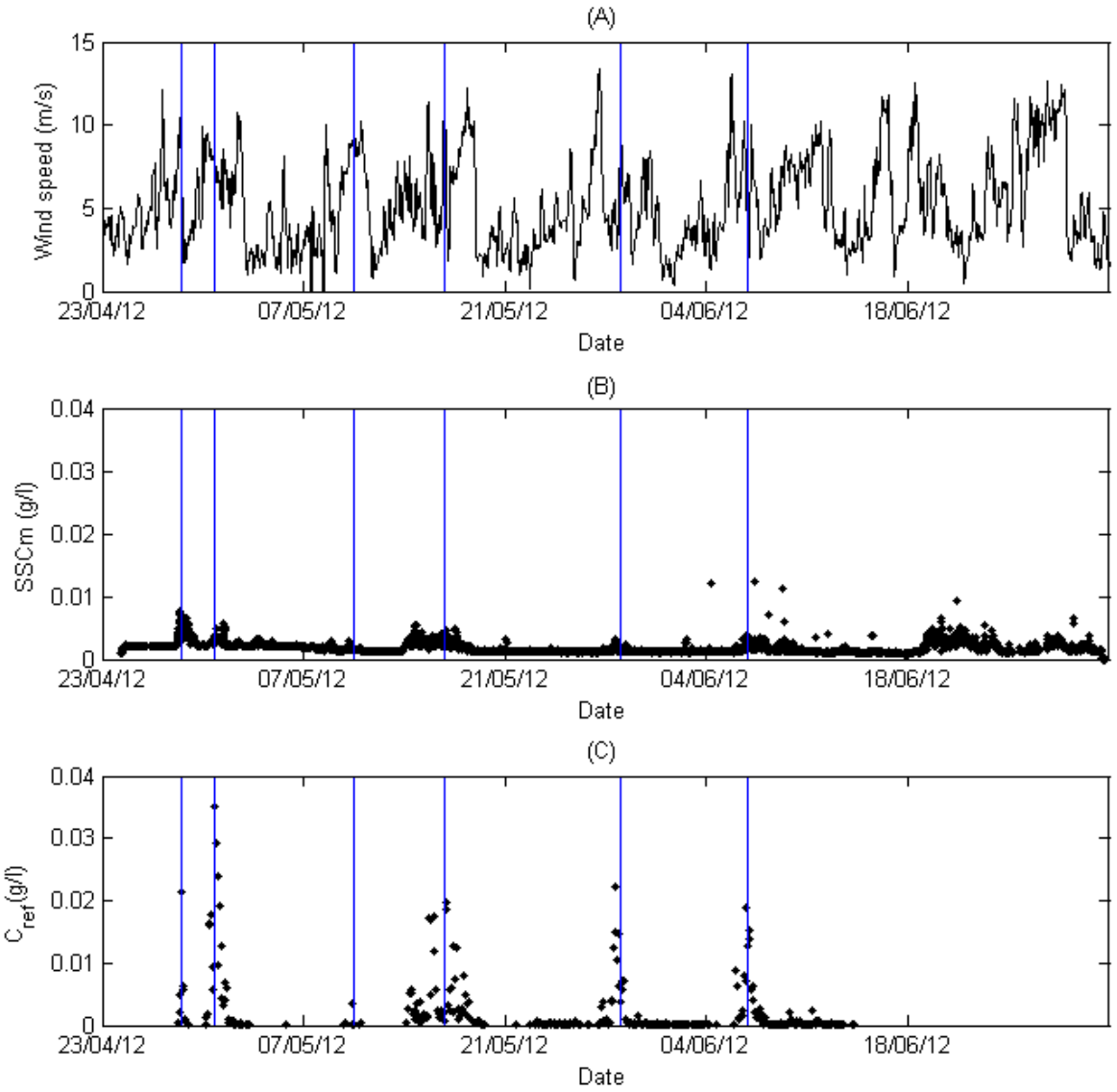

Figure 3-58: Near-bed SSC measurements at site 10 for deployment D3. Panels: (A) wind speed (proxy for H_s as no wave data was collected during D3), (B) *SSCm,* and (C) C_{ref}.

3.6.4 Sand Fluxes

Using the *SSCs* profiles generated from the ABS measurements and the current velocity measurements we are able to estimate the horizontal suspended-sand transport, or flux, (*Q*), which is defined as

$$Q = \int_0^h C_z U_z dz$$

where C_z is the time-averaged suspended-sand concentration at elevation z above the bed (units of kg/m^3), U_z is the time-averaged current speed at elevation *z* above the bed (m/s), *h* is the water depth (m), and the integration is conducted over the entire water column (from *z* = 0 to *z* = *h*). The units of *Q* are kg of sand transported per second per metre width of sea

bed. Note that this is a gross transport, as opposed to a net transport, since we are treating U_z (current speed) is a scalar quantity (i.e., has no directionality).

The integral was evaluated numerically, using the ABS profiles for C_z, and terminating the integral at the level where measured C_z fell below 0.001 g/l. This is a very small concentration, which will give only a very small additional contribution to Q, even when combined with a strong current. C_z typically fell below 0.001 g/l by 0.75 m above the sea bed, which is below the lowest measurement bin of the ADCP. Therefore, U_z was simply set to the current speed recorded in the ADCP bin closest to the sea bed.

Q for sites 6, 7, 8 and 10 are shown in Figure 3-59, Figure 3-60, Figure 3-61 and Figure 3-62, respectively. In each of these figures, the three events (labelled E1, E2 and E3) that generated the three largest sediment fluxes have been identified.

Integrating Q (with respect to time) over the duration of an event yields the total mass of sand per unit width of sea bed transported over that event. The gross transport so calculated, along with information about Q, is shown in Table 3-23. In the final column of the table, the volume of sand transported over each of the three largest events is shown. For this, gross transport expressed as sediment mass was converted to volume of sediment using a bulk density of 1600 kg/m^3.

Table 3-23 shows that the most sediment transported during any one event was 3355 kg/m, which equates to 2.1 cubic metres of mobile sediment per metre of sea bed. This occurred at site 7 during event E1. While this event transported the greatest amount of sediment, it did not produce the largest instantaneous sediment flux, which was 0.13 kg/s/m, measured at site 6 during E3. Figure 3-59 shows that the largest instantaneous sediment flux was driven by the largest current speeds experienced during the entire field programme. The maximum instantaneous sediment fluxes measured at site 8 and 10 were several orders of magnitude less than those measured at sites 6 and 7. Thus, the gross sand transport during events at sites 8 and 10 was considerably smaller than the gross sand transport at sites 6 and 7.

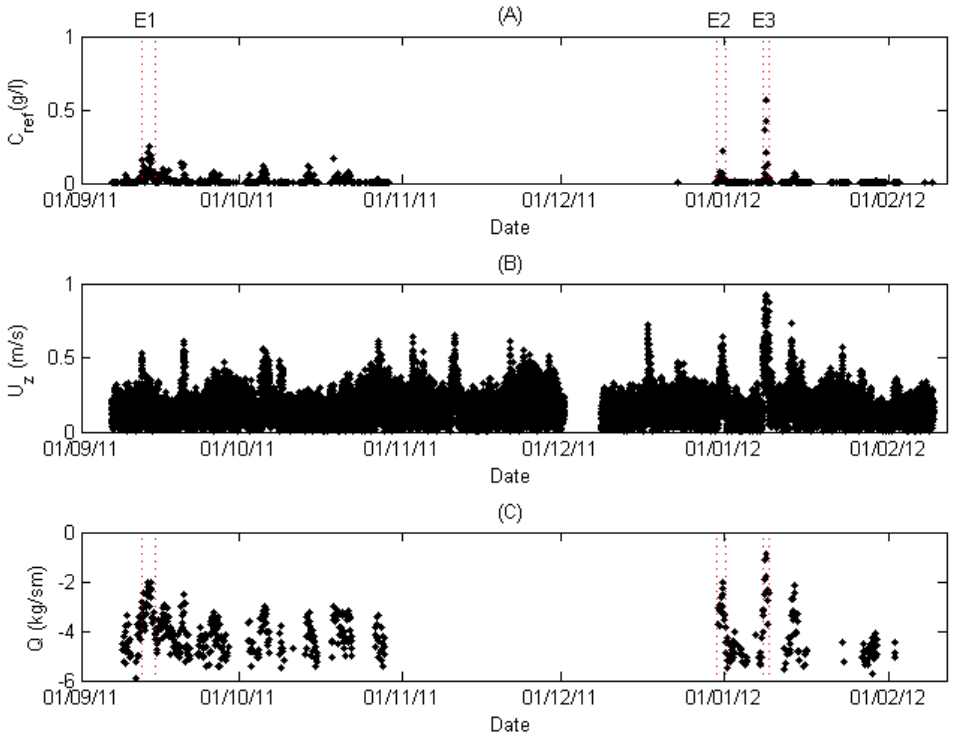

Figure 3-59: Suspended-sand flux at Site 6 for deployments D1 and D2. Panels: (A) C_{ref}, (B) U_z and (c) Q (plotted on a log scale e.g., -2 is 10^{-2} or 0.01).

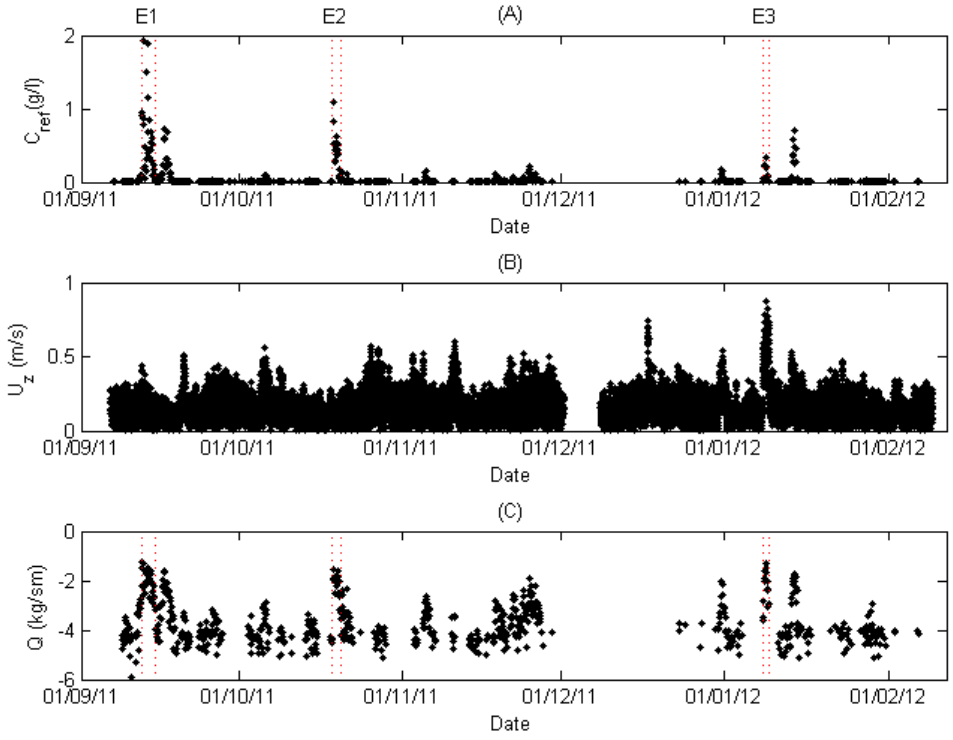

Figure 3-60: Suspended-sand flux at Site 7 for deployments D1 and D2. Panels: (A) C_{ref}, (B) U_z and (c) Q (plotted on a log scale).

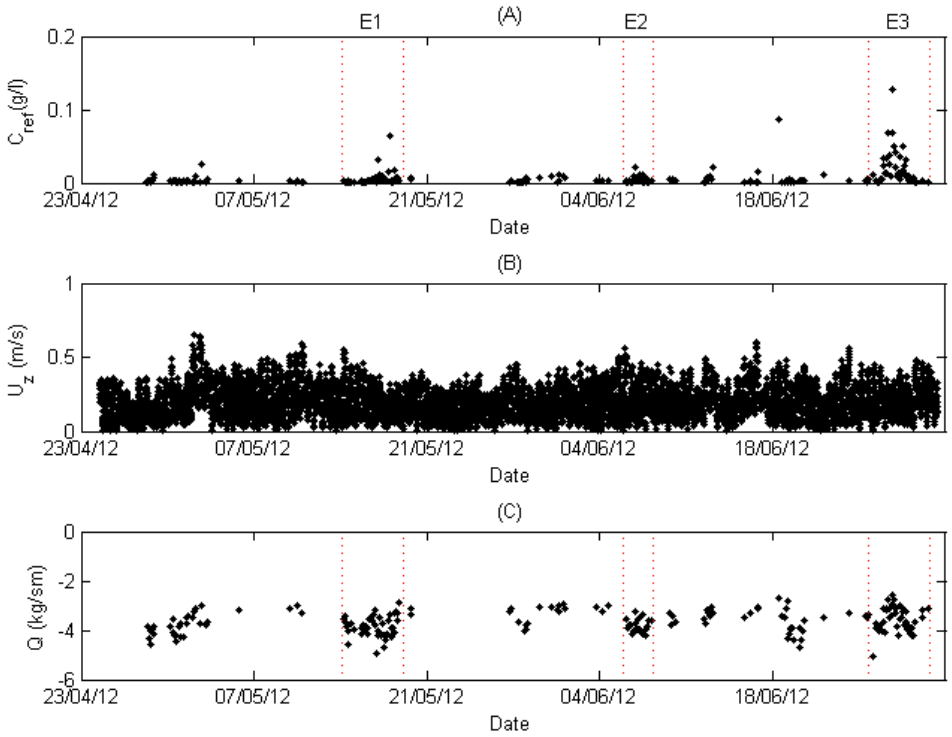

Figure 3-61: Suspended-sand flux at Site 8 for deployment D3. Panels: (A) C_{ref}, (B) U_z and (c) Q (plotted on a log scale).

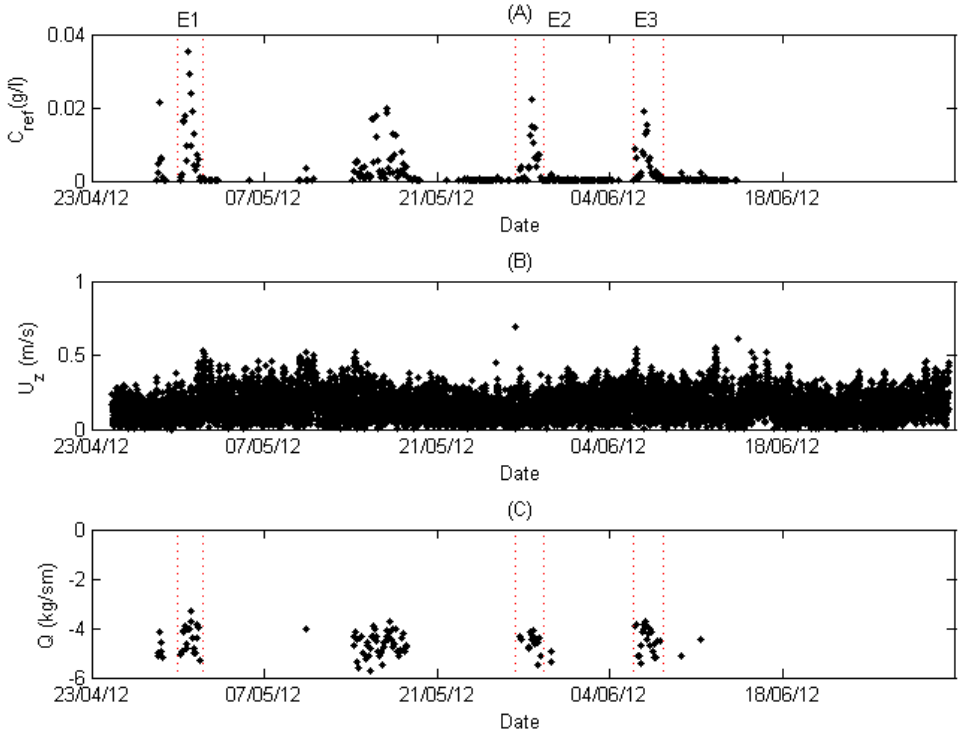

Figure 3-62: Suspended-sand flux at Site 10 for deployment D3. Panels: (A) C_{ref}, (B) U_z and (c) Q (plotted on a log scale).

Site	Event	Duration (days)	Maximum instantaneous flux (Q) (kg/ms)	Gross mass flux over the event (kg/m)	Gross volume flux over the event (m^3/m)
6	E1	2.3	0.0099	494	0.309
6	E2	1.5	0.0099	202	0.126
6	E3	1.0	0.1336	2405	1.503
7	E1	2.4	0.0558	3355	2.097
7	E2	1.5	0.0279	1210	0.756
7	E3	1.0	0.0519	1254	0.783
8	E1	4.5	0.0013	70	0.044
8	E2	2.1	0.0005	33	0.020
8	E3	4.6	0.0026	173	0.108
10	E1	1.8	0.0004	11	0.007
10	E2	2.2	0.0001	4	0.002
10	E3	2.2	0.0002	9	0.006

Table 3-23: Summary of suspended-sand fluxes for all sites.

4 Summary

A comprehensive set of current, wave and suspended-sediment measurements has been obtained in the South Taranaki Bight (STB) during three deployment periods which cover an approximate 7-month period 09 September 2011 to 01 July 2012 (excluding gaps between deployments). This report presents and synthesises the field measurements.

Current velocities were measured at five sites in the STB and represent a significant dataset in their own right. The data show the prevailing patterns of circulation in the STB. Tidal currents account for a significant proportion of the measured currents at all sites, with the proportion of variance explained by the tidal constituents ranging from 40% at site 5 to 78 % at site 7. The amplitude (maximum speed) of the main twice-daily lunar (M2) or average tide ranged between 0.13 m/s at site 5 to 0.25 m/s at site 8. At all sites the M2 tide was oriented in the SE–NW direction (parallel with the coastline). Note: higher velocities will occur during spring tides.

The tidal currents, however, only tell part of the story. Currents in the STB were substantially affected by meteorological conditions. Large current speeds of around 1 m/s were measured on a number of occasions during periods of high winds. Winds blowing from the W and the SE sectors had the most pronounced influence on currents. Winds not only increased current speeds but also greatly altered current direction. During strong winds, currents could set in a constant direction for more than 24 hours; during calm conditions, currents reversed approximately every 6.2 hours with the tides re-asserting dominance.

At sites 5, 6, 8 and 10 during periods of light winds the prevailing current drift was towards the SE; during calm periods at site 7 the prevailing current drift was towards the NE. Drift directions were significantly altered by moderate to strong SE winds which turned the drift towards the NW. During times of moderate to strong W to NW winds, the prevailing SE drift was enhanced.

These results have implications for the hydrodynamic and sediment modelling as both tidal and meteorological forcing are responsible for observed water movements in the STB. The current measurements provide a comprehensive, reliable and consistent dataset for the calibration and verification of a hydrodynamic model.

Waves were measured at eight sites in the STB, in water depths ranging from 50 m to 9 m near the coast. Wave measurements in both deep and shallow water have captured the transformation of the wave train as it moves from deep to shallow water.

The wave data clearly show that the STB is a high-energy environment. At the deep sites, significant wave heights in excess of 4 m were routinely observed. The highest significant wave height of 7.1 m was recorded on 03/03/2012 at 05:40. The spectral mean wave period at the surface at that time was 8.4 seconds and the waves arrived from the south. Locals winds at Whanganui preceding this weather-bomb event were strong (~17 m/s or 61 km/hr) and blew from the SSW.

Waves greater than 2 m in height arrived mainly from either the S–SSE or from the SW–WSW sectors. There was a reduction in wave height moving from the offshore deeper sites into the shallower sites close to the shoreline. There was also a reduction in wave height

moving in a S–SE direction, caused by sheltering of the prevailing SW to WSW swell by the tip of the South Island.

The wave measurements provide a comprehensive, reliable and consistent dataset for the calibration and verification of a wave model.

Temperature and salinity measurements show that the water column in the STB was generally well mixed with only small vertical differences in temperature and salinity. Lower salinity is likely to be found in the vicinity of major rivers in the STB (e.g., Patea, Waitotara and Whanganui).

Concentrations in the water column of suspended sands and suspended fine sediments (clays, silts and muds) were made at several sites and heights above the bed within the STB.

In the near-surface waters, the maximum *SSCm* (muds, silts, clays) was 0.025 g/l, which was recorded at site 5. At sites 5, 6 and 7 *SSCm* varied over the deployment period, with peaks in *SSCm* tending to occur during or just after periods of significant rainfall. At these times it is likely that rivers were discharging fine sediments into the STB, which were then being transported in suspension through the measurement site. Some of the peaks in *SSCm* also coincided with times of large H_s. While it is possible that large waves resuspended fine sediments from the sea bed and increased *SSCm* near the surface, it is also possible that the increase resulted from an increase in optical backscatter generated by the entrainment of air bubbles into the water column by an energetic sea. For most of the time, the near-surface background *SSCm* was typically less than 0.01 g/l, which is close to the lower detection limit of the OBS.

Near the sea bed, the maximum *SSCm* was 0.08 g/l, which was recorded at site 7. Peaks in *SSCm* near the bed did not always coincide with peaks in wave height, which implies that the increase in *SSCm* was not always driven by local resuspension. Instead, fine suspended sediment may have been advected through the measurement site from some “upstream" location.. During the times in which the peaks in *SSCm* did coincide with peaks in wave heights, the OBS may have been responding to the increased *SSCs* and not to any increase in *SSCm*. During calm periods, background *SSCm* at the bed was similar to the background *SSCm* at the surface (~ 0.01 g/l), which is close to the lower detection limit of the OBS.

When there was any sand in suspension, *SSCs* close to the sea bed was typically much greater than *SSCm* . The largest suspended-sand reference concentration (i..e, *SSCs* at the sea bed) was 1.9 g/l, which was measured at site 7. At all sites, periods of increased *SSCs* coincided with periods of large waves, thus highlighting the importance of waves in resuspending sand from the seabed in the STB. During calm periods, no sand was found to be in suspension. *SSCs* at sites 6 and 7 were much larger than *SSCs* at sites 8 and 10.

Using the measurements of *SSCs* and current velocity, horizontal suspended-sand flux (*Q*) was estimated. Over the duration of the largest event, 3355 kg of sand per metre width of sea bed was transported in suspension by currents. This equates to a volume of ~ 2 m^3 of sand transported per metre width of sea bed. These are gross transport rates.

Overall, the field dataset provides a coherent picture of currents, waves and suspended-sediment concentrations in the STB. The datasets can be used with confidence in the

development of numerical models of current flows, waves and suspended-sediment plume dispersion in the STB.

Information relating to TTR's additional scientific work undertaken since 2014 has been provided and the conclusions is this report remain valid.

5 Acknowledgements

We thank the many people who assisted in the field, especially Matt McGlone, Braden Crocker, Pete Notman and Mike Carson. We would also like to thank Dr Mal Green for his review of this report.

6 References

Green, M.O., Black, K.P. (1999) Suspended-sediment reference concentration under waves: field observations and critical analysis of two predictive models. *Coastal Engineering*, 38(3): 115–141.

Green, M.O., Vincent, C.E., Trembanis, A.C. (2004) Suspension of coarse and fine on a wave-dominated shoreface, with implications for the development of rippled scour depressions. *Continental Shelf Research,* 24(3): 317–335.

Hurther, D., Thorne, P.D., Bricault, M., Lemmin, U., Barnoud, J.-M. (2011) A multi-frequency Acoustic Concentration and Velocity Profiler (ACVP) for boundary layer measurements of fine-scale flow and sediment transport processes. *Coastal Engineering*, 58(7): 594–605.

MacDiarmid, A., Anderson, O., Beaumont, J., Gorman, R., Hancock, N., Julian, K., Schwarz, J., Stevens, C., Sturman, J., Thompson, D., Torres, L. (2010) South Taranaki Bight iron sand mining baseline environmental study. *NIWA client report* WLG2010-46.

Moate, B.D., Thorne, P.D. (2012) Interpreting acoustic backscatter from suspended sediments of different and mixed mineralogical composition. *Continental Shelf Research ,* 46: 67–82.

Teledyne RD Instruments Inc. WAVES PRIMER: Wave Measurments and the RDI ADCP Waves Array Technique: 30.

Thorne, P.D., Hanes, D.M. (2002) A review of acoustic measurement of small-scale sediment processes. *Continental Shelf Research*, 22(4): 603–632.

Appendix A Additional deployment information

Site #	Deployment #	ID	Instrument	Serial No. (freq)	Time period (NZST) (in water)	Duration (days)	Elevation of first bin (mab)	Vertical bin size (m)	Ibb (mins)	BD (mins)	Sampling rate (Hz)	Mean water level (m)
5	1	S5/D1	ADCP	6270 (600kHz)	06/09/11 11:30 to 09/11/11 08:45	64	2.1	0.5	15	2	2	26
5	2	S5/D2	ADCP	16530 (600kHz)	08/12/11 07:45 to 22/01/12 08:00	45	2.1	0.5	15	2	2	26
6	1	S6/D1	ADCP	10842 (600kHz)	06/09/11 16:30 to 01/12/11 13:15	86	2.1	0.5	15	2	2	23
6	2	S6/D2	ADCP	10842 (600kHz)	08/12/11 12:30 to 09/02/12 12:15	63	2.1	0.5	15	2	2	23
7	1	S7/D1	ADCP	7900 (600kHz)	06/09/11 14:15 to 01/12/11 10:15	86	2.1	0.5	15	2	2	31
7	2	S7/D2	ADCP	16525 (600kHz)	08/12/11 10:15 to 09/02/12 10:00	63	2.1	0.5	15	2	2	31
8	3	S8/D3	ADCP	7900 (600kHz)	24/04/12 11:45 to 01/07/12 08:30	68	3.5	2	15	2	2	45
10	3	S10/D3	ADCP	4876 (300kHz)	24/04/12 16:20 to 01/07/12 10:20	68	2.7	0.5	10	2	2	42

Table A-1: Additional deployment information for current measurements. List of symbols: mab = metres above bed; Ibb = interval between bursts and BD = burst duration.

Site #	Deployment #	ID	Instrument	Instrument serial No. (freq)	Period (in water)	Duration (days)	Ibb (mins)	BD (mins)	Sampling rate (Hz)	Mean water level (m)
1	1	S1/D1	DWG	2608 (n/a)	07/09/11 14:00 to 04/11/11 14:00	58	60	17.1	0.5	12
1	2	S1/D2	DWG	2608 (n/a)	08/12/11 15:00 to 08/02/12 13:30	62	90	17.1	0.5	12
2	1	S2/D1	DWG	914 (n/a)	07/09/11 15:00 to 21/10/11 21:00	44	60	17.1	0.5	15
2	2	S2/D2	DWG	914 (n/a)	08/12/11 15:00 to 08/02/12 13:30	62	90	17.1	0.5	15
3	1	S3/D1	DWG	2607 (n/a)	07/09/11 16:00 to 04/11/11 14:00	58	60	17.1	0.5	9
3	2	S3/D2	DWG	2408 (n/a)	09/12/11 10:30 to 08/02/12 12:00	61	90	17.1	0.5	11
4	1	S4/D1	DWG	2312 (n/a)	07/09/11 17:00 to 04/11/11 14:00	58	60	17.1	0.5	13
4	2	S4/D2	DWG	2312 (n/a)	09/12/11 09:00 to 08/02/12 12:00	61	90	17.1	0.5	11
5	1	S5/D1	ADCP	6270 (600kHz)	06/09/11 11:30 to 09/11/11 08:45	64	180	20	2	26
5	2	S5/D2	ADCP	16530 (600kHz)	08/12/11 07:45 to 22/01/12 08:00	45	60	20	2	26
6	1	S6/D1	ADCP	10842 (600kHz)	06/09/11 16:30 to 01/12/11 13:15	86	60	20	2	23
6	2	S6/D2	ADCP	10842 (600kHz)	08/12/11 12:30 to 09/02/12 12:15	63	60	20	2	23
7	1	S7/D1	ADCP	7900 (600kHz)	06/09/11 14:15 to 01/12/11 10:15	86	60	20	2	31
7	2	S7/D2	ADCP	16525 (600kHz)	08/12/11 10:15 to 09/02/12 10:00	63	60	20	2	31
9	1*	S9	WRB		21/09/11 19:40 to 23/04/12 03:40	214	30	24	4	>50

Table A-2: Additional deployment information for wave measurements. List of symbols: mab = metres above bed; Ibb = interval between bursts and BD = burst duration.

Site #	Deployment #	ID	Instrument	Serial No. (freq)	Time period (NZST) (in water)	Duration (days)	Elevation above bed (mab)	Ibb (mins)	Mean water level (m)
7	1	S7/D1	MicroCAT (Cand T)	7284	08/09/11 15:00 to 19/09/11 06:32	11	22	2	31
7	1	S7/D1	MicroCAT (Cand T)	7285	No data: Battery failure	-	2	2	31
7	1	S7/D1	RBR (T)	19982	22/09/11 12:00 to 08/12/11 09:00	77	15	1	31
7	1	S7/D1	RBR (T)	19994	22/09/11 12:00 to 08/12/11 09:00	77	9	1	31
7	2	S7/D1	MicroCAT (Cand T)	7284	22/12/11 07:30 to 11/03/12 15:58	80	22	2	31
7	2	S7/D1	MicroCAT (Cand T)	7285	22/12/11 07:30 to 11/03/12 15:58	80	2	2	31
7	2	S7/D1	RBR (T)	19982	22/12/11 07:30 to 11/03/12 16:00	80	15	1	31
7	2	S7/D1	RBR (T)	19994	22/12/11 07:30 to 11/03/12 16:00	80	9	1	31
9	1	S9/D1	MicroCAT (Cand T)	7280	08/09/11 14:46 to 08/12/11 11:28	91	3	2	>50
9	2	S9/D2	MicroCAT (Cand T)	7280	No data: instrument not recovered	-	3	2	>50
10	3	S10/D3	MicroCAT (Cand T)	5675	No data: instrument damaged when trawled	-	40	2	42
10	3	S10/D3	MicroCAT (Cand T)	7284	22/05/12 15:00 to 16/06/2012 10:28	25	22	2	42
10	3	S10/D3	MicroCAT (Cand T)	7285	22/05/12 15:00 to 16/06/2012 10:28	25	2	2	42
10	3	S10/D3	RBR (T)	19998	No data: instrument damaged when trawled	-	28	1	42
10	3	S10/D3	RBR (T)	19996	No data: instrument damaged when trawled	-	15	1	42
10	3	S10/D3	RBR (T)	19997	No data: instrument damaged when trawled	-	9	1	42

Table A-3: Additional deployment information for temperature and salinity measurements. List of symbols: mab = metres above bed and ibb = interval between bursts.

Site #	Deployment #	ID	Instrument	Instrument serial No.	Time period (NZST) (in water)	Duration (days)	Ibb (mins)	BD (mins)	Sampling rate (Hz)	Mean water level (m)
5	1	S5/D1	OBS -near-surface	10295	06/09/11 10:45 to 25/10/11 17:45	49	15	1.7	10	26
5	2	S5/D2	OBS -near-surface	10295	22/12/11 06:00 to 08/02/11 12:40	48	20	1.7	10	26
6	1	S6/D1	ABS	ABS#2	06/09/11 18:00 to 29/10/11 12:00	53	120	15	80	23
6	1	S6/D1	OBS -near bed	11871	06/09/11 16:30 to 09/10/11 20:00	33	15	1.7	10	23
6	1	S6/D1	OBS -near-surface	10600	06/09/11 16:15 to 12/09/11 11:00	6	15	1.7	10	23
6	2	S6/D2	ABS	ABS#2	22/12/11 11:00 to 09/02/12 11:00	49	120	15	80	23
6	2	S6/D2	OBS -near bed	11871	22/12/11 10:45 to 09/02/12 12:15	49	15	1.7	10	23
6	2	S6/D2	OBS -near-surface	10600	22/12/11 11:00 to 09/02/12 11:00	49	20	1.7	10	23
7	1	S7/D1	ABS	ABS#1	06/09/11 18:00 to 01/12/11 10:00	86	120	15	80	31
7	1	S7/D1	OBS -near bed	11870	06/09/11 14:00 to 01/12/11 09:45	86	15	1.7	10	31
7	1	S7/D1	OBS -near-surface	10597	06/09/11 14:00 to 23/10/11 11:45	47	15	1.7	10	31
7	2	S7/D2	ABS	ABS#1	22/12/11 09:00 to 09/02/12 09:00	49	120	15	80	31
7	2	S7/D2	OBS -near bed	11870	22/12/11 07:30 to 22/01/12 16:45	31	15	1.7	10	31
7	2	S7/D2	OBS -near-surface	10597	Instrument lost (No data)		15	1.7	10	31
8	3	S8/D3	ABS	ABS#1	24/04/12 12:00 to 01/07/12 08:00	68	120	15	80	45
8	3	S8/D3	OBS -near bed	11870	24/04/12 06:00 to 15/05/12 19:30	22	15	1.7	10	45
8	3	S8/D3	OBS -near-surface	10600	24/04/12 13:45 to 12/06/12 20:15	49	15	1.7	10	45
10	3	S10/D3	ABS	ABS#2	24/04/12 16:00 to 14/06/12 09:00	51	120	15	80	
10	3	S10/D3	OBS -near bed	11871	24/04/12 06:00 to 01/07/12 17:15	68	15	1.7	10	
10	3	S10/D3	OBS -near-surface	10295	24/04/12 17:00 to 09/05/12 20:30	15	15	1.7	10	

Table A-4: Additional deployment information for SSC measurements. List of symbols: mab = metres above bed; ibb = interval between bursts and BD = burst duration.

Appendix B Tidal constituents

S5/D1

	Frequency (degrees/h)	Amplitude (m/s)	Phase (°; NZST)	Orientation (°True)
K1	15.04107	0.026 ± 0.011	87.3 ± 24.0	174.0 ± 16.6
N2	28.43973	0.029 ± 0.004	159.8 ± 8.2	163.5 ± 10.3
M2	28.98410	0.131 ± 0.005	190.3 ± 2.1	156.8 ± 2.4
S2	30.00000	0.022 ± 0.004	189.9 ± 15.6	150.5 ± 14.7
M4	57.96821	0.006 ± 0.002	129.5 ± 25.8	5.1 ± 21.6

S5/D2

	Frequency (degrees/h)	Amplitude (m/s)	Phase (°; NZST)	Orientation (°True)
K1	15.0411	0.029 ± 0.012	130.3 ± 25.5	160.0 ± 18.5
N2	28.4397	0.027 ± 0.007	164.4 ± 15.0	156.0 ± 11.9
M2	28.9841	0.118 ± 0.006	182.4 ± 3.4	160.9 ± 2.4
S2	30.0000	0.020 ± 0.006	164.5 ± 34.3	173.8 ± 28.3

S6/D1

	Frequency (degrees/h)	Amplitude (m/s)	Phase (°; NZST)	Orientation (°True)
O1	13.94304	0.019 ± 0.008	91.3 ± 29.0	144.8 ± 25.8
K1	15.04107	0.035 ± 0.008	97.1 ± 14.6	150.8 ± 13.3
MU2	27.96821	0.018 ± 0.005	132.3 ± 16.1	146.3 ± 12.5
N2	28.43973	0.056 ± 0.005	154.6 ± 4.9	142.8 ± 4.3
M2	28.98410	0.216 ± 0.005	185.1 ± 1.2	138.6 ± 1.1
S2	30.00000	0.032 ± 0.005	170.9 ± 9.9	134.5 ± 11.0
SK3	45.04107	0.010 ± 0.002	204.8 ± 12.1	162.2 ± 9.6
M4	57.96821	0.012 ± 0.002	312.2 ± 8.6	143.1 ± 7.8
MS4	58.98410	0.007 ± 0.002	337.8 ± 16.0	143.9 ± 15.9
S4	60.00000	0.004 ± 0.002	207.7 ± 31.0	162.6 ± 20.0

S6/D2

	Frequency (degrees/h)	Amplitude (m/s)	Phase (°; NZST)	Orientation (°True)
O1	13.9430	0.017 ± 0.008	80.2 ± 27.7	139.2 ± 27.7
K1	15.0411	0.045 ± 0.008	116.1 ± 11.6	141.1 ± 10.3
N2	28.4397	0.056 ± 0.007	151.8 ± 7.6	142.8 ± 6.5
M2	28.9841	0.211 ± 0.007	181.7 ± 1.9	137.8 ± 1.5
S2	30.0000	0.030 ± 0.009	164.1 ± 18.7	143.7 ± 17.4
SK3	45.0411	0.013 ± 0.004	250.4 ± 17.5	166.9 ± 11.7
M4	57.9682	0.011 ± 0.003	282.5 ± 15.3	143.1 ± 14.1

S7/D1

	Frequency (degrees/h)	Amplitude (m/s)	Phase (°; NZST)	Orientation (°True)
O1	13.94304	0.016 ± 0.007	99.8 ± 31.9	147.7 ± 27.8
K1	15.04107	0.033 ± 0.007	98.4 ± 13.5	149.3 ± 13.0
MU2	27.96821	0.015 ± 0.006	137.3 ± 21.1	150.6 ± 20.1
N2	28.43973	0.055 ± 0.005	158.4 ± 5.5	141.7 ± 5.9
M2	28.98410	0.215 ± 0.006	186.6 ± 1.6	138.1 ± 1.3
S2	30.00000	0.032 ± 0.006	173.6 ± 9.9	135.5 ± 9.6
SK3	45.04107	0.008 ± 0.002	190.7 ± 20.3	166.0 ± 12.2
M4	57.96821	0.005 ± 0.002	249.2 ± 26.2	150.1 ± 25.3
MS4	58.98410	0.012 ± 0.002	299.7 ± 10.1	141.3 ± 10.8
S4	60.00000	0.005 ± 0.002	204.4 ± 31.3	141.6 ± 27.4

S7/D2

	Frequency (degrees/h)	Amplitude (m/s)	Phase (°; NZST)	Orientation (°True)
O1	13.9430	0.020 ± 0.008	85.9 ± 23.6	137.7 ± 25.9
K1	15.0411	0.045 ± 0.007	116.5 ± 9.9	139.5 ± 10.6
N2	28.4397	0.055 ± 0.008	152.2 ± 8.1	141.8 ± 8.2
M2	28.9841	0.205 ± 0.007	181.9 ± 2.1	138.8 ± 2.1
S2	30.0000	0.026 ± 0.008	168.1 ± 24.7	144.3 ± 20.4
SK3	45.0411	0.011 ± 0.005	241.5 ± 27.7	168.7 ± 14.7
M4	57.9682	0.012 ± 0.003	284.5 ± 13.7	136.0 ± 11.8

S8/D3

	Frequency (degrees/h)	Amplitude (m/s)	Phase (°; NZST)	Orientation (°True)
O1	13.94304	0.012 ± 0.005	84.8 ± 30.1	160.2 ± 27.4
K1	15.04107	0.038 ± 0.005	107.1 ± 7.6	139.3 ± 7.5
N2	28.43973	0.065 ± 0.005	166.5 ± 5.2	136.6 ± 5.3
NU2	28.51258	0.012 ± 0.005	164.9 ± 26.5	136.6 ± 23.9
M2	28.98410	0.248 ± 0.005	193.6 ± 1.2	133.2 ± 1.2
S2	30.00000	0.036 ± 0.006	189.4 ± 9.5	136.2 ± 9.2
M3	43.47616	0.006 ± 0.002	273.8 ± 24.9	159.1 ± 21.8
MK3	44.02517	0.007 ± 0.003	157.4 ± 26.6	150.3 ± 22.3
M4	57.96821	0.008 ± 0.002	296.9 ± 12.9	142.9 ± 13.7

	S10/D3			
	Frequency (degrees/h)	**Amplitude (m/s)**	**Phase (°; NZST)**	**Orientation (°True)**
K1	15.0411	0.037 ± 0.007	103.3 ± 11.4	138.9 ± 11.2
N2	28.4397	0.056 ± 0.007	162.6 ± 7.0	142.8 ± 6.8
M2	28.9841	0.200 ± 0.007	189.2 ± 2.3	138.4 ± 1.8
S2	30.0000	0.025 ± 0.007	156.4 ± 19.0	148.6 ± 17.2
M3	43.4762	0.006 ± 0.002	270.8 ± 27.8	163.9 ± 27.5
M4	57.9682	0.007 ± 0.002	289.0 ± 21.7	142.5 ± 21.1

Appendix C Instrument calibrations

OBS Calibration

Each sensor gain and offset were determined by calibrating the sensor against a series of test suspensions of a known concentration in the laboratory. The sediment used in the calibration came from bed-sediments collected near the mouth of the Whanganui River. Reflecting the greater sensitivity to fine sediments, the collected sediment was sieved through a 63-micron sieve to form a slurry of fine sediment, and the slurry was used in calibration process. A linear regression was fitted to the calibration dataset (sensor output versus reference suspended solids concentration) to determine the sensor's gain and offset.

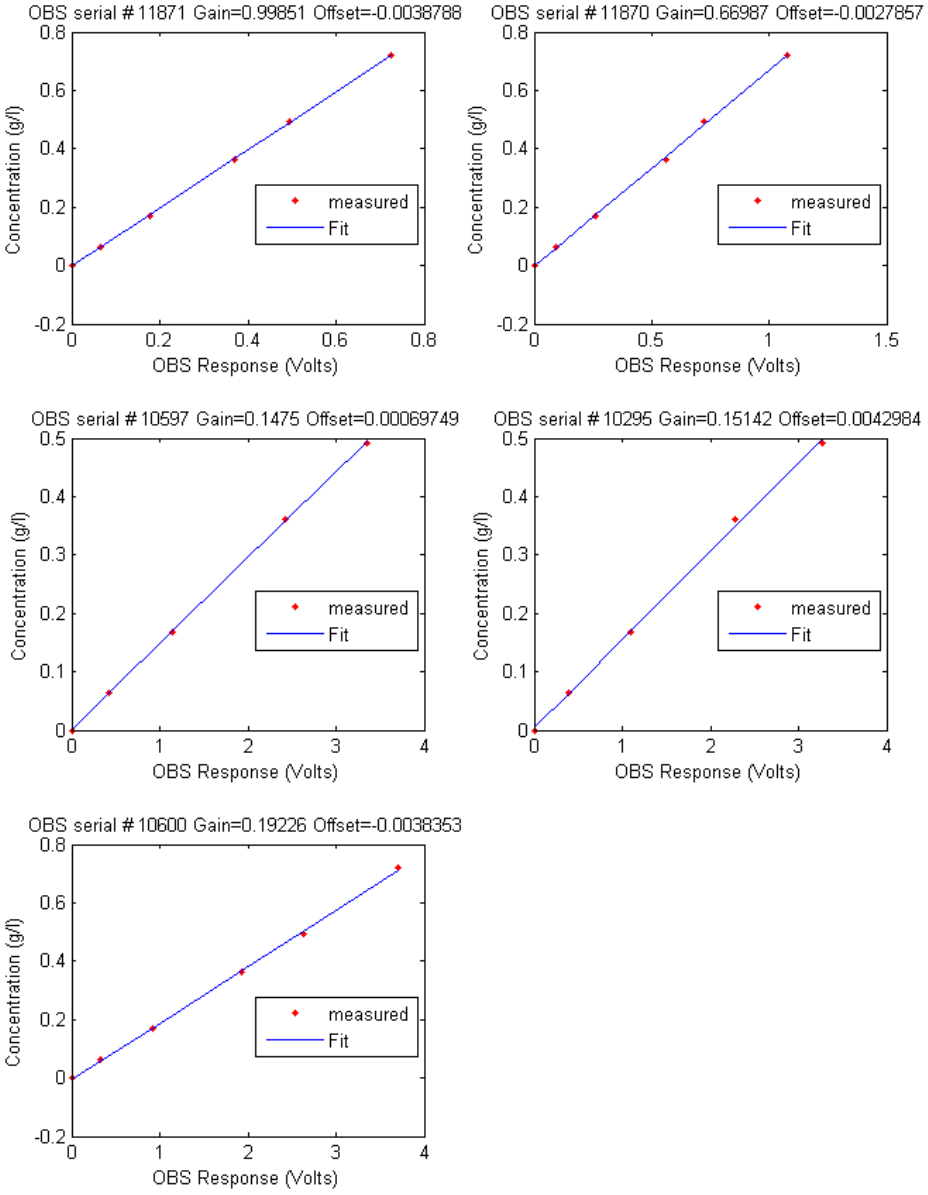

Figure C-1: OBS calibration data.

ABS Calibration

The K_t values were obtained by minimising the differences (in a least squares sense) between the known concentration and the concentration obtained by the ABS through the inversion process across all 4 test concentrations. The results of this minimisation are shown in Figure C-2.

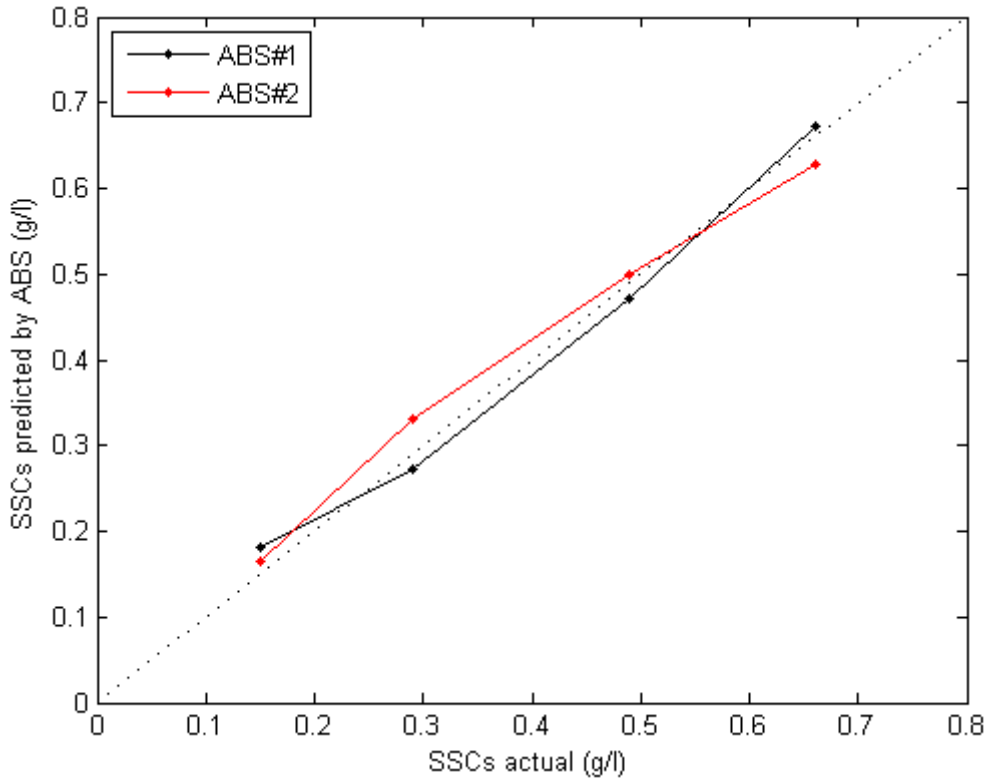

Figure C-2: ABS calibration results. (Note the dotted line represents y=x).